

TECHNISCHE UNIVERSITÄT MÜNCHEN

Fakultät für Chemie

Lehrstuhl für Technische Chemie II

# Promoted Bimetallic PdAu Catalysts for Gas Phase Vinyl Acetate Synthesis

Elisabeth Katharina Hanrieder

Vollständiger Abdruck der von der Fakultät für Chemie der Technischen Universität München zur Erlangung des akademischen Grades eines

Doktors der Naturwissenschaften (**Dr. rer. nat.**)

genehmigten Dissertation.

Vorsitzender: Univ.-Prof. Dr. Klaus Köhler

Prüfer der Dissertation:

1. Univ.-Prof. Dr. Johannes A. Lercher

2. Hon.-Prof. Dr. Richard W. Fischer

Die Dissertation wurde am 25.04.2016 bei der Technischen Universität München eingereicht und durch die Fakultät für Chemie am 12.07.2016 angenommen.



## **Acknowledgements**

There are many people who accompanied me during the time of my PhD thesis and who encouraged me to succeed.

Foremost, I would like to thank Prof. Dr. Johannes A. Lercher for giving me the opportunity to work on an interesting and challenging research topic, for enlightening discussions, for the guidance and the freedom to set up my own research ideas.

My deepest gratitude goes to Prof. Dr. Andreas Jentys, who had always an open ear for me, who stimulated discussions with excellent advices and ideas. Thank you for being my (scientific) teacher, for patiently correcting my papers and for your encouraging support throughout my thesis.

I would like to express my sincere gratitude to Prof. G.L. Haller (Yale University, US). The conversations regarding CO adsorption were really helpful.

I would like to thank Xaver Hecht for his numerous decisive advices to make my setups running. Martin Neukamm is acknowledged for elemental analysis and Andreas Marx for his computer expertise. I would like to mention Stefanie Maier, Ulrike Sanwald, Bettina Federmann and Karen Schulz who ran the show.

I am grateful to the Wacker Chemie AG for the financial support and Dr. Jürgen Eberle, Dr. Christoph Rüdinger, Dr. Anne Alber and Dr. Anja Roscher for the helpful discussions, their interest and the excellent collaboration.

Moreover, I would like to thank all participants of the Workshops of the Wacker-Institut für Siliciumchemie and Prof. Dr. Dr. h.c. Bernhard Rieger for fruitful discussions.

My students did a great job and contributed immensely to the present work. I would like to thank Sylvia Albersberger, Teresa Schachtl, Verena Höpfl, Bastian Richter, Thomas Moser, Franziska Deiser, Christoph Gnad, Magdalena Dinkel, Stefanie Mayr, Michael Grübel, Marius Bilke and Christoph Schmücker. Particularly I want to announce Sylvia for numerous discussions and her support during her Master's thesis.

I acknowledge my former colleague Dr. Stefanie Simson, for providing me an excellent introduction to the topic during my Master's thesis and for her constructive ideas during my PhD studies.

It is my pleasure to thank all my colleagues, especially those in our office: Peter Hintermeier, Maximilian Werner Hahn, Matthias Steib and in former times Anastacia Pashigreva, Vishnuvartan Muthusamy, Yanzhe Yu, Martha Dömök and Ana Hrabar.

At this point, I would like to mention: Franzi and Renate with sons and all my relatives, uncles, aunts and cousins who helped me in any kind of situation. Last but not least, I am deeply grateful to my sister Maria and my parents Lydia and Bernhard, who supported me during my whole life. I also want to say thank you to Roswitha and Martin Müller. Very special thanks go to my dear Sebastian for a wonderful time, for your patience and understanding in positive as well as in difficult moments.

Lisl

## Abbreviations

Å	Ångström
AAS	Atom Absorption Spectroscopy
AcOH	Acetic Acid
Au	Gold
a.u.	Arbitrary units
at %	Atomic percent
atm.	Atmosphere
BET	Brunauer-Emmet-Teller
°C	Degree Celsius
cm	Centimeter
CN	Coordination Number
COD	Crystallographic Open Database
CuK <sub>α</sub>	K <sub>α</sub> radiation of the copper X-ray tube
d	Diameter
D <sub>3h</sub>	Point group
DFT	Density Functional Theory
DRIFT	Diffuse Reflectance Infrared Fourier Transform
(G)eV	(Giga) electron volt
ε	Molar extinction / absorption coefficient
EXAFS	Extended X-Ray Absorption Fine Structure
fcc	Face centered cubic
FTIR	Fourier Transform Infrared Spectrometer
FWHM	Full Width at Half Maximum
g	Gram
GC	Gas Chromatography
h	Hour
HDK	Hochdisperse Kieselsäure
HR-TEM	High Resolution Transmission Electron Microscopy
IR	Infrared
in situ	Under reaction conditions
IWI	Incipient Wetness Impregnation
(k)J	(kilo) Joule
K	Kelvin
KOAc	Potassium Acetate
kV	Kilovolt
λ	Wavelength

---

L	Liter
mA	Milliampere
mol	Mol
mol-%	Mol percent
min	Minute
mL	Milliliter
ML	Monolayer
mm	Millimeter
nm	Nanometer
Pa	Pascal
Pd	Palladium
Pd(OAc) <sub>2</sub>	Palladium Acetate
PVA	Poly Vinyl Acetate
PVOH	Poly Vinyl Alcohol
PZC	Point of Zero Charge
R	Rydberg constant (8.3145 J/(mol*K))
rds	Rate determining step
r.t.	Room temperature
s	Second
S	Selectivity
SEM	Scanning Electron Microscopy
SiC	Silicon Carbide
T <sub>c</sub>	Order-Disorder Temperature
TCD	Thermal Conductivity Detector
TOF	Turn over Frequency
TOS	Time on Stream
TUM	Technische Universität München
VA	Vinyl Acetate
wt %	Weight percent
XAS	X-Ray Absorption Spectroscopy
XANES	X-Ray Absorption Near Edge Structure
XPS	X-Ray Photoelectron Spectroscopy
XRD	X-Ray Diffraction

## **Abstract**

The activity and selectivity of silica supported bimetallic PdAu catalysts for the structure sensitive acetoxylation of ethene to vinyl acetate is drastically enhanced by the addition of potassium acetate (KOAc). Surface and bulk sensitive studies on the role of KOAc allowed to establish a complete reordering mechanism of PdAu on an atomistic level. Reasons for deactivation of PdAu were resolved by systematically exploring the location and the interaction of different alkali metal acetates regarding the active site Pd.

## **Zusammenfassung**

Die Aktivität und Selektivität Silika-geträgerter PdAu Katalysatoren für die struktursensitive Acetoxylierung von Ethen zu Vinylacetat wird durch Zugabe von Kaliumacetat (KOAc) signifikant gesteigert. Durch Oberflächen- und Partikelkern- sensitive Studien zur Rolle von KOAc konnte ein vollständiger Restrukturierungsmechanismus von PdAu auf atomarer Ebene aufgestellt werden. Gründe für die Deaktivierung von PdAu wurden durch systematische Studien zur Lage und der Wechselwirkung unterschiedlicher Alkalimetallacetate hinsichtlich dem aktiven Zentrum Pd aufgeklärt.

## Table of Contents

<b>Acknowledgements</b> .....	<b>I</b>
<b>Abbreviations</b> .....	<b>II</b>
<b>Abstract</b> .....	<b>IV</b>
<b>Table of Contents</b> .....	<b>V</b>

### CHAPTER 1

<b>1. General Introduction</b> .....	<b>1</b>
1.1. Vinyl Acetate (VA) Synthesis - From Past to Presence .....	2
1.2. PdAu Alloy System .....	4
1.3. PdAu Surface.....	6
1.3.1. Ligand and Ensemble Effect.....	7
1.3.2. Surface and Bulk Composition.....	7
1.3.3. Adsorbate Induced Surface Segregation.....	8
1.4. CO Chemisorption on PdAu Surfaces .....	9
1.5. Proposed Mechanisms for VA Synthesis .....	10
1.5.1. Heterogeneous Pathway to VA.....	11
1.5.2. Homogeneous Pathway to VA.....	11
1.5.3. Supported Liquid Phase (SLP) Mechanism.....	14
1.5.4. Comparison of the Reaction Mechanisms .....	15
1.6. Active Sites for VA Synthesis .....	15
1.7. Influence of the Promoter .....	18
1.7.1. Homogeneous Reaction System .....	18
1.7.2. Heterogeneous Reaction System .....	21
1.8. References .....	24
1.9. Scope of the Thesis.....	31

### CHAPTER 2

<b>2. Atomistic Engineering of Catalyst Precursors - Dynamic Reordering of PdAu Nanoparticles during Vinyl Acetate Synthesis enhanced by Potassium Acetate</b> .....	<b>32</b>
2.1. Introduction .....	33
2.2. Experimental.....	34
2.2.1. Synthesis.....	34
2.2.2. X-Ray Powder Diffraction.....	34
2.2.3. Low Temperature IR Spectroscopy during CO Adsorption .....	35
2.2.4. In Situ IR Spectroscopy .....	35
2.2.5. Catalytic Reactions .....	35

2.3.	Results and Discussion .....	36
2.3.1.	Vinyl Acetate Synthesis on KOAc Promoted and Unpromoted PdAu/SiO <sub>2</sub> .....	36
2.3.2.	KOAc Enhances Reactive Reordering of PdAu Particles in the Heterogeneous Pathway to VA Synthesis .....	36
2.3.2.1.	Effect of KOAc on the Pd <sub>x</sub> Au <sub>y</sub> Bulk Composition .....	36
2.3.2.2.	Effect of KOAc on the PdAu Surface Composition during VA Synthesis .....	39
2.3.3.	Formation of Reactive Pd Species in Presence and Absence of KOAc .....	44
2.3.3.1.	Surface Structures in Presence and Absence of KOAc .....	44
2.3.3.2.	Exploring the Catalysts in the Working State .....	47
2.3.4.	Dynamic Reconstruction of KOAc Promoted and Unpromoted PdAu/SiO <sub>2</sub> .....	49
2.4.	Conclusions .....	50
2.6.	References .....	51
2.7.	Appendix .....	55

## CHAPTER 3

<b>3. Impact of Alkali Acetate Promoters on the Dynamic Ordering of PdAu catalysts during Vinyl Acetate Synthesis .....</b>	<b>60</b>
3.1. Introduction .....	61
3.2. Experimental Section .....	62
3.2.1. Synthesis .....	62
3.2.2. Catalytic Reactions .....	62
3.2.3. Elemental Analysis .....	62
3.2.4. IR Spectroscopy of Adsorbed CO .....	63
3.2.5. X-Ray Absorption Spectroscopy .....	63
3.3. Results and Discussion .....	64
3.3.1. Deactivation Behavior of PdAu/MOAc/SiO <sub>2</sub> (M <sup>+</sup> = Li <sup>+</sup> , Na <sup>+</sup> , K <sup>+</sup> , Cs <sup>+</sup> ) .....	64
3.3.2. Impact of the Pd Surface Concentration on Deactivation of PdAu .....	66
3.3.2.1. Pd Surface Enrichment on PdAu/MOAc/SiO <sub>2</sub> (M <sup>+</sup> = Li <sup>+</sup> , Na <sup>+</sup> , K <sup>+</sup> , Cs <sup>+</sup> ) during Reaction .....	66
3.3.2.2. Interaction of the Promoter with the Pd Enriched Surface of PdAu .....	68
3.3.3. Stability of the Pd/M <sup>+</sup> -O Adlayer on PdAu/MOAc/SiO <sub>2</sub> (M <sup>+</sup> = Li <sup>+</sup> , Na <sup>+</sup> , K <sup>+</sup> , Cs <sup>+</sup> ) .....	69
3.3.4. Deactivation of PdAu/MOAc/SiO <sub>2</sub> (M <sup>+</sup> = Li <sup>+</sup> , Na <sup>+</sup> , K <sup>+</sup> , Cs <sup>+</sup> ) .....	72
3.4. Conclusions .....	72
3.5. References .....	74
3.6. Appendix .....	77



**CHAPTER 4**

<b>4. Interaction of Alkali Acetates with PdAu.....</b>	<b>81</b>
4.1. Introduction .....	82
4.2. Experimental.....	82
4.2.1. Synthesis.....	82
4.2.2. Elemental Analysis .....	83
4.2.3. X-Ray Powder Diffraction.....	83
4.2.4. IR Spectroscopy of Adsorbed CO .....	83
4.2.5. X-Ray Absorption Spectroscopy at the Pd-K and Au-L <sub>3</sub> -edge .....	84
4.3. Results and Discussion .....	84
4.3.1. Pd Surface Enrichment on PdAu Particles Induced by MOAc (M <sup>+</sup> = Li <sup>+</sup> , Na <sup>+</sup> , K <sup>+</sup> , Cs <sup>+</sup> ).....	84
4.3.2. Interaction of MOAc (M <sup>+</sup> = Li <sup>+</sup> , Na <sup>+</sup> , K <sup>+</sup> , Cs <sup>+</sup> ) with Pd on PdAu .....	87
4.3.3. Chemical Nature of the Pd/M <sup>+</sup> Adlayer.....	90
4.4. Conclusions .....	92
4.5. References .....	93
4.6. Appendix .....	95

**CHAPTER 5**

<b>5. Summary .....</b>	<b>100</b>
-------------------------	------------

**CHAPTER 6**

<b>6. Zusammenfassung .....</b>	<b>102</b>
---------------------------------	------------

<b>Curriculum Vitae.....</b>	<b>104</b>
------------------------------	------------

<b>Liste der Publikationen.....</b>	<b>105</b>
-------------------------------------	------------

# Chapter 1

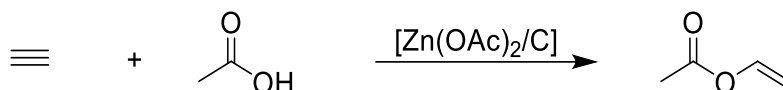
## General Introduction

The synthesis of vinyl acetate (VA) is one of the most important industrial processes involving the heterogeneous catalytic acetoxylation of ethene. First produced in 1912 as a by-product in the liquid phase synthesis of ethylidene diacetate,<sup>[1]</sup> VA is an important substance for a wide range of applications. About 50 % of the global VA production is radically polymerized to polyvinyl acetate (PVA) which is part of water-based paintwork materials, various types of glue, tiles for floors, acrylic fibers, paper coatings and textiles. Copolymers like ethene vinyl acetate (EVA) are used in shoe soles, toothpaste or foils. Moreover, VA monomer is the starting material for polyvinyl alcohol (PVOH), which is also used on a large scale for fibers.<sup>[2-3]</sup> Products based on VA are ubiquitous in modern life because of their good adhesive, optical, electrical and fiber-forming properties.

In 2010, the global production of VA was 4.7 million metric tons.<sup>[4]</sup> Further growth of almost 4.6 % per year is expected revealing high market potential for VA synthesis. Main producers are Celanese (USA), Lyondell Basell (USA), Dow Chemical (USA), DuPont (USA), Ineos (Great Britain) and Wacker Chemie (Germany).<sup>[5]</sup> Over the past 90 years, the technology of VA production has been constantly improved.<sup>[6-7]</sup> Especially, structural properties of silica-supported bimetallic PdAu catalysts have been widely investigated. The challenge for today`s scientists is to establish a better understanding of mechanistic aspects under the influence of promoters in order to improve existing PdAu catalysts and to develop new catalytic systems.

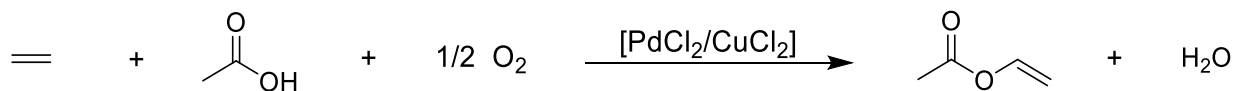
## 1.1. Vinyl Acetate (VA) Synthesis - From Past to Presence

First synthesized in 1912 by Fritz Klatte, vinyl acetate (VA) was produced via the heterogeneous acetoxylation of acetylene, based upon vapor phase reaction over a zinc acetate catalyst, typically supported on activated carbon until 1965.<sup>[8-9]</sup> The role of carbon goes beyond merely providing a medium for dispersing  $\text{Zn}(\text{OAc})_2$ . Carbon donates electrons to Zn thereby promoting acetylene adsorption.<sup>[9]</sup> High reaction yields up to 99% based on acetylene are obtained at 160-210 °C and 0.4 bar overpressure in fixed or fluidized bed reactors.<sup>[10]</sup> However, the expense and scarcity of acetylene made this process unattractive.<sup>[11]</sup>



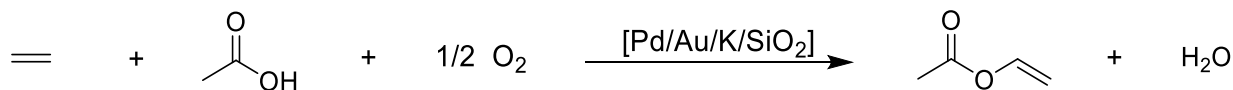
**Scheme 1.1.** Gas phase acetoxylation of acetylene.

In the early 1960s, Moiseev<sup>[12]</sup> and Smidt<sup>[13-14]</sup> first reported the homogeneous, liquid phase process using palladium salts such as  $\text{PdCl}_2$  or  $\text{Pd}(\text{OAc})_2$  with cocatalysts like sodium acetate.<sup>[15]</sup> VA is formed by reaction of ethene with Pd acetate in acetic acid solution accompanied by the reduction of  $\text{Pd}^{2+}$  to Pd black.<sup>[16]</sup>  $\text{Pd}^0$  has to be oxidized by  $\text{CuCl}_2$ , which is successively reoxidized with  $\text{O}_2$ . The applied conditions are 100-130 °C and 30-40 bar pressure. This process is closely related to the homogeneous Wacker process<sup>[13, 17]</sup> using almost the same catalyst to form acetaldehyde.<sup>[10, 16]</sup>



**Scheme 1.2.** Liquid phase acetoxylation of ethene.

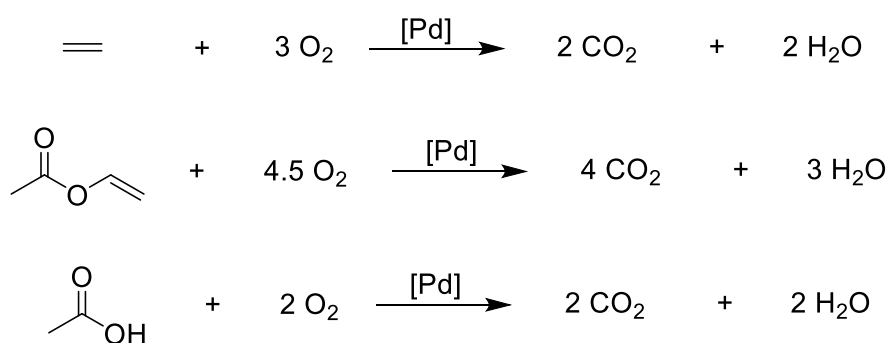
In the late 1960s, a heterogeneous gas phase process developed by Hoechst and Bayer proved more favorable. Corrosion by chloride compounds in the liquid phase process could be eliminated and selectivities increased.<sup>[18]</sup> Currently, VA is produced on a large scale via a related gas-phase acetoxylation procedure.<sup>[16, 19]</sup> The three component reaction with ethene, oxygen and acetic acid to VA is exothermic ( $\Delta H_R = -178 \text{ kJ/mol}$ ).<sup>[20]</sup>



**Scheme 1.3.** Gas phase acetoxylation of ethene.

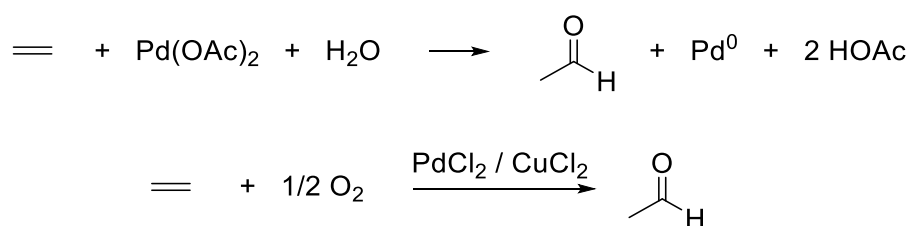
The reaction, operating at 140 to 180 °C and at pressures of 5 to 10 atm.<sup>[21]</sup> is usually performed in fixed-bed multi-tubular reactors.<sup>[22]</sup> Silica-supported bimetallic PdAu catalysts promoted with potassium acetate in large excess are the most relevant catalysts.<sup>[19, 23-24]</sup> The optimized catalyst composition was found to be 1.5 wt% Pd, 0.75 wt% Au with 5.0 wt% KOAc at selectivity levels between 93 and 95 %.<sup>[25]</sup> Besides PdAu, potassium promoted PdCd and PdBa systems<sup>[26]</sup> as well as Pd-K-Bi-Pt<sup>[27]</sup> and Pd doped with Sb, Bi, Se or Te<sup>[27-28]</sup> also

catalyze VA formation. Addition of a second metal to Pd is important since Pd agglomerates favor the total combustion of ethene ( $\Delta H_R = -1304$  kJ/mol), vinyl acetate<sup>[18, 29]</sup> or acetic acid ( $\Delta H_R = -683$  kJ/mol), lowering the selectivity towards VA synthesis.<sup>[30]</sup> The oxidation rates follow the order  $C_2H_4 > VA > AcOH$ . Early studies claimed that  $CO_2$  derived primarily from ethene.<sup>[31-32]</sup> However, Chrathorne et al.<sup>[18]</sup> claimed that  $CO_2$  derived equally from AcOH and  $C_2H_4$  and that the combustion of VA is not significant, as it may not strongly interact with the catalyst.<sup>[18]</sup> The ethene combustion kinetics in the presence and absence of acetic acid were essentially the same, suggesting that ethene combustion is primarily responsible for  $CO_2$  formation in the synthesis of vinyl acetate.  $r_{CO_2}$  increases significantly with an increase in the temperature.<sup>[33]</sup> Presumably the relative contribution of ethene and acetate decomposition to the formation of  $CO_2$  will depend on the rate at which the acetate species react with ethene compared to their decomposition rate.<sup>[34]</sup>



**Scheme 1.4.** Total combustion of ethene, VA and acetic acid to  $CO_2$  and  $H_2O$ .

Acetaldehyde can form via a Wacker-type reaction in the presence of water<sup>[14]</sup> or by the oxidation of ethene (Wacker process).<sup>[17]</sup> By adding alkali metal salts, the selectivity to VA is enhanced.



**Scheme 1.5.** Formation of acetaldehyde from ethene.

Further, however negligible byproducts depending on the reaction conditions in homogeneous VA synthesis are ethylidene diacetate and butenes.<sup>[35]</sup>

## 1.2. PdAu Alloy System

PdAu alloys have been reported to increase the activity of a wide range of reactions. The addition of Au to Pd leads to a catalytic improvement in VA synthesis<sup>[36]</sup>, in H<sub>2</sub>O<sub>2</sub> formation (1.9 106 tons/a) from H<sub>2</sub> and O<sub>2</sub><sup>[37-38]</sup>, in methanol decomposition to H<sub>2</sub> and CO<sup>[39]</sup>, in oxidation reactions<sup>[40-48]</sup>, in the hydrogenation of allyl alcohol<sup>[49-50]</sup>, in hydrodechlorination reactions<sup>[51]</sup>, in the hydrodesulfurization of dibenzothiophene<sup>[52]</sup> or in direct ethanol fuel cells<sup>[53]</sup>. The use of bimetallic catalysts increases the resistance to particle sintering and changes the geometry as well as the electronic properties of the active sites.<sup>[54]</sup>

Palladium and gold crystallize both in face centered cubic structures, exhibit similar electronegativity, metal radii and number of valence electrons. These are reasons, why PdAu alloys are completely miscible over the entire range of composition forming a continuous series of solid solution.<sup>[55-56]</sup> At lower temperatures Au<sub>3</sub>Pd-<sup>[57]</sup>, AuPd- and AuPd<sub>3</sub>-<sup>[58]</sup> superstructures are observed.<sup>[59-61]</sup>

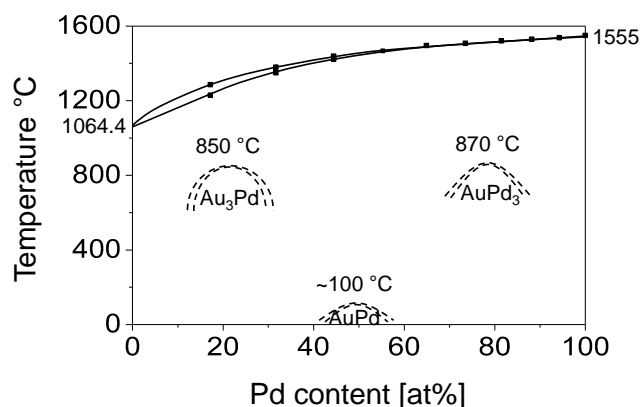


**Figure 1.1.** Phase diagram of the PdAu system.<sup>[61]</sup>

All of these long-range order (LRO) phases show fcc crystal structures like AuCu<sub>3</sub> and AuCu. The LRO transition temperature in a 50 at-% Pd alloy is estimated to be at about 100 °C<sup>[60-61]</sup> whereas Sluiter et al.<sup>[62]</sup> found an order-disorder temperature between 100-200°C for the PdAu superstructure.<sup>[62]</sup> Short-range ordering in PdAu alloys, detected by diffuse X-ray scattering, was observed at 40 at% Pd quenched from 350 °C.<sup>[61]</sup> (The quenching history has no effect on the lattice parameter of the alloy.<sup>[63]</sup>)

Heats of formation of PdAu alloys at 300 K are exothermic over the entire composition range. Maximum stability occurs at ~ 40 at% Pd with an enthalpy of ~ -7.8 kJ/mol.<sup>[61, 64-65]</sup> The large negative enthalpies are indicative of an attractive interaction between the alloy constituents and a tendency to order.<sup>[11]</sup> Additionally, it implies that the alloy structure is stabilized by the energetically more favorable Pd-Au bonds compared to Au-Au or Pd-Pd bonds.<sup>[66-67]</sup>

The lattice parameters vary from 0.389 nm for pure Pd and 0.408 nm for pure Au with a small negative deviation of 0.0004 nm at about 30 at% Pd from Vegard's law.<sup>[68]</sup> Thus, the PdAu system seems to be well described by a two-band model, an extended theory of the free electron theory of Bloch. Under the assumption that the band shape does not change with composition, the principle effect of adding a soluble metal is an alteration of the Fermi energy,  $E_F$  of the electrons.<sup>[69-70]</sup> The valence electrons lie in a broad s-orbital that

overlaps with a narrow d-band. In pure Pd, 9.4 and 0.6 electrons are in the d-band and in the s-orbital, respectively. Thus, there are 0.6 positive holes in the d-band of Pd, which can be filled with the s-electrons of a monovalent atom like Au or Ag according to the alloy concentration.<sup>[64, 71]</sup> In this manner, Mott<sup>[69-70]</sup> and Kim<sup>[72]</sup> explained the large electrical resistivity of the transition metals and their alloys. However, the rigid band model represents an extreme as the outermost shells of d and s electrons are equally redistributed among the component atomic sites that have substantial ionic character. Consequently, elements of an alloy should become indistinguishable according to the band theory model. At 40 at% Pd in PdAu alloys, the paramagnetism of Pd is zero and the d-band orbitals were completely filled with electrons. d-band vacancies are essential in bonding activated complexes and to create reactivity in low temperature catalysis.<sup>[73]</sup> So zero reactivity is assumed for Pd<sub>40</sub>Au<sub>60</sub>. However, catalysis does not take place in the bulk phase but on the PdAu surface where the picture is more complicated.<sup>[64]</sup>

Further doubts on the band theory model were cast by photoemission studies indicating two separate/split instead of one common d-band.<sup>[74]</sup> It is considered more likely that the d-band is always full on the Au atoms. According to this extreme, the minimum polarity model,<sup>[75]</sup> atomic sites in an alloy remain neutral since they have the same electronic configuration as in the pure metal. This implies that the geometrical arrangement of the Pd atoms with respect to the Au atoms on the surface may be of importance since the atoms will appear different to an adsorbing species.<sup>[64]</sup> However, studies of the electronic structure of PdAg and PdAu alloys from Meitzner and Sinfelt indicate that the true state lies between these extremes.<sup>[74]</sup>

To gain a deeper insight into the electronic structure of mono- and bimetallic particles, several techniques have been applied. In order to investigate the density of unfilled states  $E_F$ , XAS studies have been applied to AuPd alloys. Reifnsnyder et al.<sup>[76]</sup> determined a negative feature near 3eV in Au L<sub>3</sub> XANES difference spectra of PdAu alloy films and PdAu/SiO<sub>2</sub> catalysts, due to loss of white line intensity. This feature is relatively insensitive to alloy composition and indicates a decrease in the density of unoccupied d<sub>5/2</sub> states relative to bulk Au. This decrease results from a change in d band hybridization and not from charge transfer as the extent of charge transfer is small for PdAu alloys.<sup>[77]</sup> XANES spectroscopy at the L<sub>3</sub> and L<sub>2</sub> (electron excitations from 2p core levels to the unoccupied d-states) absorption edges of PdAu alloys confirms that electron transfer to the Pd 4d band is much smaller<sup>[74, 78-79]</sup> than predicted by the rigid band model of Mott.<sup>[70]</sup> Nonetheless, the PdAu d-d interaction is believed to have an important effect on the electronic structure of the alloys. In particular, the Au d<sub>5/2</sub> partial DOS is broadened and shifted to higher binding energy (relative to  $E_F$ ) with increasing Pd content.<sup>[76]</sup>

Soft X-ray photoelectron spectroscopy (sXPS) has been applied to examine the width, shape, and energetic level of the valence band. A clear hybrid state between the 4d Pd band and the 5d Au band could be detected.<sup>[44, 80]</sup> The binding energy of core level electrons and the valence d-band occupation in the bimetallic particles were significantly altered in comparison to the monometallic particles. Lee et al.<sup>[81]</sup> reported that the Pd 3d<sub>3/2</sub> and the Au 4f<sub>7/2</sub> core levels shift to lower binding energies upon alloying in agreement with the core level shifts of Au 4f<sub>7/2</sub> and Pd 3d<sub>3/2</sub>. These authors also assert that the core-level binding energy shifts conform to a charge compensation model and propose that Au gains sp-type electrons and loses d-electrons whereas Pd loses sp-

electrons and gains d-electrons.<sup>[81]</sup> Together with the core shell structure it is supposed to be the main reason for the observed changes in the catalytic behavior.<sup>[82]</sup>

### 1.3. PdAu Surface

According to Goodman<sup>[83]</sup>, two questions are important in the study of bimetallic alloy surfaces. What is the nature of the hetero-nuclear metal-metal bond? How does the hetero-nuclear bond formation affect the physical chemical properties of the metal?<sup>[83]</sup>

The formation of a surface metal-metal bond can perturb the electronic, chemical, and catalytic properties of a metal. Charge transfer is an important component in surface metal-metal bonds that involve different elements. The larger the charge transfer, the stronger the energy of the bimetallic bond. On a surface, the formation of a hetero-nuclear metal-metal bond induces a flow of electron density toward the element with the larger fraction of empty states in its valence band. In the case of PdAu, Pd offers ~0.55 d band holes and thus, electrons from Au are transferred to Pd. This behavior indicates that the nature of a hetero-nuclear metal-metal bond depends strongly on the structural geometry of the bimetallic system.<sup>[84]</sup> However, the electron flow from Au to Pd is contrary to the trend predicted from the electronegativity (Allred, Rochow) which is 1.30 (Pd) and 1.42 (Au). Consequently, electrons should flow from Pd to Au as the electronegativity is the ability of a chemically bonded atom to attract electrons to itself. This statement is true but oversimplified for a metal on the surface. The electronegativity of an atom in a given compound depends on the orbitals involved in the chemical bond. Changes in the coordination geometry can influence the hybridization of the orbitals. Thus the electronegativity and therefore the properties of a bulk atom (3D) can drastically differ from the identical atom on the surface (2D).<sup>[84]</sup> A reduction in the atomic coordination number produces a narrowing of the valence band at the surface. Consequently, charge flows between the surface atoms and the bulk to maintain a common  $E_F$  of the composite. Bimetallic surfaces with the strongest Pd-substrate bonds have the weakest Pd-CO bonds. The behavior seen for the 2D metal overlayers is different from that expected for bulk metals stressing the need to investigate the nature of the surface metal-metal bond.<sup>[83]</sup>

In catalysis and especially for structure sensitive reactions like VA synthesis that require larger ensemble sizes,<sup>[85]</sup> the surface topography is of interest.<sup>[86]</sup> Both the activity and the selectivity can be improved in these systems by the optimal design of the specific sites and bifunctional ensembles. Au is added to Pd to improve the activity for VA synthesis by about a factor of 2 and the selectivity by about 5%.<sup>[85]</sup> For alloys combining catalytically active and inactive elements, the increase in chemical selectivity on geometrically optimized surfaces has been described in terms of the different size and concentration of clusters of the active element. For these reasons both the composition of the surface layer as a function of the bulk composition as well as the relative presence of different cluster types on the surface is important for the fundamental understanding of reactions on these surfaces.<sup>[87]</sup>

### 1.3.1. Ligand and Ensemble Effect

Alloying effects on the PdAu surface affecting heterogeneous catalysis are divided into ligand and ensemble effects.<sup>[88]</sup> Ligand effects describe the formation of hetero-nuclear metal-metal bonds (see 1.3.) involving either charge transfer between the metals or orbital rehybridization of one or both of the metals.<sup>[89]</sup> Ensemble effects refer to changes in the catalytic properties of an ensemble of atoms in the surface when the chemical composition of the ensemble changes. Surface adsorption properties can be described by either the ligand or/and the ensemble effect.<sup>[90]</sup> In PdAu systems, charge transfer from Au to Pd is limited<sup>[79]</sup> while marked ensemble effects have been observed.<sup>[91-92]</sup>

In experimental and theoretical studies, separation of these two effects is difficult. Variations in the ratio of Pd and Au atoms in an adsorption site changes automatically the ligands around the adsorption site. Liu et al.<sup>[88]</sup> used extensive DFT calculations to show that the ligand effects can be accounted for by changes in the d-band centers of the surface metal atoms. Upon alloying, Au gains s, p electrons and loses d electrons whereas Pd loses s, p electrons but gains d electrons.<sup>[89, 93-94]</sup> Charge transfer between Pd and Au helps to explain why Au is able to fully isolate Pd. There exists some Coulomb Pd-Pd repulsion in bulk Pd whereas Pd-Au attraction is realized as a result of net charge transfer from Pd to Au. For late-transition metals like Pd and Au, the d-character is much more important than s, p-character in defining their chemisorption and catalytic properties. For Pd, gaining d electrons shifts the d band center away from  $E_F$ , which leads to weaker interaction between adsorbates and surface Pd atoms.<sup>[88]</sup> Theoretical calculations demonstrate that the Pd d band for Pd monomers surrounded by Au is much lower in energy than that for Pd monolayer or bulk Pd surfaces. Thus, the electronic effect induced by alloying with Au causes the Pd d-band to be more localized below  $E_F$ .<sup>[95]</sup> There is another reason that causes the Pd d band to narrow, a lattice mismatch between Pd and Au, as Pd has a lattice constant 5% smaller than Au.<sup>[89]</sup> Upon alloying, Pd adopts the lattice constant of Au in some cases.<sup>[93, 96]</sup> The increase in Pd-Pd bond length causes  $E_F$  within the Pd d band to rise. This also enhances the atomic-like character of Pd atoms and correspondingly, weakens binding toward reactants. From both charge transfer and bond length arguments, Au is able to weaken the binding strength of Pd by perturbing its d band. However, this does not mean that Au weakens the catalytic activity of Pd. In contrast, enhanced activity of Pd within PdAu alloys is frequently found as compared to pure Pd.<sup>[97]</sup> Thus, the ligand effect related to the electronic structure of the adsorption site is a good measure of the metal d band center and the reactivity.<sup>[88]</sup>

The ensemble effect is described by a simple linear interpolation model in which the adsorption energy at a mixed site is the appropriate average of the properties of the constituents.<sup>[88-89]</sup> In VA synthesis, the enhanced activity of Pd in PdAu compared to monometallic Pd is described by the ensemble effect (see section 1.6.).

### 1.3.2. Surface and Bulk Composition

In the surface composition model, the surface is regarded as a simple array of individual Pd and Au atoms. Since the surface Pd concentration will decrease linearly with increasing Au concentration, no abrupt change



in catalytic activity with alloy composition is expected.<sup>[64]</sup> Early studies from Jablonski et al.<sup>[98]</sup> indicate that the surface and bulk PdAu structures equilibrate in 500s at 600 °C. Even at room temperature PdAu systems indicate interdiffusion.<sup>[99]</sup> The regular solution parameter  $\Omega$  for PdAu is largely negative and thus a strong tendency towards ordering is expected.<sup>[98]</sup> The metallic radii and heats of vaporization of Pd and Au are similar leading to the assumption that the surface and bulk composition are closely related.<sup>[56]</sup> In contrast, the regular solution model predicts a small extent of surface enrichment over most of the composition range in equilibrated PdAu systems (in inert atmosphere or vacuum).<sup>[76]</sup> Indeed, annealing a 1:1 PdAu mixture at 800 K led to a surface composition of Au<sub>0.8</sub>Pd<sub>0.2</sub> which, however, can be systematically controlled by altering the bulk PdAu alloy concentration.<sup>[89-90]</sup> A significant Au enrichment of the first atomic PdAu surface plane compared to the bulk was observed at 800 K, while the second and deeper planes had compositions close to the bulk value in agreement with the ion scattering results of Swartzfager et al.<sup>[100]</sup> Since the excess enthalpies of PdAu alloys are negative, the alloys will have short-range order.<sup>[87]</sup> In agreement to Christensen et al.<sup>[101]</sup> who theoretically studied the phase diagrams for surface PdAu alloys found that during heating Au segregates to the surface<sup>[89, 102-106]</sup> due to its surface energy in the ideal solution model ( $\Delta H_{\text{mix}} = 0$ ) (Segregation energy (eV/atom) of -0.14 eV). The surface free energy of Pd (2.043 J/m<sup>2</sup>)<sup>[107]</sup> is higher than that of Au (1.626 J/m<sup>2</sup>).<sup>[108]</sup> Hence, to minimize the surface free energy, Au preferentially decorates the surface.<sup>[89]</sup> In general, the surface segregation of an alloy component depends on the enthalpy of mixing, the atomic sizes of the metals and the surface free energies (which are proportional to the heats of sublimation).<sup>[94]</sup>

### 1.3.3. Adsorbate Induced Surface Segregation

As stated in 1.3.2., Pd diffuses to more stable sites in the subsurface and bulk of Au at high temperatures (~400 K). However, in the presence of reactive species Pd will actually segregate back to the surface as single atoms, clusters<sup>[109]</sup> and adsorbates significantly affect surface enrichment in PdAu alloys.<sup>[76]</sup> According to Haire et al.<sup>[110]</sup>, on a thermodynamic basis, surface composition will adjust so that the surface becomes enriched in the element which interacts more strongly with the adsorbate.<sup>[110]</sup> Thus, chemisorption of O, CO or H<sub>2</sub> induced the reverse trend in surface segregation, a Pd surface enrichment, due to the higher chemisorption bond energy of O and CO on Pd than on Au.<sup>[64, 97, 103, 111]</sup> Exposure to air resulted in selective reoxidation of the Pd atoms and subsequent reduction led to deposition of a Pd-rich shell on the surface of the remaining Au core.<sup>[112]</sup> Analysis of Pd d-band provides evidence of strong Pd–O affinity and a small effect of the Pd substitution on the d-band densities of states of neighboring Au atoms.<sup>[113]</sup> This effect was also observed for Pt-Au alloys. Although Au has a lower work function than Pt and is therefore more stable on the surface (5.3 eV compared to 5.6 eV), CO induces fluxional behavior in the PtAu particles that draw Pt to the surface due to the stronger Pt-CO bond.<sup>[114]</sup> Additionally, the adsorption of acetic acid at 300 K is found to cause measurable segregation of Pd to the surface of PdAu alloys for all surface compositions tested. The effect of adsorbate-induced segregation may be more dramatic at the PdAu(100) surface. Therefore the remarkable catalytic behavior reported by Chen et al.<sup>[115]</sup> for VA synthesis may require a more complex explanation than the proposed ensemble effect.<sup>[116]</sup>

## 1.4. CO Chemisorption on PdAu Surfaces

Carbon monoxide molecules adsorbing on metal atoms or ions interact with the metal valence d-electron forming metal-carbon-oxygen bonds according to Hückel molecular orbital theory, which increases the metal-carbon bond strength but decreases the carbon-oxygen bond strength. In this model, only effects in the  $\pi$ -bonding system are considered whereas  $\sigma$ -bonds are assumed constant. This model qualitatively explains the occurrence of several carbon-oxygen stretching frequencies in the IR spectra of CO adsorbed on metals, on evaporated and supported metals, IR band positions as a function of coverage, the effect of adsorbing other gases in addition to previously chemisorbed CO and band shifts on alloys compared to pure metals.<sup>[117]</sup> Thus, C-O vibrations give direct information on the C-O bond strength as function of the electronic state of the substrate.<sup>[118]</sup> On reduced Pd(111) linearly, bridged and hollow adsorbed CO appeared at  $\sim 2105$ , 1995 and  $1883\text{ cm}^{-1}$ , depending on the temperature and pressure. The bonding strength of CO on Pd monomer sites is much weaker than that on contiguous Pd sites, thus reducing the poisoning effect of CO. The transition from hollow to bridging adsorption occurs at  $\sim 850$ -900 K and the transition from bridging to a-top/ hollow at  $\sim 250$  K. Weak features at  $2096\text{ cm}^{-1}$  between 250-720 K are likely due to small amounts of CO adsorbed on top of Pd atoms and could represent either a slight disorder on the CO overlayer or a mismatch between the compressed CO overlayer and Pd surface.<sup>[119]</sup> Bands below  $2000\text{ cm}^{-1}$  for bridged adsorbed CO are affected by intermolecular interactions of adsorbed CO species which is more important on bigger particles than on smaller ones.<sup>[120]</sup> Additionally, M-CO complexes depend directly on the effective charge of the adsorbent. Bands at 2120 and 2150–2160  $\text{cm}^{-1}$  correspond to  $\text{Pd}^+$ -CO and  $\text{Pd}^{2+}$ -CO complexes according to Pestryakov.<sup>[121]</sup>

Modified chemisorptive properties at step/edge sites and particle size dependent CO frequencies were observed by Rainer et al.<sup>[92]</sup>. Indeed, Mejía-Rosales et al.<sup>[122]</sup> described the final PdAu alloy particle structure is neither a cuboctahedral nor an icosahedral structure but as a truncated octahedron with a very rough surface, in the sense that the surface contains many defect sites such as kinks, edges, vacancies, and di-vacancies. The effect of alloying Pd with Au is the formation of new structures and the increase of surface roughness.<sup>[122]</sup> Thus, peak widths broaden with greater surface heterogeneity and/or disorder of the CO overlayer.

The relative distribution of CO adsorbed in linear or multifold way depends on the particle size. For particles smaller 3 nm, threefold hollow bound CO are entirely absent at 100K.<sup>[92]</sup> Chou et al.<sup>[123]</sup> found that also the calorimetric heat of adsorption of CO depended on the crystallite size of Pd. For poorly dispersed samples (average crystallite sizes up to 1000 nm)  $Q_{\text{ad}}$  were close to 22 kcal/mol.  $Q_{\text{ad}}$  increased sharply to 35 kcal/mol when the average Pd crystallite size dropped below 3 nm. Changes in the electronic properties from decreasing Pd crystallite sizes appear to be the major factor causing the stronger bond strengths.  $Q_{\text{ad}}$  was not noticeably affected by the support.<sup>[123]</sup>

The zero coverage effective desorption activation energy and the preexponential factor for CO on Pd(111) were found to be 35.5 kcal/mol and  $10^{13.5}\text{ s}^{-1}$ , respectively from 87 to 200 K.<sup>[124]</sup> Initial isosteric heats of adsorption of 30 and 38 kcal/mol were determined for Pd(111) and Pd(100).<sup>[125]</sup>

Isosteric heat of adsorption of CO on Pd extrapolated to zero coverage was determined to be 38.9 kcal/mol on 6-7 nm particles. The size dependency has been attributed either to intrinsic particle size effects, resulting from changes in the average metal atom coordination number, or to an enhancement in the relative contribution from the metal-support interaction.<sup>[126]</sup>

In contrast to CO adsorption on Pd, on Au CO will adsorb only in linear mode at  $\sim 2104\text{ cm}^{-1}$ . CO does adsorb on Au(100) down to 125 K<sup>[92]</sup> but weakly and reversibly on Au at 300 K.<sup>[127]</sup> The initial heat of CO adsorption on Au/SiO<sub>2</sub> was low (70 kJ/mol) in agreement with the low CO uptakes. Heats of CO adsorption on Au increase sharply with decreasing cluster size of Au from 12.5 kcal/mol (3.1 nm particles) to 18.3 kcal/mol (1.8 nm particles). Heat of CO adsorption on bulk Au films is 13.4 kcal/mol.<sup>[128]</sup> Additionally, the nature of the active sites and the oxidation state(s) of gold can be estimated by especially IR spectroscopy of adsorbed CO. Different ionic Au sites (Au<sup>3+</sup>, Au<sup>+</sup>, Au<sup>0</sup>, Au<sup>-</sup>) can be detected dependent on the CO frequency. The most stable surface carbonyls are expected for Au<sup>+</sup> (2200 - 2150 cm<sup>-1</sup>, not removed by evacuation), Au<sup>-</sup> followed by Au<sup>0</sup>, Au<sup>3+</sup> (decompose at low temperatures, Au<sup>3+</sup>-CO at 2207 cm<sup>-1</sup>, Au<sup>3+</sup>-(CO)<sub>2</sub> at 2205 cm<sup>-1</sup>, Au<sup>3+</sup>-(CO) at 2170 cm<sup>-1</sup>) and Au<sup>δ+</sup> (2155 - 2130 cm<sup>-1</sup>). Generally, the higher  $\nu_{\text{CO}}$ , the higher the oxidation state of the gold site.<sup>[129]</sup> However, complications during CO adsorption on supported gold arise as CO can reduce gold cations easily and induce other changes of gold nanoclusters. To minimize reactive adsorption of CO, it is advantageous to perform experiments at low temperatures and/or in the presence of O<sub>2</sub>.<sup>[129]</sup>

Generally, the frequency of adsorbed CO increases with surface coverage due to increased CO dipole-dipole coupling as the distance of the CO molecules in CO islands has a pronounced effect on the CO frequency. A decrease in CO frequency in coadsorbed layers is mainly due to geometrical dilution effects in Pd by Au and not due to a reduced bond strength of CO.<sup>[118]</sup> In order to check for CO coverage effects, transient <sup>12</sup>CO-<sup>13</sup>CO experiments are carried out as CO coupling effects are eliminated by a mixture of <sup>12</sup>CO/<sup>13</sup>CO. Eischens et al.<sup>[130]</sup> found that the changes in the CO spectra of C<sup>12</sup>O and C<sup>13</sup>O on Pt during variation of the surface coverage are due to interaction effects. In contrast, Primet et al.<sup>[131]</sup> explained this phenomenon based on surface heterogeneity as consequence of Pd surface islands formation,<sup>[132]</sup> repulsive interactions between adsorbed atoms and changes in work function of the adsorbent surface induced by the adsorbed gas. <sup>12</sup>CO and <sup>13</sup>CO experiments on Pt crystallites show that the CO molecules are free of dipole-dipole coupling. The CO stretching frequencies are interpreted in terms of electronic transfer as the surface coverage increased, the heat of adsorption decreased.<sup>[131]</sup> Blyholder et al.<sup>[117]</sup> attributed the coverage-dependent CO frequency shift to the population decrease of the CO  $\pi^*$  orbitals due to a competition of the metallic d-electrons.<sup>[117]</sup>

## 1.5. Proposed Mechanisms for VA Synthesis

Several possible reaction pathways for VA synthesis have been proposed in literature. In general, the active site Pd remains Pd<sup>0</sup> or is oxidized to either Pd<sup>1+</sup> or Pd<sup>2+</sup> during reaction.<sup>[16, 32]</sup>

### 1.5.1. Heterogeneous Pathway to VA

Nakamura et al.<sup>[32]</sup> suggested that dissociative adsorption and activation of ethene leads to formation of a vinyl species that couples with an adsorbed acetate species to produce VA. Pd remained in metallic form throughout the reaction.<sup>[32]</sup> Oxygen either can be directly involved in the C–H activation steps or can simply provide a thermodynamic sink for produced hydrogen. It is regarded as a classic Langmuir - Hinshelwood mechanism derived from kinetic studies from Han et al.<sup>[23]</sup> Ethene activation to form vinyl species and the coupling of vinyl with acetate to VA have the highest activation barriers and may be steps that control the rate.<sup>[85]</sup> In accordance, Plata et al. confirmed the C-O coupling to be the rate determining step.<sup>[133]</sup> So, one of the most important intermediates for this reaction is the acetate.<sup>[134]</sup>

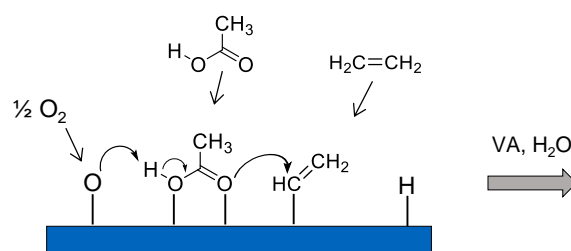
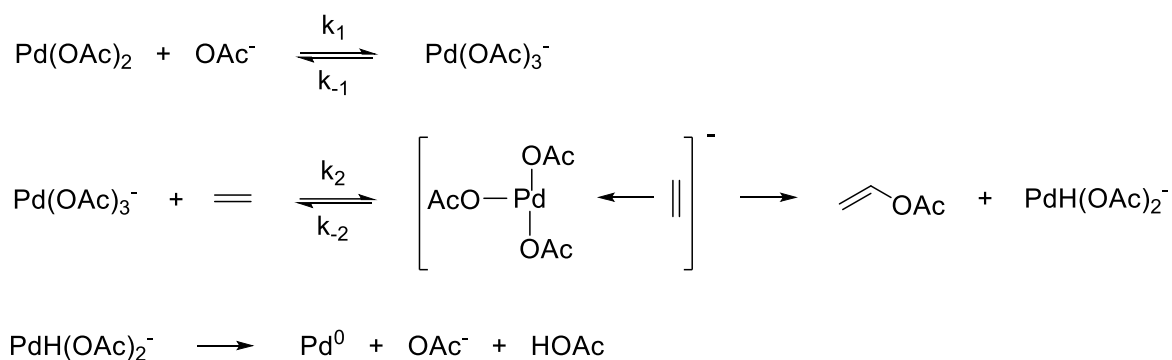


**Figure 1.2.** Reaction mechanism for heterogeneous VA formation by Nakamura et al.<sup>[32]</sup> and Moiseev et al.<sup>[12]</sup>

Stacchiola et al.<sup>[34]</sup> found that acetate is likely bound in  $\eta^2$ <sup>[12]</sup> than in  $\eta^1$ <sup>[135]</sup> mode in the heterogeneous VA reaction pathway.<sup>[34]</sup> However, whether vinyl or ethene reacts with acetate, remained unclear. Ethylidyne is formed on the surface as it becomes depleted of acetate species, and is most likely not involved in the formation of VA. Ethylidyne species thermally decompose to yield hydrogen and carbon at  $\sim 450$  K on clean Pd(111), which will oxidize to form H<sub>2</sub>O and CO<sub>2</sub>, respectively.<sup>[34]</sup>

### 1.5.2. Homogeneous Pathway to VA

Samanos et al.<sup>[31]</sup> proposed a classic homogeneous nucleophilic addition reaction shown in Scheme 1.6 to take place on Pd/SiO<sub>2</sub> or Pd/Al<sub>2</sub>O<sub>3</sub>.<sup>[136]</sup> Under typical industrial operating conditions, the adsorption of acetic acid and water on the support is substantial.<sup>[18, 31]</sup> An adsorbed, condensed acetic acid film with approximately three monolayers in thickness on PdAu/SiO<sub>2</sub> catalysts was evident in isotopic transient kinetics and TPD studies.<sup>[18]</sup> After oxidation of Pd to quadratic planar Pd(OAc)<sub>2</sub>, addition of a third acetate species presumably from the alkali acetate promoter leads to the formation of [Pd(OAc)<sub>3</sub>]<sup>-</sup> (“K<sub>2</sub>Pd<sub>2</sub>(OAc)<sub>6</sub>”<sup>[137]</sup>, “Pd-promoter acetate compound”<sup>[136]</sup>).  $\pi$  adsorbed ethene reacts with an adsorbed acetate nucleophile to form an ethyl acetate-like intermediate. Subsequent  $\beta$ -H elimination is assumed to be rate-determining<sup>[31, 35]</sup> in contrast to reoxidation of Pd<sup>0</sup> in the presence of an oxidant like benzoquinone or Cu<sup>2+</sup>.<sup>[15]</sup> The reoxidation could occur in air, but solubility of O<sub>2</sub> in AcOH is low.<sup>[18]</sup> Except the reductive elimination to Pd<sup>0</sup>, all reaction steps are equilibrium reactions.



**Scheme 1.6.** Liquid phase mechanism proposed by Samanos and van Helden et al.<sup>[31, 35]</sup>

In the Samanos pathway<sup>[31]</sup>, ethene directly couples with  $\eta^2$ -acetate, whereas in the Moiseev pathway<sup>[12]</sup>, ethene chemisorbs as vinyl species on Pd to form vinyl acetate. Figure 1.3 schematically illustrates the Samanos pathway.<sup>[31]</sup>

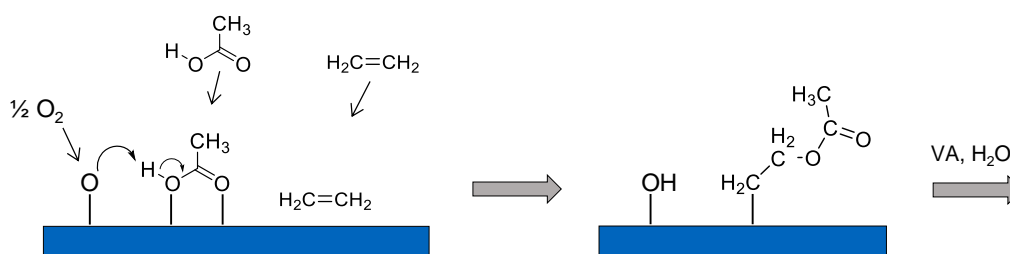


**Figure 1.3.** Homogeneous-like pathway proposed by Samanos et al.<sup>[31]</sup>

Acetate adsorbs with the molecular plane oriented perpendicular to the palladium surface with the oxygen atoms located almost above the palladium sites such that the carbon atom in the carboxylate is positioned directly above a bridge site. The saturation coverage is  $\sim 1/3$  of a monolayer (where coverages are referenced to the palladium atom site density on the surface).<sup>[138]</sup>

According to Kragten et al.<sup>[139]</sup> (Figure 1.4.), electron-donating ethene coordinates in  $\eta^2$  to Pd by substitution of a terminal acetate (1).  $\text{C}_2\text{H}_4$  coordination proceeds via a *ligand path* to end up in a trigonal bipyramidal coordinated Pd(II) typical for square planar substitutions. In contrast, the *solvation path* requires first the generation of a vacancy on Pd by first dissociation of an acetate and addition of an AcOH solvent molecule, which is substituted by ethene. However, vacancy formation on Pd is highly endothermic with 78 kJ/mol and therefore not favorable compared to the slightly exothermic ligand path. At high acetate concentrations, vacancy formation is inhibited in all paths, which is reflected by a negative reaction order in acetate. In the next step (2), acetate and ethene couple either via an *inner-* or an *outer sphere* mechanism. In the inner-sphere mechanism, ethene and acetate both coordinated to Pd couple to form ethyl acetate (back-bonded 6 membered ring) by  $\beta$  H transfer to Pd (3). The outer-sphere mechanism involves coupling of Pd coordinated ethene with acetate from the solution. The H from  $\text{C}_2\text{H}_4$  is transferred to a neighboring acetate on the coordinatively saturated Pd, which prohibits back bonding of ethyl acetate (2). The reaction energy is unfavorable in both mechanisms with the outer sphere attack by acetate is more probable to take place as it is far less endothermic. Theory suggests the  $\beta$ -H transfer (3) as the rate-determining step.<sup>[133, 139]</sup> The activation energy is predicted to

be 67 kJ/mol in good agreement with reported value of 71 kJ/mol.<sup>[140]</sup> Solvent effects are explicitly taken into account in all steps.<sup>[139]</sup> Figure 1.4 illustrates the energy diagram for the inner and outer sphere mechanism.<sup>[139]</sup>

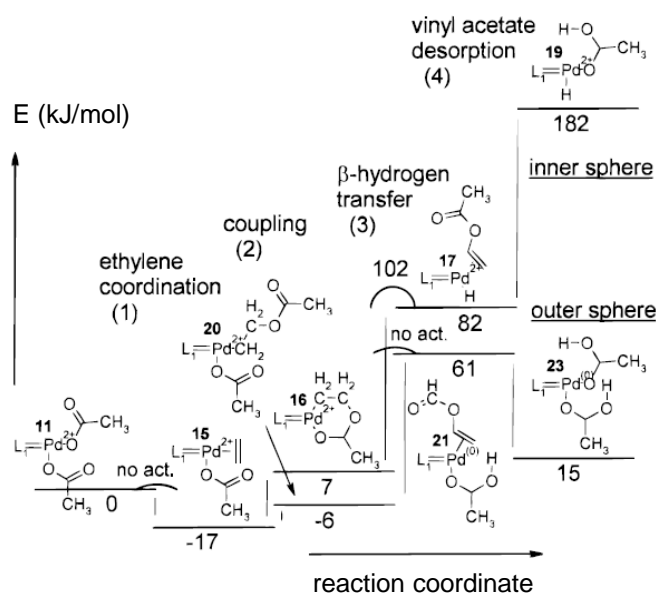


**Figure 1.4.** Energy diagrams of the inner- and the outer sphere mechanisms.<sup>[139]</sup>

In contrast, theoretical first shell analysis studies from Neurock et al.<sup>[141]</sup> concentrate on the inner-sphere mechanism on oxidized Pd<sub>3</sub>O<sub>2</sub> (Pd<sub>3</sub>O<sub>3</sub>). Adsorption steps of AcOH and C<sub>2</sub>H<sub>4</sub>, formation of ethyl acetate and  $\beta$  C-H scission to desorb VA and associated H<sub>2</sub>O were included. Figure 1.5 depicts the DFT predicted energy diagram for the elementary reaction steps.

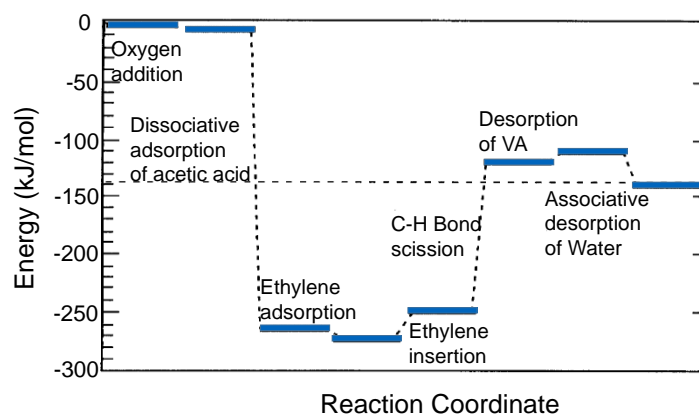


**Figure 1.5.** DFT predicted energies for the steps involved in the inner-sphere mechanism.<sup>[141]</sup>

The overall energy of reaction for VA synthesis is calculated to -142 kJ/mol (experimental -138 kJ/mol). Dissociative AcOH adsorption is highly exothermic (-260 kJ/mol) as acetate is stabilized on oxygen precovered Pd surfaces.<sup>[142]</sup> Ethene binds to Pd preferentially in  $\pi$  configuration (-5 kJ/mol) with increasing oxygen coverage.<sup>[143-144]</sup> Ethene insertion into the local Pd-acetate bond and  $\beta$  C-H scission are highly endothermic (together +131 kJ/mol) whereas VA desorption required only 9 kJ/mol. The Pd-hydride forms a stable Pd-OH group by attacking adsorbed oxygen. O-H is substantially stronger than Pd-H and the  $\beta$  C-H

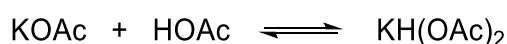
bond scission step is reduced in energy from +131 kJ/mole to -10 kJ/mole making the thermodynamics of this step much more favorable. Analysis of the thermodynamics suggest that ethene insertion may become rate limiting.<sup>[141]</sup>

Stacchiola et al.<sup>[34]</sup> showed that ethene from the gas phase reacts with a model-catalyst surface of  $\eta^2$ -acetate moieties adsorbed on a Pd(111) surface precovered with oxygen to form VA. Later, this group noticed the C=O stretching vibration of the acetoxyethyl-palladium intermediate at 1718  $\text{cm}^{-1}$  in the reaction between the acetate species and  $\text{C}_2\text{D}_4$  with hydrogen involved in the rate-determining step.<sup>[145]</sup> The intermediate provides clear evidence for the occurrence of the Samanos pathway, which is essentially the same as that observed for the stoichiometric oxidation of ethene to VA by soluble Pd acetate.<sup>[146-147]</sup> Also the activation energies calculated for elementary steps carried out on acetate-saturated palladium surfaces reveal that the reaction proceeds via the Samanos mechanism consistent with experimental results on acetate-saturated Pd(111) surfaces. The rate-limiting step involves a  $\beta$ -hydride elimination from the adsorbed acetoxyethyl intermediate (apparent calculated activation barrier of 53 kJ/mol agrees well with the experimental barrier of 55 kJ/mol from kinetic measurements). Higher acetate coverages lower the electron density on the oxygen, making it less nucleophilic, and decrease the occupation of the antibonding C-O  $\sigma^*$  state which lowers the activation energy.<sup>[145]</sup>

### 1.5.3. Supported Liquid Phase (SLP) Mechanism

Supported liquid-phase catalysts combine the desirable features of both homogeneous (on  $\text{Pd}^{2+}$ ) and heterogeneous catalysis (on  $\text{Pd}^0$ ). The catalyst support immobilizes both catalyst species and prevent the association of unsaturated catalytic centers, thus enhancing the catalytic activity.<sup>[136, 148-149]</sup>

As pointed out by Samanos et al. and Crathorne et al.<sup>[18, 31]</sup>, the adsorption of water and acetic acid on the PdAu/SiO<sub>2</sub> under industrial relevant conditions in three molecular layers is substantial. This layer is insufficient to provide a full coordination sphere and thus should not be considered as true liquid. The catalyst components (support, PdAu particles and KOAc promoter) maximize AcOH retention to establish a liquid-film like layer where Pd can be oxidized to Pd acetate. KOAc forms a dimer compound with AcOH ( $\text{KH}(\text{OAc})_2$ ) which melts under reaction conditions.



**Scheme 1.7.** Formation of  $\text{KH}(\text{OAc})_2$ .

Additionally, KOAc can convert Pd acetates to mixed  $\text{KPd}^{2+}$  acetates considered as the active site (Scheme 1.9.) The determination of the solubility of the active complexes in liquid films under reaction conditions is crucial to understand the mechanisms in more detail.<sup>[150]</sup>

### 1.5.4. Comparison of the Reaction Mechanisms

Nakamura et al.,<sup>[151]</sup> Samanos<sup>[31]</sup> and also quantum chemical Monte Carlo simulations from Neurock<sup>[85]</sup> assume that the coupling of a surface ethylenic and acetate species to form VA is the rate-determining step (rds).<sup>[115, 152]</sup>

The reaction proceeds presumably via a Langmuir Hinshelwood mechanism.<sup>[21, 23]</sup> For PdAu catalysts, the reaction orders in C<sub>2</sub>H<sub>4</sub> and O<sub>2</sub> are positive.<sup>[23]</sup> The dissociative adsorption of O<sub>2</sub> is unlikely to be the rds as alloying Pd with Au leads to decreased coverage of C<sub>2</sub>H<sub>4</sub> on PdAu surfaces enhancing the adsorption capacity for oxygen. Additional intensified mobility of adsorbed oxygen under reaction conditions is likely responsible for the high reactivity of PdAu catalysts in VA synthesis.<sup>[23, 132]</sup>

Both reaction mechanisms have three expected main steps, ethene-acetate coupling (C-O formation),  $\beta$ -hydrogen elimination and catalyst reoxidation. For the homogeneous system, the barriers for the three main steps are 74.9, 96.2, and 92.1 kJ/mol, respectively. The rate-determining step involves therefore the  $\beta$ -hydrogen transfer in agreement with previous experimental considerations. For the heterogeneous counterpart the reaction shows a major reaction bottleneck (127.4 kJ/mol) associated to the formation of the C-O bond on the surface.<sup>[133]</sup>

The reoxidation process is far simpler in the heterogeneous situation. The homogeneous reaction takes place at lower temperatures than the heterogeneous (i.e., 50-60 °C to be compared with 130-200 °C). This agrees well with the calculated barriers for the rate-determining step that are significantly higher in the heterogeneous version of the catalyst (i.e., 127 vs 96 kJ/mol for the homogeneous case). In conclusion, homogeneous and heterogeneous processes in the case of VA synthesis are closely linked.<sup>[133]</sup>

### 1.6. Active Sites for VA Synthesis

Catalytic activity is attributed to some form of Pd active site while Au was shown to be negligibly active for VA synthesis.<sup>[11, 23, 115, 153]</sup>

There is a debate in literature on the valence state of active Pd. Moiseev et al.<sup>[12]</sup> argued that Pd<sup>0</sup> is highly selective and active. Nakamura et al.<sup>[32, 151]</sup> suggested a type of Pd<sup>+</sup> acetate in agreement with EPR studies from Smejkal et al.<sup>[154]</sup> who supposed paramagnetic Pd<sup>+</sup> species probably from Pd acetate as key intermediate in the reaction mechanism.<sup>[154]</sup> However, there is consensus about the formation of Pd<sup>2+</sup> acetate on the Pd particles and in the acetic acid layer.<sup>[31, 155-157]</sup> Reilly et al.<sup>[150]</sup> supposed the presence of solid/heterogeneous Pd<sup>0</sup> and Pd<sup>+</sup> / Pd<sup>2+</sup> complexes all three contributing to the reaction within a supported liquid phase mechanism.

Both, the homogeneous and the heterogeneous mechanisms are consistent that the reaction requires a large ensemble of metal atoms and is therefore likely to be structure sensitive including a strong dependence on metal particle size and on the local structure of the ensemble.<sup>[11]</sup> Nevertheless, a mechanism analogous to the homogeneous route makes it difficult to account for the promoting influence of gold. The fact that the majority of the palladium component in these samples was present as a non-alloyed and highly dispersed form might



also be problematic in relation to the promoting influence of gold.<sup>[156]</sup> However, Samanos et al.<sup>[31]</sup> found that very highly dispersed palladium catalysts had very low activity for VA formation. This was attributed to the very small particles being inaccessible to the ethene feed as they are completely embedded within the acetic acid/acetate liquid layer (ethene has very low solubility in acetic acid).<sup>[31]</sup> VA formation may therefore be restricted to the larger PdAu alloy particles accessible to gaseous ethene.<sup>[156]</sup>

Considering VA synthesis on the heterogeneous PdAu particles, addition of a second dissimilar metal like Au to Pd significantly enhances the overall catalytic activity, selectivity<sup>[158]</sup> and stability.<sup>[105]</sup> In principal, the catalytic modifications may be caused by two effects described in section 1.3.1. The ligand effect refers to electronic modifications from charge transfer effects between Pd and Au atoms that can alter the strength of Pd-adsorbate bonds.<sup>[76]</sup> By affecting bond lengths, the ligand effects cause the Pd d band to be more filled, moving the d-band center away from  $E_F$ . Charge transfer between the metals or orbital rehybridization of one or both metallic components make Pd more “atomic like” therefore binding reactants and products more weakly. For certain reactions, this eliminates a so-called “self-poisoning” effect and enhances activity/selectivity.<sup>[97]</sup> However, experiments have not provided conclusive evidence of ligand effects in supported PdAu catalysts.<sup>[92]</sup> Early studies assigned the promoting influence of Au to an electronic interaction, modifying the adsorption strength of various species on the metal surface and enhancing the desorption rate of VA. Single crystal studies showed that the added Au had significant effects on the surface chemistry of Pd.<sup>[156]</sup> Secondly, the ensemble or dilution effect refers to structural modifications in the surface atom geometry to create hetero-nuclear bonds.<sup>[76, 92, 115]</sup> Dilution of surface Pd atoms by inert Au atoms modifies the arrangement of a finite number of atom sites required for facilitating a particular catalytic process (reactant and product adsorption) in structure-sensitive reactions such as VA synthesis.<sup>[76, 78, 97, 120]</sup> The ensemble effect makes the desired chemisorption bonds preferable.<sup>[90]</sup> Consequently, investigations on the surface composition of bimetallic clusters by e.g. CO adsorption is critical in understanding the properties of supported bimetallic catalysts.

Note that one cannot vary the composition of the catalyst surface without affecting both the distribution of the ensembles and changing the electronic structure of the individual constituent atoms in the surface. Hence, a synergy between ensembles and ligand effects in affecting chemisorption exists.<sup>[97]</sup>

Chen et al. could reveal details regarding the PdAu ensembles active for VA formation from single crystal studies at 453 K.<sup>[115, 153]</sup> Pd was vapor deposited onto Au (100) and Au (111) substrates, followed by annealing for 10 min at 550 K. The rate towards VA, expressed as the number of VA molecules produced per Pd active site per second (TOF), is significantly enhanced on PdAu(100) compared with PdAu(111). For the optimum surface of ~ 0.07 ML of PdAu(100), (ML, defined as one Pd atom per substrate Au atom) the density of Pd monomers is highest.<sup>[111]</sup> In contrast, Chen et al. suggested an equimolar mixture of Pd and Au was shown to have a surface Pd coverage of 0.2 ML and to exhibit exclusively monomeric Pd sites as determined by LEISS and IRAS after annealing to 700 K.<sup>[115]</sup> These activity studies and additional CO-IRAS, STM and LEISS studies confirm that the critical reaction site for VA synthesis consists of two noncontiguous, suitably spaced Pd surface monomers.<sup>[30, 104, 159]</sup> Further increasing of Pd coverage leads to decreased TOF numbers. Single

isolated Pd sites are less efficient than a Pd monomer pair.<sup>[153]</sup> Figure 1.6 illustrates plots of VA formation rates of PdAu surfaces as a function of the Pd coverage.

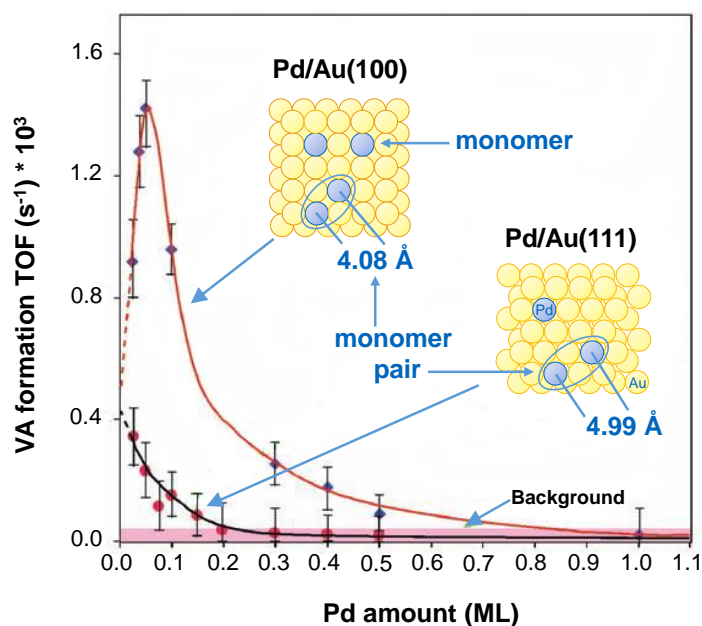


**Figure 1.6.** VA formation as a function of Pd coverage.<sup>[11, 105, 115]</sup>

The optimum Pd-Pd distance to couple vinyl and acetate species is  $\sim 3.3$  Å. Larger Pd ensembles containing contiguous Pd atoms are not required and are less efficient than a pair of Pd monomers separated from one another by 4.08 Å on Pd/Au(100). The rate to VA on Pd/Au(111) is lower than on Pd/Au(100) as the distance of 4.99 Å is far away from the ideal distance of 3.3 Å to efficiently reactive intermediates.

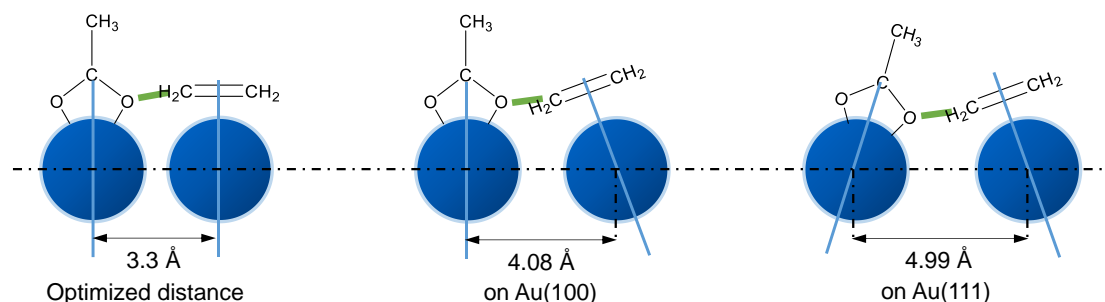


**Figure 1.7.** Scheme for VA synthesis from acetic acid and ethene on two isolated Pd monomers in the optimized distance of 3.3 Å, 4.08 Å on Pd/Au(100) and 4.99 Å on Pd/Au(111).<sup>[11, 105]</sup>

So, the role of Au is to modify active Pd ensembles and to isolate Pd monomer sites that facilitate the coupling of critical surface species to product (rate enhancement). Contiguous Pd sites, though active for VA synthesis, are also active for ethene decomposition and combustion to  $\text{CO}_x$  and  $\text{H}_2\text{O}$ . By forming surface isolated Pd monomers, the path of ethene decomposition is blocked due to absence of Pd bridging and/or tri-hollow sites. Consequently, Au addition prevents undesirable ethene decomposition pathways to ethylidyne, CO,  $\text{CO}_2$  and surface carbon and higher selectivities and activities are achieved.<sup>[11, 30, 89, 97, 105, 116, 153, 160]</sup> Ethene oxidation rates depend linearly on the Au content. At Au > 0.1 wt%, the catalyst operates stable.<sup>[25]</sup> Au inhibits the

decomposition of VA and AcOH and favors its desorption.<sup>[36, 156]</sup> Au suppresses carbide formation in PdAu alloys<sup>[161]</sup> and converts eventual formed CO to CO<sub>2</sub>. Furthermore, adding small amounts of Au to Pd keeps all Pd atoms as Pd<sup>0</sup> while on monometallic Pd catalysts, Pd<sup>2+</sup> has been detected by XPS.<sup>[162]</sup> It is plausible that the electronic and geometric properties of Pd particles can be tuned by formation of a Au<sub>x</sub>Pd<sub>y</sub> alloy surface with highly optimized sites for VA synthesis.<sup>[40, 76, 98]</sup> The theory of two of suitably spaced, isolated Pd monomers as active site was confirmed by application of PdSn alloys with 50% surface concentration of Pd showing a maximum in the VA formation rate.<sup>[163]</sup>

In contrast to the studies of Goodman et al., Neurock<sup>[85]</sup> applied DFT calculations to elucidate active sites for VA synthesis. He suggested that the structure-sensitive VA synthesis over Pd requires rather large ensembles consisting of several Pd atoms.<sup>[85]</sup> The activation of ethene to vinyl requires at least a four-atom Pd ensemble in order to accommodate the vinyl and hydrogen surface product states. The oxygen-assisted activation of ethene requires six atom ensembles. The ensemble size necessary for vinyl and acetate coupling is even larger.<sup>[85]</sup>

Acetic acid and oxygen preferentially dissociate at Pd sites and remain bound to Pd. The addition of Au into the Pd lattice promotes the formation of adsorbed monodentate acetate<sup>[156]</sup> and opens up sites where ethene can preferentially adsorb and stably coexist with both acetate and oxygen.<sup>[116]</sup> Calculated barriers for C–H and C–C activation, which are steps necessary for decomposition, are substantially higher on alloyed surfaces. The gold sites by themselves are inactive for C–H and C–C activation. In addition, they impart both geometric and electronic effects that act to raise the C–H and C–C activation at neighboring sites.<sup>[85]</sup>

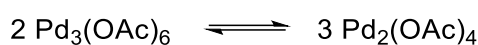
So, is the reaction promoted essentially by two Pd atoms or larger Pd ensembles? The spacing between Pd monomers controls the catalytic activity of PdAu catalysts in the VA formation only if a vinyl surface species is involved in the rate-determining step of the reaction.<sup>[152]</sup> However, the findings of Stacchiola et al.<sup>[34, 145-146]</sup> suggest the coupling of  $\eta^2$  acetate with ethene from the gas phase as rate-determining step. The C–C bond of weakly  $\pi$ -bonded ethene on Pd monomer is only slightly longer than the gas-phase value (1.333 Å).<sup>[152]</sup> Following this conclusion there would be no need of a particular distance between two Pd sites or a special Pd ensemble as not vinyl but ethene couples with acetate. Additionally, computational results from Mazzone et al.<sup>[152]</sup> could not support the speculation that the different spacing of Pd monomers in the critical reaction site could be responsible for the experimentally detected enhancement of the VA formation rate on PdAu(100) compared to PdAu(111).

## 1.7. Influence of the Promoter

### 1.7.1. Homogeneous Reaction System

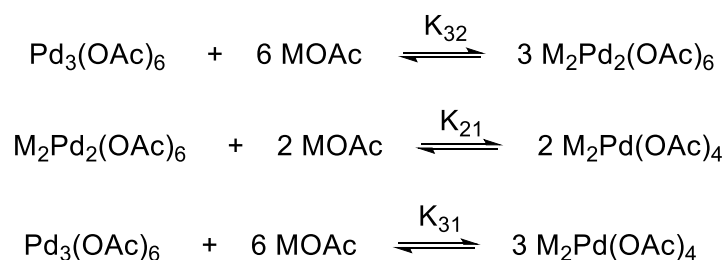
Pd is known to be soluble in glacial acetic acid films on the support under oxidizing conditions in form of palladium acetate.<sup>[16]</sup> Metallic Pd is slowly oxidized by O<sub>2</sub> at 1 atm. in hot (100 °C) acetic acid and retaining quantities in solution is easy.<sup>[164]</sup> Thus, a homogeneous, Wacker-like route to VA via inner- or outer sphere

mechanism is possible at least as a side reaction to the heterogeneous process. Gusevskaya et al.<sup>[165]</sup> has shown that the oxidation of propene in AcOH on supported Pd catalysts proceeds both on the solid catalyst surface and in solution due to Pd leaching. However, the activity of dissolved metal complexes is not more than 30 % of the total activity.<sup>[165]</sup> Solved Pd acetate can exist as trimeric Pd<sub>3</sub>(OAc)<sub>6</sub> (*D*<sub>3h</sub> symmetry, same structure as the crystal<sup>[16, 166-168]</sup>) or as linear dimeric Pd<sub>2</sub>(OAc)<sub>4</sub> but not in monomeric Pd(OAc)<sub>2</sub> form in AcOH. Stoyanov<sup>[169]</sup> showed, that the equilibrium between cyclic trimer (Pd<sub>3</sub>(OAc)<sub>6</sub>) and linear dimer (Pd<sub>2</sub>(OAc)<sub>4</sub>) depends on the solvent applied. In AcOH, the equilibrium is shifted towards the trimeric form because of the variation of the composition of the outer-spheric solvation shells.<sup>[169]</sup> With addition of chloroform to AcOH, dimeric Pd acetate forms successively with 10 to 22% dimeric Pd acetate in 50 vol% CHCl<sub>3</sub>.<sup>[169]</sup> Trimeric Pd<sub>3</sub>(OAc)<sub>6</sub> is formed in benzene as well.<sup>[170-171]</sup> Thus, trimeric Pd<sub>3</sub>(OAc)<sub>6</sub> is one of the most stable forms of palladium(II) acetate in solution with a solubility as function of the temperature.<sup>[16, 169]</sup>



**Scheme 1.8.** Equilibrium between trimeric Pd<sub>3</sub>(OAc)<sub>6</sub> and linear dimeric Pd<sub>2</sub>(OAc)<sub>4</sub>.

In the presence of alkali metal acetates MOAc, Pd acetate can exist in three different species, related by equilibria that can be controlled through the addition of MOAc.<sup>[171-172]</sup>



**Scheme 1.9.** Equilibrium between trimeric Pd<sub>3</sub>(OAc)<sub>6</sub>, dimeric M<sub>2</sub>Pd<sub>2</sub>(OAc)<sub>6</sub> and monomeric M<sub>2</sub>Pd(OAc)<sub>4</sub> with M<sup>+</sup> = alkali ion.

Pandey et al.<sup>[171]</sup> calculated K<sub>32</sub> for NaOAc to be 7.77 10<sup>4</sup> M<sup>-5</sup> and for LiOAc to be 1.76 10<sup>2</sup> M<sup>-5</sup>. The transformation from Pd trimers to dimers proceeds by a SN<sub>2</sub> attack of acetate ions or by acetic acid molecules to break the acetate bridges in Pd<sub>3</sub>(OAc)<sub>6</sub>. It is a slow reaction as the non-labile bridging acetates in Pd<sub>3</sub>(OAc)<sub>6</sub> have to be broken. The labile terminal acetates in dimeric and monomeric Pd acetate species are expected to react more rapidly with e.g. olefins.<sup>[16, 171-172]</sup> At 0.5 M LiOAc, 0.2 M NaOAc<sup>[171]</sup> and between 0.1-0.2 M KOAc,<sup>[16]</sup> trimers decomposed completely into dimers. Dimers are converted into monomers above 0.4 M NaOAc but this equilibrium is on the side of the dimer as K<sub>21</sub> for NaOAc is 7.6 10<sup>4</sup> M<sup>-1</sup>. K<sub>21</sub> for LiOAc was too small to determine. At a total Pd concentration of 0.0128 M and at 1.0 M NaOAc the dimer is only about 16% converted to monomers. However, at 1.225 10<sup>-4</sup> M Pd<sub>3</sub>(OAc)<sub>6</sub>, the conversion of dimers at 1.0 M NaOAc is 79%. K<sub>31</sub> was found to be 1.14 10<sup>3</sup> M<sup>-4</sup> (NaOAc) and 2.38 M<sup>-4</sup> (LiOAc).<sup>[171]</sup> The concentration needed to completely convert all Pd acetate trimers to dimers is proportional to the solvation energy of the alkali metal cation. The greater this energy, the more the equilibrium is shifted in the direction of decomposed active Pd

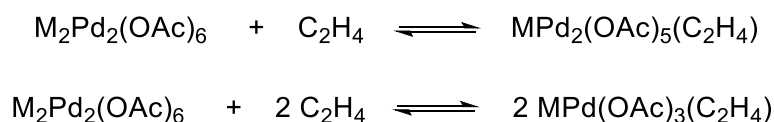
acetate.<sup>[16]</sup> The solvation energy of  $M^+$  depends on the number of AcOH directly bound to  $M^+$  (first coordination sphere) and the number of total molecules.<sup>[173]</sup>

**Table 1.1.** Properties of alkali ions.<sup>[173]</sup>  $Z$  is the charge of the ion and  $r$  is the radius.<sup>[174]</sup>

	<b>Li<sup>+</sup></b>	<b>Na<sup>+</sup></b>	<b>K<sup>+</sup></b>	<b>Cs<sup>+</sup></b>
<b>Ionic radii [Å]</b>	0.90	1.16	1.52	1.81
<b>Hydrated radii [Å]</b>	3.40	2.76	2.32	2.28
<b>Hydration numbers</b>	25.3	16.6	10.5	9.9
<b>Hydration enthalpies [-kJ/mol]</b>	519	406	322	264
<b><math>Z^2/r</math> [Å<sup>-1</sup>]<sup>[174]</sup></b>	1.1	0.86	0.66	0.55

Although Table 1.1 indicates numbers on the hydration of alkali ions in water, the behavior can be transferred to the acetic acid liquid. The smallest cation  $Li^+$  exerts most influence on water with 25 water molecules in the hydration sphere. Consequently, solvated  $Li^+$  will not exchange with other anions.<sup>[173]</sup> Thus,  $LiOAc/AcOH$  hardly reacts with  $Pd_3(OAc)_6$  to form  $Li_2Pd_2(OAc)_6$  in accordance with the low  $K_{32}$  for  $LiOAc$ . In contrast,  $KOAc$  and  $CsOAc$  most efficiently decomposes  $Pd_3(OAc)_6$ .<sup>[16]</sup>

Dimeric  $M_2Pd_2(OAc)_2$  reacts with ethene to form an active but labile  $\pi$  complex  $MPd_2(OAc)_5(C_2H_4)$  (fast) or an inactive, non-labile  $\pi$  complex  $MPd(OAc)_3(C_2H_4)$  (slow). Lower  $C_2H_4$  concentration favor  $MPd_2(OAc)_5(C_2H_4)$ <sup>[172]</sup> which increased the rate to VA.<sup>[175]</sup>



**Scheme 1.10.** Equilibrium reaction between dimeric  $M_2Pd_2(OAc)_6$  and ethene.

By changing the concentration of  $MOAc$ , the activity and selectivity towards VA is affected. Increasing the amount of  $MOAc$  is accompanied by reaching a maximum rate of VA at 0.2 M  $NaOAc$ .<sup>[175]</sup> The solution then contains mainly catalytically active dimers. A decrease in activity by excess acetate is probably due to the blocking of vacancies by acetate<sup>[139]</sup> or due to the formation of inactive monomers  $Na_2Pd(OAc)_4$ .<sup>[175]</sup> In agreement, Rony predicted the existence of an optimum loading of the catalyst solution related to the overall activity in supported liquid phase catalysts.<sup>[176]</sup>

The use of excess  $LiCl$  was found to completely inhibit the formation of VA as acetate groups are entirely displaced by chloride ions<sup>[25]</sup> and ethene dimerized to butylenes.<sup>[35]</sup> The chloride-free systems are expected to offer enhanced reactivity as  $E^0$  is 0.91 v. for  $Pd^{2+}_{aq}/Pd^0$  and 0.59 v. for  $PdCl_4^{2-}/Pd^0 + 4Cl^-$ .<sup>[164]</sup> Thus, the overall rate of homogeneous VA synthesis depends strongly on the promoter counter ion and indicates that nucleophilic attack of the bonded olefin by  $OAc^-$  proceeds via a coordinated acetate ligand within an inner sphere mechanism.<sup>[35]</sup>

In the liquid phase system, palladium acetate reacted with ethene to yield VA at 70 °C. The reaction is first order in palladium and the promoter acetate. Thus, the reaction rate dramatically increased by the addition of small alkali acetate amounts. The mechanism proceeds via square planar  $C_2H_4 \cdot PdOAcX_2^-$  whereas the rate is strongly influenced by X in the order  $Cl_2 < (OAc)_2 < OAcCl \cdot Fe(OAc)_3$ . The higher rate with ferric acetate than with LiCl may be attributed to the increased charge transfer to Pd in the intermediate which accelerates the attack of coordinated acetate.<sup>[35]</sup> However, solutions of several  $Pd^{2+}$  salts on charcoal are non-selective for VA synthesis as acetaldehyde is formed. The reduction of  $Pd^{2+}$  salt result in precipitation of Pd metal.<sup>[136]</sup> However,  $Pd^0$  is expected to be converted to Pd acetate during the reaction as platinum group metals are oxidized by hydrogen acids in the presence of oxygen.<sup>[177]</sup> In the presence of alkali metal acetate salts Pd is readily converted to palladium acetate.<sup>[32]</sup> Furthermore,  $PdCl_2$  solves in AcOH as soon as LiOAc was present in AcOH.<sup>[178]</sup>

On non-promoted Pd acetate catalysts, large amounts of acetaldehyde in addition to VA were formed.<sup>[179]</sup> Likely, a lithium-palladium acetate complex is involved in the selective oxidation<sup>[136]</sup> like the observed  $Na_2Pd_2(OAc)_6$  complex by Winstein et al.<sup>[175]</sup> Elimination of  $\beta$  H from the ethyl palladium complex results in  $Pd^0$ . However, Pd acetate is not significantly reduced to  $Pd^0$  by ethene in the presence of lithium acetate<sup>[180]</sup> and Pd is readily oxidized to Pd acetate in AcOH/O<sub>2</sub>. Coordination of ethene to Pd sensitized the attack of the acetate ion on the olefin.<sup>[136]</sup>

Conclusively, alkali acetates promote VA formation by stabilizing reaction intermediates and activating Pd as the assumed reactive site for VA synthesis.

### 1.7.2. Heterogeneous Reaction System

On catalyst surfaces, electropositive promoters such as alkalis are present in ionic state.<sup>[181-182]</sup> The promoting effect of alkali metals is interpreted in terms of electronic effects. In order to understand these effects, the theoretical understanding of the energy states of alkali atoms adsorbed on Rh(111) at low coverages is explained.<sup>[183-186]</sup> Adsorption of alkali atoms on a metal surface leads to hybridization of the s and p energy levels of the alkali atom with the n metal electronic states. The band positions relative to the Fermi level  $E_F$  are determined by the competition between the atom's desire to fill its valence shell and the electron affinity of the metal. Figure 1.8 illustrates the hybridized 3s and 3p bands of Na chemisorbed on a metal.<sup>[183-186]</sup>

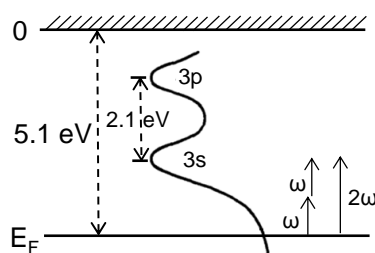


**Figure 1.8.** Schematic energy diagram for the hybridized 3s and 3p bands of a Na atom chemisorbed on a metal d surface with respect to  $E_F$ .<sup>[183]</sup>

The 3s band lies above  $E_F$  and is therefore mostly unoccupied. As a result, the adatom appears ionic with electrons partially transferred from the adatom toward the metal, creating a surface dipole. The wave functions of the hybridized ns states below  $E_F$  have greater amplitudes in the atom-metal bond region than those above  $E_F$ . The ns band is about 2 eV above  $E_F$ , the widths of the ns and np bands are of the order of 2 eV and the spacing between the ns and np bands is not very different from that in the atomic case. The ns-np transition energies are 2.1, 1.6, and 1.4 eV for Na, K, and Cs, respectively. In the case of a bare  $Rh^{3+}$  surface,  $E_F$  is 5.1 eV below the vacuum level.<sup>[187]</sup> As the alkali coverage increases, interaction between the adsorbed alkali atoms becomes important. Each alkali atom experiences a potential created by the surface dipoles on the neighboring alkali atoms.<sup>[188]</sup> This potential shifts the energy bands of the alkali together with the vacuum level downward with respect to  $E_F$ , and partially immerses the ns band in the Fermi sea. The alkali atoms now appear more neutral and a further increase of the alkali coverage induces little additional level shift.<sup>[188]</sup>

The electron transfer from the adatom toward the metal increases the heat of adsorption of CO and weakens the C-O bond. In some cases the dissociation of CO is promoted. The weakening of the C-O bond is manifested in the downward frequency shift of the C-O stretching frequencies in RAIRS.<sup>[189]</sup>

Lithium decreased the initial heat of hydrogen adsorption and Na and K increased the initial heat of CO adsorption by 10 kJ/mol to 165 kJ/mol.<sup>[190]</sup> According to XPS studies of Praliaud et al.<sup>[182]</sup> it is difficult to distinguish between chemical shifts caused by either, i. e., a change in the electronic state of palladium (via an electron-donating alkali metal-oxygen composite) or a modification of the palladium surroundings.<sup>[182]</sup> These electronic effects appear to be due to both long and short range forces operating between CO and potassium. Short range interactions may cause the tilting of CO molecules, side on bonding of CO or the formation of K-CO complexes. Rehybridization of CO orbitals from sp to  $sp^2$  has been considered, as bonding involves the  $\pi$  CO molecular orbital.<sup>[189]</sup>

In agreement, Ertl et al.<sup>[191]</sup> found that preadsorbed potassium on iron increased the adsorption energy of hydrogen by 2 kcal/mol and lowered the sticking coefficient for hydrogen adsorption by a factor of 2. K adsorption causes an increase in the CO dissociation rate, an increase in the CO heat of desorption from 27 to 39 kcal/mol with increasing K coverage and a decrease in the  $CH_4$  formation rate.<sup>[191]</sup> The additional electron density alters the chemisorptive bonding of adsorbed species promoting the rate by ligand effects.<sup>[192]</sup> Strongin et al.<sup>[193]</sup> found that adsorbed potassium reduced the adsorption enthalpy of ammonia on iron during ammonia synthesis. The decrease in blocked surface sites increased the rate to ammonia.<sup>[193]</sup>

The described electronic changes upon alkali adsorption are expected to be present on PdAu/KOAc/SiO<sub>2</sub>. However, under VA synthesis conditions, the existence of a liquid-film like AcOH adlayer on the catalyst surface in the presence of O<sub>2</sub> opens additional possibilities for KOAc to interact with solid PdAu particles.

MOAc itself immobilizes AcOH within the liquid surface layer<sup>[18, 36, 156-157, 194]</sup>, dissolves in the water/acetic acid layer and/or forms a dimer species with AcOH (Scheme 1.8.).<sup>[150]</sup>  $KH(OAc)_2$  melts at 148 °C during reaction conditions and forms a protective molten salt coating on the catalyst surface<sup>[195]</sup> that suppresses direct ethene combustion and increases the selectivity in this way (Supported liquid-phase catalysis).<sup>[150]</sup> Since all catalyst components (support, PdAu particles, MOAc promoters) maximize the AcOH surface concentration, the existence of the liquid-film like AcOH layer is supposed to be detrimental for the reaction.<sup>[11]</sup>

Provine et al.<sup>[36]</sup> found that KOAc facilitates VA desorption and enhanced the rate for VA. However, KOAc increased AcOH combustion to CO<sub>2</sub> and CO but suppressed ethene combustion.<sup>[36]</sup> KOAc is involved in the solvation of Pd to form complexes, which presumably form the active centers of the catalyst by establishing an equilibrium between Pd acetate solvated in KOAc/AcOH and PdK complexes (see section 1.7.1.).<sup>[150]</sup>

Augustine et al.<sup>[135]</sup> employed in situ DRIFTS-MS and kinetic studies to determine the role of acetic acid on gas phase VA synthesis on heterogeneous Pd/ $\alpha$ -Al<sub>2</sub>O<sub>3</sub> catalysts. For solutions containing KOAc and Pd acetate a band at 1730 cm<sup>-1</sup> was observed which is assigned to the carboxylate stretch vibration of a terminal acetate species bound to a palladium dimer in a monodentate ester-like configuration. This species is considered to be a key intermediate in heterogeneous VA synthesis as observed on a working Pd catalyst.<sup>[135, 156]</sup>



## 1.8. References

- [1] <http://www.atsdr.cdc.gov/ToxProfiles/tp59-c4.pdf>.
- [2] <http://www.dow.com/productsafety/finder/vinyl.htm>.
- [3] <http://www.vinylacetate.org/what.shtml>.
- [4] <http://www.sriconsulting.com/WP/Public/Reports/vam/>.
- [5] P. S. Voskanyan, *Catal. Ind.* **2013**, *5*, 90-97.
- [6] S. A. Miller, *Ethylene and its industrial derivatives* Benn, London, **1969**.
- [7] B. Elvers, S. Hawkins, *Ullman's Encyclopedia of Industrial Chemistry Vol. A27*, VCH Verlagsgesellschaft GmbH, Weinheim, **1996**.
- [8] K. B. S. Prasad, K. B. S. Saibabu, R. Vaidyeswaran, *J. Catal.* **1981**, *72*, 338-346.
- [9] B. A. Morrow, *J. Catal.* **1984**, *86*, 328-332.
- [10] D. D. Kragten, *PhD Thesis*, Technische Universiteit Eindhoven, **1999**.
- [11] D. Kumar, M. S. Chen, D. W. Goodman, *Catal. Today* **2007**, *123*, 77-85.
- [12] I. I. Moiseev, M. N. Vargaftic, Y. L. Syrkin, *Dokl. Akad. Nauk. USSR* **1960**, *133*, 377.
- [13] J. Smidt, W. Hafner, R. Jira, R. Sieber, J. Sedlmeier, A. Sabel, *Angew. Chem.* **1962**, *74*, 93-102.
- [14] J. Smidt, W. Hafner, R. Jira, J. Sedlmeier, R. Sieber, R. Rüttinger, H. Kojer, *Angew. Chem.* **1959**, *71*, 176-182.
- [15] G. S. Grover, R. V. Chaudhari, *Chem. Eng. J.* **1986**, *32*, 93-99.
- [16] D. D. Kragten, R. A. van Santen, M. K. Crawford, W. D. Provine, J. J. Lerou, *Inorg. Chem.* **1999**, *38*, 331-339.
- [17] J. E. Baekvall, B. Akermark, S. O. Ljunggren, *J. Am. Chem. Soc.* **1979**, *101*, 2411-2416.
- [18] E. A. Crathorne, D. Macgowan, S. R. Morris, A. P. Rawlinson, *J. Catal.* **1994**, *149*, 254-267.
- [19] T. C. Bissot, *U.S. 4,048,096* **1977**.
- [20] [http://www.chemie.tu-darmstadt.de/claus/akclaus/forschung\\_2/methoden/vinylacetatvam/vam.de.jsp](http://www.chemie.tu-darmstadt.de/claus/akclaus/forschung_2/methoden/vinylacetatvam/vam.de.jsp).
- [21] D. Kumar, Y. Han, M. Chen, D. Goodman, *Catal. Lett.* **2006**, *106*, 1-5.
- [22] <http://www.nacatsoc.org/20nam/abstracts/P-S9-21B.pdf>.
- [23] Y. F. Han, J. H. Wang, D. Kumar, Z. Yan, D. W. Goodman, *J. Catal.* **2005**, *232*, 467-475.
- [24] Sennewald, *U.S. 3,631,079* **1971**.
- [25] P. S. Voskanyan, *Catal. Ind.* **2010**, *2*, 167-172.
- [26] H.-J. Eberle, R. Heidenreich, J. Weis, *Ger. DE 10 2006 058 800 A1* 2008.06.19, **2008**.
- [27] S. A. Schunk, C. Baltes, A. Sundermann, *Catal. Today* **2006**, *117*, 304-310.
- [28] T. Komatsu, K. Inaba, T. Uezono, A. Onda, T. Yashima, *Appl. Catal. A* **2003**, *251*, 315-326.
- [29] F. Calaza, D. Stacchiola, M. Neurock, W. T. Tysoe, *Surf. Sci.* **2005**, *598*, 263-275.
- [30] M. Chen, D. W. Goodman, *Chinese J. Catal.* **2008**, *29*, 1178-1186.
- [31] B. Samanos, P. Boutry, R. Montarnal, *J. Catal.* **1971**, *23*, 19-30.
- [32] S. Nakamura, T. Yasui, *J. Catal.* **1970**, *17*, 366-374.

- [33] Y. F. Han, D. Kumar, C. Sivadinarayana, D. W. Goodman, *J. Catal.* **2004**, *224*, 60-68.
- [34] D. Stacchiola, F. Calaza, L. Burkholder, W. T. Tysoe, *J. Am. Chem. Soc.* **2004**, *126*, 15384-15385.
- [35] R. van Helden, C. F. Kohll, D. Medema, G. Verberg, T. Jonkhoff, *Recl. Trav. Chim. Pays-Bas* **1968**, *87*, 961-991.
- [36] W. D. Provine, P. L. Mills, J. J. Lerou, *Stud. Surf. Sci. Catal.* **1996**, *101*, 191-200.
- [37] P. Landon, P. J. Collier, A. J. Papworth, C. J. Kiely, G. J. Hutchings, *Chem. Commun.* **2002**, 2058-2059.
- [38] J. K. Edwards, B. E. Solsona, P. Landon, A. F. Carley, A. Herzing, C. J. Kiely, G. J. Hutchings, *J. Catal.* **2005**, *236*, 69-79.
- [39] T. T. David, *Plat. Metals Rev.* **2004**, *48*, 169-172.
- [40] A. M. Venezia, L. F. Liotta, G. Pantaleo, V. La Parola, G. Deganello, A. Beck, Z. Koppány, K. Frey, D. Horváth, L. Guzzi, *Appl. Catal. A* **2003**, *251*, 359-368.
- [41] T. V. Choudhary, D. W. Goodman, *Appl. Catal. A* **2005**, *291*, 32.
- [42] M. Hosseini, S. Siffert, H. L. Tidahy, R. Cousin, J. F. Lamonier, A. Aboukais, A. Vantomme, M. Roussel, B. L. Su, *Catal. Today* **2007**, *122*, 391-396.
- [43] A. M. Venezia, V. L. Parola, B. Pawelec, J. L. G. Fierro, *Appl. Catal. A* **2004**, *264*, 43-51.
- [44] S. Marx, A. Baiker, *J. Phys. Chem. C* **2009**, *113*, 6191-6201.
- [45] D. I. Enache, J. K. Edwards, P. Landon, B. Solsona-Espriu, A. F. Carley, A. A. Herzing, M. Watanabe, C. J. Kiely, D. W. Knight, G. J. Hutchings, *Science* **2006**, *311*, 362-365.
- [46] L. Prati, A. Villa, F. Porta, D. Wang, D. Su, *Catal. Today* **2007**, *122*, 386-390.
- [47] W. Hou, N. A. Dehm, R. W. J. Scott, *J. Catal.* **2008**, *253*, 22-27.
- [48] A. Maclennan, A. Banerjee, Y. Hu, J. T. Miller, R. W. J. Scott, *ACS Catal.* **2013**.
- [49] R. W. J. Scott, O. M. Wilson, S.-K. Oh, E. A. Kenik, R. M. Crooks, *J. Am. Chem. Soc.* **2004**, *126*, 15583-15591.
- [50] P. Dash, N. A. Dehm, R. W. J. Scott, *J. Mol. Catal. A* **2008**, *286*, 114-119.
- [51] K. N. Heck, B. G. Janesko, G. E. Scuseria, N. J. Halas, M. S. Wong, *J. Am. Chem. Soc.* **2008**, *130*, 16592-16600.
- [52] A. M. Venezia, V. La Parola, B. Pawelec, J. L. G. Fierro, *Proc. Int. Conf. Science, Technol. Ind.* **2003**.
- [53] L. Y. Chen, N. Chen, Y. Hou, Z. C. Wang, S. H. Lv, T. Fujita, J. H. Jiang, A. Hirata, M. W. Chen, *ACS Catal.* **2013**, *3*, 1220-1230.
- [54] R. Pellegrini, G. Leofanti, G. Agostini, L. Bertinetti, S. Bertarione, E. Groppo, A. Zecchina, C. Lamberti, *J. Catal.* **2009**, *267*, 40-49.
- [55] H. P. Myers, L. Wallden, B. Karlsson, *Philosoph. Magazine* **1968**, *18*, 725-744.
- [56] Y. L. Lam, M. Boudart, *J. Catal.* **1977**, *50*, 530.
- [57] A. Nagasawa, Y. Matsuo, J. Kakinoki, *J. Phys. Soc. Jpn.* **1965**, *20*, 1881.
- [58] Y. Matsuo, A. Nagasawa, J. Kakinoki, *J. Phys. Soc. Jpn.* **1966**, *21*, 2633.
- [59] [http://ruby.chemie.uni-freiburg.de/Vorlesung/intermetallische\\_3\\_2.html](http://ruby.chemie.uni-freiburg.de/Vorlesung/intermetallische_3_2.html).
- [60] R. Elliott, F. Shunk, *J. Phase Equilib.* **1982**, *2*, 482-484.

- [61] H. Okamoto, T. Massalski, *J. Phase Equilib.* **1985**, *6*, 229-235.
- [62] M. H. F. Sluiter, C. Colinet, A. Pasturel, *Phys. Rev. B* **2006**, *73*, 174204.
- [63] U. Devi, C. N. Rao, K. K. Rao, *Acta Metall.* **1965**, *13*, 44-45.
- [64] E. G. Allison, G. C. Bond, *Catal. Rev.* **1972**, *7*, 233 - 289.
- [65] R. Oriani, W. K. Murphy, *Acta Metall.* **1962**, *10*, 879-885.
- [66] M. Aschoff, S. Speller, J. Kuntze, W. Heiland, E. Platzgummer, M. Schmid, P. Varga, B. Baretzky, *Surf. Sci.* **1998**, *415*, L1051-L1054.
- [67] G. Mazzone, I. Rivalta, N. Russo, E. Sicilia, *J. Phys. Chem. C* **2008**, *112*, 6073-6081.
- [68] A. Maeland, T. B. Flanagan, *Canad. J. Phys.* **1964**, *42*, 2364-2366.
- [69] N. F. Mott, *Proc. Phys. Soc.* **1935**, *47*, 571-588.
- [70] N. Mott, H. T. Jones, **1936**.
- [71] D. D. Eley, P. Luetic, *Trans. Faraday Soc.* **1957**, *53*, 1483-1487.
- [72] M. J. Kim, W. F. Flanagan, *Acta Metall.* **1967**, *15*, 747-752.
- [73] A. Couper, D. D. Eley, *Discuss. Faraday Soc.* **1950**, *8*, 172-184.
- [74] G. Meitzner, J. H. Sinfelt, *Catal. Lett.* **1995**, *30*, 1-10.
- [75] N. D. Lang, H. Ehrenreich, *Phys. Rev.* **1968**, *168*, 605-622.
- [76] S. N. Reifsnnyder, H. H. Lamb, *J. Phys. Chem. B* **1998**, *103*, 321-329.
- [77] P. A. P. Nascente, S. G. C. de Castro, R. Landers, G. G. Kleiman, *Phys. Rev. B* **1991**, *43*, 4659-4666.
- [78] C. J. Baddeley, R. M. Ormerod, A. W. Stephenson, R. M. Lambert, *J. Phys. Chem.* **1995**, *99*, 5146-5151.
- [79] B. E. Koel, A. Sellidj, M. T. Paffett, *Phys. Rev. B* **1992**, *46*, 7846-7856.
- [80] T.-U. Nahm, R. Jung, J.-Y. Kim, W. G. Park, S. J. Oh, J. H. Park, J. W. Allen, S. M. Chung, Y. S. Lee, C. N. Whang, *Phys. Rev. B* **1998**, *58*, 9817-9825.
- [81] Y.-S. Lee, Y. Jeon, Y.-M. Chung, K.-Y. Lim, C.-N. Whang, S.-J. Oh, *J. Korean Phys. Soc.* **2000**, *37*, 451-455.
- [82] H. Falsig, B. Hvolbæk, I. S. Kristensen, T. Jiang, T. Bligaard, C. H. Christensen, J. K. Nørskov, *Angew. Chem. Int. Ed.* **2008**, *47*, 4835-4839.
- [83] D. W. Goodman, *Surf. Sci.* **1994**, *299-300*, 837-848.
- [84] J. A. Rodriguez, D. W. Goodman, *Science* **1992**, *257*, 897-903.
- [85] M. Neurock, *J. Catal.* **2003**, *216*, 73-88.
- [86] A. D. O. Cinneide, J. K. A. Clarke, *Catal. Rev.* **1972**, *7*, 213.
- [87] S. M. Foiles, *J. Vac. Sci. Technol. A* **1987**, *5*, 889-891.
- [88] P. Liu, J. K. Nørskov, *Phys. Chem. Chem. Phys.* **2001**, *3*, 3814-3818.
- [89] C. W. Yi, K. Luo, T. Wei, D. W. Goodman, *J. Phys. Chem. B* **2005**, *109*, 18535-18540.
- [90] T. Wei, J. Wang, D. W. Goodman, *J. Phys. Chem. C* **2007**, *111*, 8781-8788.
- [91] F. Maroun, F. Ozanam, O. M. Magnussen, R. J. Behm, *Science* **2001**, *293*, 1811-1814.
- [92] D. Rainer, *J. Vac. Sci. Technol. A* **1997**, *15*, 1653-1662.
- [93] A. Sárkány, O. Geszti, G. Sáfrán, *Appl. Catal. A* **2008**, *350*, 157-163.

- [94] J. Rodriguez, *Surf. Sci. Rep.* **1996**, *24*, 223-287.
- [95] M. Zhang, Q. Hao, Y. Yu, *Comput. Theoret. Chem.* **2013**, *1019*, 33-38.
- [96] A. F. Lee, C. J. Baddeley, C. Hardacre, R. M. Ormerod, R. M. Lambert, G. Schmid, H. West, *J. Phys. Chem.* **1995**, *99*, 6096-6102.
- [97] F. Gao, D. W. Goodman, *Chem. Soc. Rev.* **2012**, *41*, 8009-8020.
- [98] A. Jablonski, S. H. Overbury, G. A. Somorjai, *Surf. Sci.* **1977**, *65*, 578.
- [99] A. Sellidj, B. E. Koel, *Phys. Rev. B* **1994**, *49*, 8367-8376.
- [100] D. G. Swartzfager, S. B. Ziemecki, M. J. Kelley, *J. Vac. Sci. Technol.* **1981**, *19*, 185-191.
- [101] A. Christensen, A. V. Ruban, P. Stoltze, K. W. Jacobsen, H. L. Skriver, J. K. Nørskov, F. Besenbacher, *Phys. Rev. B* **1997**, *56*, 5822-5834.
- [102] P. Varga, G. Hetzendorf, *Surf. Sci.* **1985**, *162*, 544-549.
- [103] G. Maire, L. Hilaire, P. Legare, F. G. Gault, A. O'Conneide, *J. Catal.* **1976**, *44*, 293-299.
- [104] K. Luo, T. Wei, C. W. Yi, S. Axnanda, D. W. Goodman, *J. Phys. Chem. B* **2005**, *109*, 23517-23522.
- [105] M. S. Chen, K. Luo, T. Wei, Z. Yan, D. Kumar, C. W. Yi, D. W. Goodman, *Catal. Today* **2006**, *117*, 37-45.
- [106] S. J. Mejía-Rosales, C. Fernández-Navarro, E. Pérez-Tijerina, J. M. Montejano-Carrizales, M. José-Yacamán, *J. Phys. Chem. B* **2006**, *110*, 12884-12889.
- [107] L. Z. Mezey, J. Giber, *Jpn. J. Appl. Phys.* **1982**, *21*, 1569-1571.
- [108] R. Anton, H. Eggers, J. Veletas, *Thin Solid Films* **1993**, *226*, 39-47.
- [109] A. E. Baber, H. L. Tierney, E. C. H. Sykes, *ACS Nano* **2010**, *4*, 1637-1645.
- [110] A. R. Haire, J. Gustafson, A. G. Trant, T. E. Jones, T. C. Q. Noakes, P. Bailey, C. J. Baddeley, *Surf. Sci.* **2011**, *605*, 214-219.
- [111] D. Tománek, S. Mukherjee, V. Kumar, K. H. Bennemann, *Surf. Sci.* **1982**, *114*, 11-22.
- [112] M. R. Knecht, M. G. Weir, A. I. Frenkel, R. M. Crooks, *Chem. Mater.* **2007**, *20*, 1019-1028.
- [113] H. Guesmi, C. Louis, L. Delannoy, *Chem. Phys. Lett.* **2011**, *503*, 97-100.
- [114] H. Lang, S. Maldonado, K. J. Stevenson, B. D. Chandler, *J. Am. Chem. Soc.* **2004**, *126*, 12949-12956.
- [115] M. Chen, D. Kumar, C.-W. Yi, D. W. Goodman, *Science* **2005**, *310*, 291-293.
- [116] T. G. Owens, T. E. Jones, T. C. Q. Noakes, P. Bailey, C. J. Baddeley, *J. Phys. Chem. B* **2006**, *110*, 21152-21160.
- [117] G. Blyholder, *J. Phys. Chem.* **1964**, *68*, 2772-2777.
- [118] F. Stoop, F. J. C. M. Toolenaar, V. Ponc, *J. Catal.* **1982**, *73*, 50-56.
- [119] W. K. Kuhn, J. Szanyi, D. W. Goodman, *Surf. Sci.* **1992**, *274*, L611-L618.
- [120] E. L. Kugler, M. Boudart, *J. Catal.* **1979**, *59*, 201-210.
- [121] A. N. Pestryakov, V. V. Lunin, S. Fuentes, N. Bogdanchikova, A. Barrera, *Chem. Phys. Lett.* **2003**, *367*, 102-108.
- [122] S. J. Mejía-Rosales, C. Fernández-Navarro, E. Pérez-Tijerina, D. A. Blom, L. F. Allard, M. José-Yacamán, *J. Phys. Chem. C* **2006**, *111*, 1256-1260.
- [123] P. Chou, M. A. Vannice, *J. Catal.* **1987**, *104*, 17-30.

- [124] X. Guo, J. J. T. Yates, *J. Chem. Phys.* **1989**, *90*, 6761-6766.
- [125] J. Szanyi, W. K. Kuhn, D. W. Goodman, *J. Vac. Sci. Technol.* **1993**, *11*, 1969-1974.
- [126] D. R. Rainer, M. C. Wu, D. I. Mahon, D. W. Goodman, *J. Vac. Sci. Technol.* **1996**, *14*, 1184-1188.
- [127] J. Shen, J. Hill, R. Watwe, S. G. Podkolzin, J. A. Dumesic, *Catal. Lett.* **1999**, *60*, 1-9.
- [128] D. C. Meier, D. W. Goodman, *J. Am. Chem. Soc.* **2004**, *126*, 1892-1899.
- [129] M. Mihaylov, H. Knözinger, K. Hadjiivanov, B. C. Gates, *Chem. Ing. Tech.* **2007**, *79*, 795-806.
- [130] R. P. Eischens, S. A. Francis, W. A. Pliskin, *J. Phys. Chem.* **1956**, *60*, 194-201.
- [131] M. Primet, *J. Catal.* **1984**, *88*, 273-282.
- [132] K. Gossner, E. Mizera, *J. Electroanal. Chem. Interfac. Electrochem.* **1979**, *98*, 37.
- [133] J. J. Plata, M. n. García-Mota, A. A. C. Braga, N. r. López, F. Maseras, *J. Phys. Chem. A* **2009**, *113*, 11758-11762.
- [134] M. Bowker, C. Morgan, V. P. Zhdanov, *Phys. Chem. Chem. Phys.* **2007**, *9*, 5700-5703.
- [135] S. M. Augustine, J. P. Blitz, *J. Catal.* **1993**, *142*, 312-324.
- [136] S. A. H. Zaidi, *Appl. Catal.* **1988**, *38*, 353-358.
- [137] E. K. Hanrieder, A. Jentys, J. A. Lercher, *ACS Catal.* **2015**, 5776-5786.
- [138] R. D. Haley, M. S. Tikhov, R. M. Lambert, *Catal. Lett.* **2001**, *76*, 125-130.
- [139] D. D. Kragten, R. A. van Santen, M. Neurock, J. J. Lerou, *J. Phys. Chem. A* **1999**, *103*, 2756-2765.
- [140] M. Tamura, T. Yasui, *Kogyo Kagaku Zasshi* **1969**, *72*, 561.
- [141] M. Neurock, W. D. Provine, D. A. Dixon, G. W. Coulston, J. J. Lerou, R. A. van Santen, *Chem. Eng. Sci.* **1996**, *51*, 1691-1699.
- [142] J. L. Davis, M. A. Barteau, *Surf. Sci.* **1991**, *256*, 50-66.
- [143] E. M. Stuve, R. J. Madix, *Surf. Sci.* **1985**, *160*, 293-304.
- [144] E. M. Stuve, R. J. Madix, *J. Phys. Chem.* **1985**, *89*, 105-112.
- [145] F. Calaza, D. Stacchiola, M. Neurock, W. T. Tysoe, *J. Am. Chem. Soc.* **2010**, *132*, 2202-2207.
- [146] D. Stacchiola, F. Calaza, L. Burkholder, A. W. Schwabacher, M. Neurock, W. T. Tysoe, *Angew. Chem. Int. Ed.* **2005**, *44*, 4572-4574.
- [147] F. Gao, Y. Wang, F. Calaza, D. Stacchiola, W. T. Tysoe, *J. Mol. Catal. A* **2008**, *281*, 14-23.
- [148] R. H. Grubbs, C. Gibbons, L. C. Kroll, W. D. Bonds, C. H. Brubaker, *J. Am. Chem. Soc.* **1973**, *95*, 2373-2375.
- [149] M. Terasawa, K. Kaneda, T. Imanaka, S. Teranishi, *J. Catal.* **1978**, *51*, 406-421.
- [150] C. R. Reilly, J. J. Lerou, *Catal. Today* **1998**, *41*, 433-441.
- [151] S. Nakamura, T. Yasui, *J. Catal.* **1971**, *23*, 315-320.
- [152] G. Mazzone, I. Rivalta, N. Russo, E. Sicilia, *Chem Comm.* **2009**, 1852-1854.
- [153] M. Chen, D. Kumar, Cheol-Woo Yi, D. W. Goodman, *Science* **2005**, *310*, 291.
- [154] Q. Smejkal, D. Linke, U. Bentrup, M. M. Pohl, H. Berndt, M. Baerns, A. Brückner, *Appl. Catal. A* **2004**, *268*, 67-76.
- [155] R. Abel, G. Prauser, H. Tiltscher, *Chem. Eng. Technol.* **1994**, *17*, 112-118.
- [156] N. Macleod, J. M. Keel, R. M. Lambert, *Appl. Catal. A* **2004**, *261*, 37-46.

- [157] M.-M. Pohl, J. Radnik, M. Schneider, U. Bentrup, D. Linke, A. Brückner, E. Ferguson, *J. Catal.* **2009**, 262, 314-323.
- [158] W. J. Bartley, S. Jobson, G. G. Harkreader, M. Kitson, M. Lemanski, *U.S.* 5,274,181 **1993**.
- [159] D. Yuan, X. Gong, R. Wu, *J. Phys. Chem. C* **2008**, 112, 1539-1543.
- [160] M. Neurock, D. Mei, *Top. Catal.* **2002**, 20, 5-23.
- [161] M. Bowker, C. Morgan, *Catal. Lett.* **2004**, 98, 67-67.
- [162] L. Prati, A. Villa, D. S. Su, D. Wang, *Catal. Sci. Technol.* **2014**.
- [163] T. Wei, D. Kumar, M. S. Chen, K. Luo, S. Axnanda, M. Lundwall, D. W. Goodman, *J. Phys. Chem. C* **2008**, 112, 8332.
- [164] R. G. Brown, J. M. Davidson, C. Triggs, *Am. Chem. Soc., Div. Petrol. Chem.* **1969**, 14, B23-B28.
- [165] A. V. Karandin, E. V. Gusevskaya, V. A. Likholobov, A. I. Boronin, E. M. Moroz, *Kinet. Catal.* **1991**, 32, 367.
- [166] D. P. Bancroft, F. A. Cotton, L. R. Falvello, W. Schwotzer, *Polyhedron* **1988**, 7, 615-621.
- [167] S. D. Kirik, R. F. Mulagaleev, A. I. Blokhin, *Acta Crystall. C* **2004**, 60, m449-m450.
- [168] L. Soptrajanova, B. Soptrajanov, *Spectrosc. Lett.* **1992**, 25, 1131.
- [169] E. Stoyanov, *J. Struct. Chem.* **2000**, 41, 440-445.
- [170] T. A. Stephenson, S. M. Morehouse, A. R. Powell, J. P. Heffer, G. Wilkinson, *J. Chem. Soc.* **1965**, 3632-3640.
- [171] R. N. Pandey, P. M. Henry, *Canad. J. Chem* **1974**, 52, 1241-1247.
- [172] R. N. Pandey, P. M. Henry, *Canad. J. Chem.* **1975**, 53, 1833-1841.
- [173] [http://www.chem.tamu.edu/rgroup/dunbar/Teaching/CHEM362/Lecture\\_33.pdf](http://www.chem.tamu.edu/rgroup/dunbar/Teaching/CHEM362/Lecture_33.pdf).
- [174] W. G. Van Der Sluys, *J. Chem. Educ.* **2001**, 78, 111-115.
- [175] S. Winstein, J. McCaskie, H.-B. Lee, P. M. Henry, *J. Am. Chem. Soc.* **1976**, 98, 6913-6918.
- [176] P. R. Rony, *J. Catal.* **1969**, 14, 142-147.
- [177] K. Fujimoto, Y. Negami, T. Takahashi, T. Kunugi, *Ind. Eng. Chem. Prod. Res. Develop.* **1972**, 11, 303-308.
- [178] R. Ninomiya, M. Sato, T. Shiba, *Bull. Jpn. Pet. Inst.* **1965**, 7, 31.
- [179] K. Fujimoto, T. Kunugi, *Kogyo Kagaku Zasshi* **1969**, 72, 1760.
- [180] G. W. Parshall, *Homogeneous Catalysis*, New York, **1980**.
- [181] S. Koukiou, M. Konsolakis, R. M. Lambert, I. V. Yentekakis, *Appl. Catal. B* **2007**, 76, 101-106.
- [182] V. Pitchon, M. Guenin, H. Praliaud, *Appl. Catal.* **1990**, 63, 333-343.
- [183] H. W. K. Tom, C. M. Mate, X. D. Zhu, J. E. Crowell, Y. R. Shen, G. A. Somorjai, *Surf. Sci.* **1986**, 172, 466-476.
- [184] N. D. Lang, A. R. Williams, *Phys. Rev. Lett.* **1976**, 37, 212-215.
- [185] N. D. Lang, A. R. Williams, *Phys. Rev. B* **1978**, 18, 616-636.
- [186] J. W. Gadzuk, *Surf. Sci.* **1967**, 6, 133-158.
- [187] W. Braun, M. Neumann, M. Iwan, E. E. Koch, *phys. stat. sol. (b)* **1978**, 90, 525-533.
- [188] S. Andersson, U. Jostell, *Surf. Sci.* **1974**, 46, 625-640.

- 
- [189] B. E. Hayden, A. W. Robinson, P. M. Tucker, *J. Electron. Spectrosc. Relat. Phenom.* **1987**, *44*, 297-304.
- [190] M. Gravelle-Rumeau-Maillot, V. Pitchon, G. A. Martin, H. Praliaud, *Appl. Catal. A* **1993**, *98*, 45-59.
- [191] G. Ertl, S. B. Lee, M. Weiss, *Surf. Sci. Lett.* **1981**, *111*, L711-L715.
- [192] C. T. Campbell, D. W. Goodman, *Surf. Sci.* **1982**, *123*, 413-426.
- [193] D. R. Strongin, G. A. Somorjai, *J. Catal.* **1988**, *109*, 51-60.
- [194] S. D. Jackson, G. J. Kelly, D. Lennon, *React. Kinet. Catal. Lett.* **2000**, *70*, 207-212.
- [195] S. Tamura, T. Yasui, *Shokubai (trans)* **1979**, *21*, 54.

## 1.9. Scope of the Thesis

The synthesis of VA is a major industrial application in selective oxidation which has been studied for decades on heterogeneous  $\text{Zn}(\text{OAc})_2/\text{C}$  and supported Pd systems as well as on homogeneous  $\text{PdCl}_2/\text{CuCl}_2$  catalysts. The addition of Au and KOAc to Pd/SiO<sub>2</sub> enhanced the catalytic activity and the intrinsic selectivity towards VA. However, the role of the promoting species KOAc on the dynamic reordering process of bimetallic PdAu catalysts is not understood.

This PhD thesis is divided into following parts:

### *Atomistic Engineering of Catalyst Precursors – Dynamic Reordering of PdAu Nanoparticles during Gas Phase Vinyl Acetate Synthesis enhanced by Potassium Acetate*

In order to improve the current understanding how the KOAc promoter enhances the catalytic activity, selectivity and stability, KOAc free and promoted, chloride free PdAu/SiO<sub>2</sub> as well as Pd/SiO<sub>2</sub> and Au/SiO<sub>2</sub> catalysts were synthesized according to patented routes. Fresh and spent samples will be studied by advanced surface and bulk sensitive analytical techniques partially under in situ conditions by infrared spectroscopy (FTIR), powder X-ray diffraction (XRD) and transmission electron microscopy (TEM). KOAc retains AcOH on the support surface and influences the dynamic reordering process towards Pd<sub>1</sub>Au<sub>1</sub> particles by the formation of  $\text{K}_2\text{Pd}_2(\text{OAc})_6$  species. The presence of intermediates from the homogenous catalyzed VA synthesis points to a supported liquid phase process. KOAc transfers acetates to Pd and forms a protective layer around PdAu thereby impeding ethene decomposition and increasing the selectivity towards VA.

### *Impact of Alkali Acetates on Deactivation of PdAu during Gas Phase Vinyl Acetate Synthesis*

Based on the findings on the formation of  $\text{K}_2\text{Pd}_2(\text{OAc})_6$  and the reordering process of PdAu influenced by KOAc, the question arises, how the different types of alkali acetate promoters MOAc ( $\text{M}^+ = \text{Li}^+, \text{Na}^+, \text{K}^+, \text{Cs}^+$ ) affect the deactivation behavior of PdAu particles. The as synthesized and reactively aged samples will be physicochemically characterized combining elemental analysis, surface and bulk sensitive methods. CO adsorption at liquid nitrogen temperature will indicate the degree of surface intermixing on samples after reaction washed for 20 min and 24 h and help to determine the existence and stability of a mixed Pd/M<sup>+</sup>-oxide adlayer on PdAu in dependence of MOAc. By comparing catalyst properties after VA synthesis, we will obtain a detailed picture of the restructuring and deactivation processes.

### *Interaction of Alkali Acetates with PdAu*

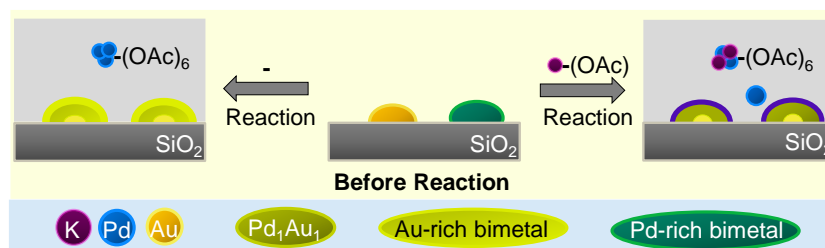
The temperature dependent formation of a mixed Pd/M<sup>+</sup>-oxide adlayer ( $\text{M}^+ = \text{Li}^+, \text{Na}^+, \text{K}^+, \text{Cs}^+$ ) as protective shell around the solid PdAu particles is believed to be the precursor for the genesis of  $\text{M}_2\text{Pd}_2(\text{OAc})_6$  species under industrial reaction conditions. Thus, the interaction of MOAc with PdAu/SiO<sub>2</sub> will be studied by (in situ) XRD, XAS and infrared spectroscopy of adsorbed CO at 100 °C to elucidate the effect of MAOc on the electronic and geometric bulk and surface properties of PdAu.



# Chapter 2

## Atomistic Engineering of Catalyst Precursors - Dynamic Reordering of PdAu Nanoparticles during Vinyl Acetate Synthesis enhanced by Potassium Acetate<sup>1</sup>

The presence of potassium acetate (KOAc) on bimetallic PdAu catalysts increases the rate of reaction for vinyl acetate (VA) formation from ethene and acetic acid by a factor of 10 and the selectivity by 20 %. The dynamic transitions of typical supported catalyst precursors with an atomic Pd/Au ratio of 2/1 were explored during synthesis in presence and absence of KOAc. The dopant induces reordering of PdAu towards a Pd<sub>1</sub>Au<sub>1</sub> phase, while Au enriched Pd<sub>39</sub>Au<sub>61</sub> bimetallic particles form primarily in the absence of KOAc. Pd-acetate species are generated via leaching of Pd from PdAu precursor particles during reaction. These species are Pd<sub>3</sub>(OAc)<sub>6</sub> and Pd<sub>2</sub>(OAc)<sub>4</sub> in absence, and K<sub>2</sub>Pd<sub>2</sub>(OAc)<sub>6</sub> in presence of KOAc. Palladium in K<sub>2</sub>Pd<sub>2</sub>(OAc)<sub>6</sub> can be readily reduced by C<sub>2</sub>H<sub>4</sub> to Pd<sup>0</sup>, while Pd<sub>3</sub>(OAc)<sub>6</sub>, which contains more stable, bridged acetate ligands remains stable. Reduced Pd either forms dispersed Pd<sup>0</sup> or is incorporated into the metal particles. KOAc enhances rates and selectivity to VA by stabilizing on the one hand active Pd species at the bimetallic surface. On the other hand, KOAc enriches acetic acid close to the surface and forms Pd surface acetates, postulated to enhance the rate and the selectivity to VA by suppressing ethene adsorption and oxidation.



<sup>1</sup> This chapter is based on the article of the same title as published in the journal ACS Catalysis. Reprinted with permission from ACS Catalysis.

## 2.1. Introduction

The heterogeneously catalyzed acetoxylation of ethene to vinyl acetate (VA) over silica-supported bimetallic palladium gold (PdAu) particles promoted with potassium acetate (KOAc) is a structure sensitive reaction.<sup>[1-2]</sup> The active sites consist of two isolated Pd surface atoms separated by Au atoms (Figure 2.1).<sup>[3]</sup>

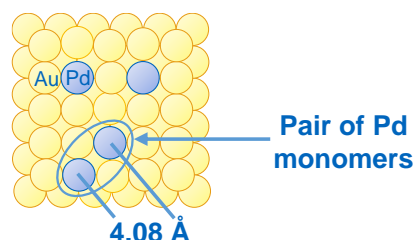
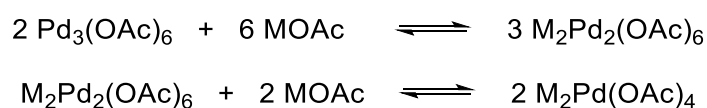


**Figure 2.1.** A pair of Pd monomers on e.g. Au(100) is proposed as active site for VA synthesis.<sup>[3]</sup>

The active surface species are typically formed under the influence of the reactant atmosphere<sup>[4]</sup> and we have recently shown that KOAc promoted Pd<sub>x</sub>Au<sub>y</sub> particles restructure into bimetallic Pd<sub>1</sub>Au<sub>1</sub> and Pd particles under reaction conditions.<sup>[5]</sup> The role of alkaline acetate promoters, which improves the overall activity and selectivity of the catalyst is hardly understood.<sup>[6]</sup>

The most widely explanation is attributing the promoting effect of alkali metals to their electronic influence on Pd. The cationic promoter's<sup>[7-8]</sup> hybridization of its s and p energy levels with the metal electronic states broadens and shifts their band positions relative to the Fermi level. This process is determined by the competition between the tendency to fill the valence shell and the electron affinity of the metal. Consequently, electrons are partially transferred from the alkali cation to the metal, creating a surface dipole.<sup>[9]</sup> In accordance with this interpretation, Gravelle-Rumeau-Maillot et al.<sup>[10]</sup> reported that the initial heat of adsorption of CO increased slightly (ca. 10 %) by the presence of K<sup>+</sup> and Na<sup>+</sup>, which is also reflected in the lower wavenumbers of adsorbed CO. While such promotion is certainly present in PdAu/KOAc catalysts, the existence of the liquid-like acetic acid (AcOH) layer on the catalyst under reaction conditions<sup>[11]</sup> leads to a more complex situation. Strong interactions of acetic acid and acetate ions with Pd allows leaching it from bimetallic particles as Pd acetate,<sup>[12]</sup> which affects the reordering of PdAu particles.

The mobile Pd acetate in liquid acetic acid exists as monomer, dimer, and trimer. The concentrations of these species are controlled by the addition of alkali metal acetates (MOAc) (Scheme 2.1).<sup>[13-15]</sup> With increasing MOAc concentration, trimeric Pd<sub>3</sub>(OAc)<sub>6</sub><sup>[16-18]</sup> is converted into active dimeric Pd<sub>2</sub>(OAc)<sub>6</sub><sup>2-</sup>, while presumably inactive monomeric Pd(OAc)<sub>4</sub><sup>2-</sup> was not formed under the conditions of the homogeneous catalytic conversion of ethene.<sup>[16, 19]</sup>



**Scheme 2.1.** Equilibrium between trimeric Pd<sub>3</sub>(OAc)<sub>6</sub>, dimeric M<sub>2</sub>Pd<sub>2</sub>(OAc)<sub>6</sub> and monomeric M<sub>2</sub>Pd(OAc)<sub>4</sub> with M<sup>+</sup> = alkali ion.

Also PdAu particles change dynamically under working conditions, as Pd leaches into AcOH, and binds to or reacts with the adsorbed molecules. These variations in structure and chemical composition, induced by reactants and intermediates, control the overall activity and selectivity in VA synthesis. Thus, atomistic information is required to analyze the nature, geometry, and environment of the active sites during catalysis.<sup>[20]</sup> Given the central role of the KOAc promoter, we explore in this contribution its impact on the reordering processes of PdAu particles and in turn on activity and selectivity.

## 2.2. Experimental

### 2.2.1. Synthesis

PdAu/SiO<sub>2</sub> catalysts were synthesized with a molar Pd/Au ratio of 2.0 to reach equal amounts of Pd in the bimetallic Pd<sub>1</sub>Au<sub>1</sub> particles and as dispersed Pd species during reaction.<sup>[5]</sup> This Pd distribution allows the best appropriate way for studying the heterogeneous pathway (on the PdAu surface) in parallel to the homogeneous pathway to VA (via Pd acetate species). Catalysts were prepared via incipient wetness impregnation according to patent DE102006058800A1.<sup>[21]</sup> Aqueous solutions of HAuCl<sub>4</sub> and PdCl<sub>2</sub> were impregnated on mesoporous SiO<sub>2</sub> (HDK<sup>®</sup>, 200 m<sup>2</sup>/g, 1.1 mL/g) followed by precipitation of Pd<sup>2+</sup> and Au<sup>3+</sup> ions with sodium carbonate and washing with ammonia solution (pH 8, 5L/8g catalyst) to remove chloride ions from the metal precursors. The PdAu/SiO<sub>2</sub> precursor was reduced in flowing H<sub>2</sub> (100 mL/min) at 300 °C for 1h with a heating rate of 5 °C/min. The Pd as well as the Au loading was ~1.5 wt.% corresponding to a molar PdAu ratio of 2.0. The catalyst was impregnated with 5 wt.% K whereas samples for IR studies were impregnated with 2 wt% of K using an aqueous solution of KOAc. A physical mixture between monometallic Pd/SiO<sub>2</sub> and Au/SiO<sub>2</sub> was prepared using 3 wt% Pd/SiO<sub>2</sub> and Au/SiO<sub>2</sub> in a molar ratio of 2/1 impregnated with 5 wt% KOAc. The term “PdAu/SiO<sub>2</sub>” refers to the unpromoted and “PdAu/KOAc/SiO<sub>2</sub>” to the promoted PdAu catalyst. The physical mixture of monometallic Pd and Au promoted with KOAc is called “(Pd+Au)/KOAc/SiO<sub>2</sub>”. Reference catalysts were impregnated with Pd(OAc)<sub>2</sub> (3 wt% Pd) and with KOAc (5 wt% K).

### 2.2.2. X-Ray Powder Diffraction

X-Ray powder diffraction measurements were conducted on a Philips X'Pert Pro System using Cu K<sub>α</sub> radiation (0.154056 nm) generated at 45 kV and 40 mA. The samples were mounted on a rotating powder holder and measured in a 2θ range of 5°–70° with a step size of 0.017°/s. Peak fitting was performed with High Score Plus software using the crystallographic open database (COD) to derive the exact peak positions and to calculate the alloy compositions using Vegard's rule.<sup>[22]</sup>

### 2.2.3. Low Temperature IR Spectroscopy during CO Adsorption

The infrared spectra were recorded on a Vertex 70 spectrometer from Bruker Optics with a resolution of  $4\text{ cm}^{-1}$ . The samples were prepared as self-supporting wafers ( $\sim 10\text{ mg/cm}^2$ ). The samples were first activated in vacuum (better than  $1 \times 10^{-7}\text{ mbar}$ ) at  $300\text{ }^\circ\text{C}$  (heating rate  $5\text{ }^\circ\text{C/min}$ ) for 1 h and reduced in  $1000\text{ mbar H}_2$  at  $300\text{ }^\circ\text{C}$  (heating rate  $5\text{ }^\circ\text{C/min}$ ). After reduction, the samples were outgassed at  $300\text{ }^\circ\text{C}$  in vacuum for 30 min and cooled to  $-150\text{ }^\circ\text{C}$  with liquid nitrogen in  $3\text{ mbar He}$  to maintain the temperature at  $-150\text{ }^\circ\text{C}$ . After recording the spectrum of the activated sample,  $1\text{ mbar CO}$  and  $50\text{ mbar of He}$  were introduced to the system. Spectra were collected during CO adsorption at  $-150\text{ }^\circ\text{C}$  until the adsorption desorption equilibrium was reached.

All IR spectra were normalized to the integrated area of the Si-O overtones of the activated sample between  $2107$  and  $1741\text{ cm}^{-1}$ . The contributions of the individual CO bands were evaluated by band fitting applying a mixed 50/50 Gaussian-Lorentzian function in the region between  $2140$  and  $2000\text{ cm}^{-1}$  using the software Grams AI. In order to extract the KOAc induced changes in the PdAu surface composition, band positions for CO adsorbed on either Pd or Au on fresh PdAu/KOAc/SiO<sub>2</sub> were fitted considering the CO band positions of Pd/KOAc/SiO<sub>2</sub> and Au/KOAc/SiO<sub>2</sub>.

### 2.2.4. In Situ IR Spectroscopy

Infrared spectra of the samples in continuous flow were collected with a resolution of  $4\text{ cm}^{-1}$  on a Thermo Fisher Nexus. The samples were pressed into self-supporting wafers ( $10\text{ mg/cm}^2$ ), cut in half and placed in a flow IR cell designed by Mirth et al.<sup>[23]</sup> The cell was vertically moved to measure either IR spectra of the wafer or the gas phase present inside the cell through the empty section in the upper half. This enabled to subtract the contributions of the gas phase (which is significant at a pressure of  $9\text{ bar}$ ) from the spectra of the adsorbed species measured.

Prior to adsorption, samples were reduced at  $250\text{ }^\circ\text{C}$  (heating rate  $5\text{ }^\circ\text{C/min}$ ) in  $\text{H}_2$  followed by  $\text{N}_2$ . Acetic acid was added using a temperature controlled saturator and oxygen as well as ethene was mixed into the  $\text{N}_2$  carrier gas stream via mass flow controllers at  $150\text{ }^\circ\text{C}$  and  $9\text{ bar}$ .

### 2.2.5. Catalytic Reactions

The activity of the catalysts for VA synthesis was studied in a 6-fold reactor setup at  $150\text{ }^\circ\text{C}$ , at  $9\text{ bar}$  total pressure and a gas composition of  $60\text{ vol } \% \text{ C}_2\text{H}_4$ ,  $13\text{ vol } \% \text{ AcOH}$ ,  $4.5\text{ vol } \% \text{ O}_2$  in  $\text{N}_2$ . SiC ( $355 - 500\text{ }\mu\text{m}$ ) was used as inert diluent to maintain a constant temperature over the catalyst bed ( $180\text{-}250\text{ }\mu\text{m}$ ). The diluent/catalyst ratio was chosen to be  $10/1$ . The product stream was analyzed using a GC (model 2014 from Shimadzu), equipped with a Haysep Q, a molecular sieve column and a TCD detector.

## 2.3. Results and Discussion

### 2.3.1. Vinyl Acetate Synthesis on KOAc Promoted and Unpromoted PdAu/SiO<sub>2</sub>

The influence of KOAc on the activity and selectivity of bimetallic PdAu catalysts in VA synthesis was studied during continued operation. The formation rates and selectivities of PdAu/SiO<sub>2</sub> and PdAu/KOAc/SiO<sub>2</sub> are compiled in Figure 2.2. The slight decrease in selectivity during the initial induction period of ~1000 minutes can be related to the increase in activity of PdAu/KOAc/SiO<sub>2</sub>. During this time, the PdAu particles undergo severe restructuring processes by leaching Pd<sup>2+</sup> from the bimetallic phase. In parallel, the overall activity increases as more active but less selective PdAu surface arrangements are generated. After this induction period, PdAu/KOAc/SiO<sub>2</sub> deactivated only by ~4 %; the selectivity increased marginally to 95 % in good agreement with ref.<sup>[24-26]</sup> In contrast, activity and selectivity of (potassium free) PdAu/SiO<sub>2</sub> decreased considerably, leading to almost complete deactivation after 6000 minutes.<sup>[27]</sup>

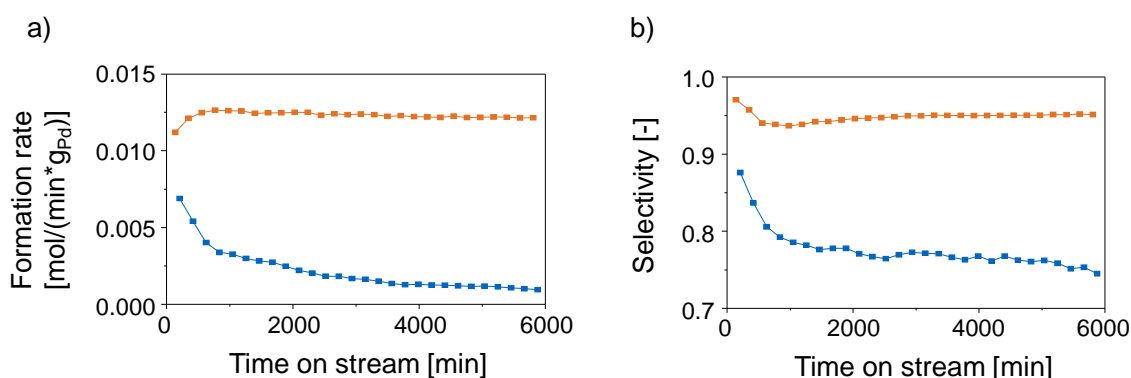


**Figure 2.2.** (a) Formation rates normalized to the concentration Pd in the bimetallic phase and (b) selectivities for PdAu/SiO<sub>2</sub> (blue) and PdAu/KOAc/SiO<sub>2</sub> (orange) with time on stream. Reaction conditions: 60 vol % C<sub>2</sub>H<sub>4</sub>, 13 vol % AcOH, 4.5 vol % O<sub>2</sub>, balance N<sub>2</sub>; total pressure, 8.8 bar; temperature, 150 °C.

### 2.3.2. KOAc Enhances Reactive Reordering of PdAu Particles in the Heterogeneous Pathway to VA Synthesis

#### 2.3.2.1. Effect of KOAc on the Pd<sub>x</sub>Au<sub>y</sub> Bulk Composition

To investigate the effect of KOAc on the bulk composition of the Pd<sub>x</sub>Au<sub>y</sub> particles during time on stream, X-ray diffractograms for fresh and used catalysts with and without KOAc were compared between 36 and 42° 2θ (Figure 2.3). The positions of Au(111) at 38.3° and Pd(111) at 40.1° indicated by bright grey and black lines, respectively, were calculated from fcc lattice constants reported in the COD database ( $a_{\text{Au}}$  at 4.060 Å and  $a_{\text{Pd}}$  at 3.890 Å). The Pd<sub>x</sub>Au<sub>y</sub> alloy compositions of fresh and used samples, derived from the fitted peak positions applying Vegard's law<sup>[22]</sup> are compiled in Table 2.1.

The potassium free PdAu/SiO<sub>2</sub> catalyst (Figure 2.3ai) before reaction consisted of Au and Pd rich particles with average compositions of Pd<sub>7</sub>Au<sub>93</sub>, Pd<sub>98</sub>Au<sub>2</sub>, and Pd<sub>69</sub>Au<sub>31</sub>. The peaks had an asymmetric shape, indicating a distribution of particles with varying composition before reaction.

After 6000 minutes time on stream (Figure 2.3aai), a small fraction of monometallic Au particles (or Au-rich core-shell particles<sup>[28-29]</sup>) remained, while diffraction lines of monometallic Pd particles were not observed. The main fraction of Pd<sub>39</sub>Au<sub>61</sub> contained significantly less Pd than expected from the overall Pd/Au ratio of 2. Thus, a considerable fraction of Pd (~64%) is concluded to be XRD amorphous, i.e., in the form of very small Pd<sup>0</sup> particles or/and dissolved Pd acetate.<sup>[4-5, 30]</sup>

On KOAc promoted PdAu/SiO<sub>2</sub> (Figure 2.3bi) the composition of the X-ray crystalline bimetallic PdAu particles changed from 2/1 (Pd<sub>69</sub>Au<sub>31</sub>) to approximately 1/1 (Pd<sub>54</sub>Au<sub>46</sub>) already upon impregnation with KOAc. We conclude that this is induced by the formation of Pd acetate. Such surface chemistry between Pd and KOAc was also observed by EPR.<sup>[31]</sup> It is hypothesized that during the impregnation process partly oxidized Pd interacts with the acetate anions, leading in turn to the removal of Pd from the bimetallic particles after impregnation.

After reaction, PdAu/KOAc/SiO<sub>2</sub> (Figure 2.3bii) mainly consisted of Pd<sub>47</sub>Au<sub>53</sub> particles (close to a Pd<sub>1</sub>Au<sub>1</sub> phase) and a small fraction of Pd<sub>4</sub>Au<sub>96</sub>, likely located in the particle core.<sup>[28-29]</sup> The content of dispersed Pd species was estimated to be 53 % of the total Pd loading, assuming that most of the Au is alloyed with Pd.<sup>[28, 30]</sup> After reaction, the fraction of dispersed Pd was lower for the promoted PdAu catalyst than for the unpromoted, which indicates that the equilibrium between leached Pd and the bimetallic PdAu phase is affected by the presence of KOAc. Thus, KOAc removes Pd from bimetallic PdAu particles, but also stabilizes the bimetallic Pd<sub>1</sub>Au<sub>1</sub> phase during reaction. In these used catalysts, the full width at half maximum is higher for PdAu/SiO<sub>2</sub> than for PdAu/KOAc/SiO<sub>2</sub>, indicating smaller PdAu particles on PdAu/SiO<sub>2</sub>. This is probably due to the higher concentration of dispersed Pd leached from the bimetallic particles on PdAu/SiO<sub>2</sub> and due to the absence of KOAc, which induces particle agglomeration on PdAu/KOAc/SiO<sub>2</sub>.<sup>[32]</sup> The loss of Pd under reaction conditions appears to be inevitable and may be retarded by the presence of KOAc, but not stopped (after 6000 minutes Pd<sub>47</sub>Au<sub>53</sub> were observed with KOAc promoted catalysts while Pd<sub>39</sub>Au<sub>61</sub> was observed in absence of KOAc). This is clearly demonstrated by a reactor study over 14 months, which reported Pd<sub>38</sub>Au<sub>62</sub><sup>[30]</sup> as a thermodynamically stable alloy having a formation enthalpy of -7.8 kJ mol<sup>-1</sup>.<sup>[33-35]</sup>

Although the PdAu surface structure is particularly important for catalysis, the bulk phase composition is also substantial for VA synthesis as it is directly connected to the surface composition by dynamic reordering and leaching Pd<sup>2+</sup> into the acetic acid film. Catalysts with an overall Pd/Au ratio of 1 showed a pronounced loss in selectivity and activity with time-on-stream compared to Pd rich samples since Pd<sub>1</sub>Au<sub>1</sub> particles initially present will also leach Pd in form of Pd<sup>2+</sup> to generate Au enriched particle surfaces that favor the combustion of C<sub>2</sub>H<sub>4</sub> to CO<sub>2</sub> over the formation of VA.

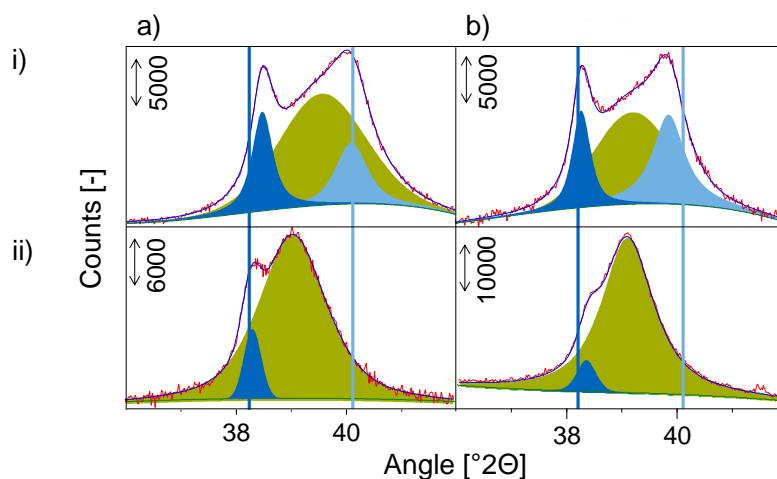


**Figure 2.3.** X-ray diffraction profiles for 111 planes (i) before and (ii) after reaction for PdAu/SiO<sub>2</sub> (a) and PdAu/KOAc/SiO<sub>2</sub> (b). The bimetallic phase (green) of the 111 plane is located between those of the pure metals: Au(111) ( $2\theta = 38.3^\circ$ ) (dark blue), Pd(111) ( $2\theta = 40.1^\circ$ ) (bright blue).

**Table 2.1.** Alloy compositions of PdAu/SiO<sub>2</sub> and PdAu/KOAc/SiO<sub>2</sub> before and after reaction determined by XRD.

	<b>Pd<sub>x</sub>Au<sub>y</sub></b>	
	<b>PdAu/SiO<sub>2</sub></b>	<b>PdAu/KOAc/SiO<sub>2</sub></b>
<b>Before reaction</b>	Pd <sub>7</sub> Au <sub>93</sub> , Pd <sub>69</sub> Au <sub>31</sub> , Pd <sub>98</sub> Au <sub>2</sub>	Au <sub>100</sub> , Pd <sub>54</sub> Au <sub>46</sub> , Pd <sub>89</sub> Au <sub>11</sub>
<b>After reaction</b>	Au <sub>100</sub> , Pd <sub>39</sub> Au <sub>61</sub>	Pd <sub>4</sub> Au <sub>96</sub> , Pd <sub>47</sub> Au <sub>53</sub>

In order to confirm the dynamic exchange of Pd between solved or dispersed Pd<sup>0</sup> and Pd in bimetallic PdAu particles, a physical mixture, (Pd+Au)/KOAc/SiO<sub>2</sub>, of monometallic Au and Pd particles (Figure 2.4a) was used as catalyst (Figure 2.4b). The XRD peaks of Au(111) and Pd(111) in the physical mixture before reaction were shifted by 0.175 and 0.080° 2θ to higher angles with respect to the reference materials (bright grey and black lines) indicating shorter distances between metal atoms in the small metal particles.

During reaction, (Pd+Au)/KOAc/SiO<sub>2</sub> (Figure 2.4b) underwent severe reordering, as the initial peaks for Au<sub>100</sub> and Pd<sub>100</sub> disappeared. Particles of Pd<sub>45</sub>Au<sub>55</sub> and Pd<sub>15</sub>Au<sub>85</sub> formed, as well as a major part of XRD invisible Pd acetate or Pd<sup>0</sup> (sub)nanoparticles (~91%). The formation of bimetallic Pd<sub>15</sub>Au<sub>85</sub> is attributed to the incorporation of Pd<sup>0</sup> into Au particles, which indicates reversibility between oxidative leaching and reductive reincorporation. The formation of the bimetallic phase on (Pd+Au)/KOAc/SiO<sub>2</sub> confirms that an oxidative dissolution of Pd<sup>2+</sup>, a transfer of Pd<sup>2+</sup> to pure Au particles in the AcOH layer and a reduction of Pd<sup>2+</sup> to incorporate Pd<sup>0</sup> in Au particles is possible under the reaction conditions of the VA synthesis. In situ reduction of Pd<sup>2+</sup> in the presence of Au nanoparticles resulted in catalytically active AuPd bimetallic catalysts.

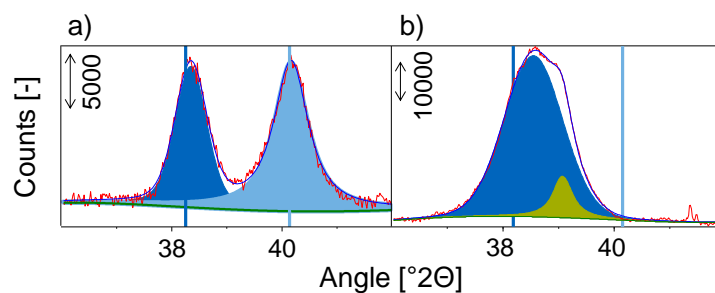


**Figure 2.4.** XRD profiles for the 111 plane of (Pd+Au)/KOAc/SiO<sub>2</sub> (a) before and (b) after reaction. The bimetallic phase (green) is located between the positions of the pure metals: Au(111) ( $2\theta = 38.3^\circ$ ) (dark blue), Pd(111) ( $2\theta = 40.0^\circ$ ) (bright blue).

TEM studies showed that the average particle size of (Pd+Au)/KOAc/SiO<sub>2</sub> decreased from initially 3.5 nm to 1-2 nm with agglomerates in the range of ~5 to 12 nm after reaction. Particle sizes below 1.0 nm were not observed (Figure A2.1, Appendix). This suggests that Pd particles loose organization by solvation in AcOH, while Au particles grow (Figure 2.4b) This suggests that Pd particles solved in AcOH (1-2 nm particles), while Au particles grew in the presence of KOAc (5-12 nm particles)(Figure 4b).<sup>[36-38]</sup> The activity normalized to the total Pd concentration and the selectivity of (Pd+Au)/KOAc/SiO<sub>2</sub> is comparable to PdAu/KOAc/SiO<sub>2</sub> (Figure A2.2, Appendix).

### 2.3.2.2. Effect of KOAc on the PdAu Surface Composition during VA Synthesis

While the preceding experiments have shown, how the nanoparticles reorganize during catalysis, the surface composition may be very different. In order to explore it we have used the IR spectra of adsorbed CO after removing the layer of KOAc or Pd acetate by washing the material with water, restoring the accessibility of the surface. Leaching of Au species by this procedure was not detected.

The IR spectra of 1.0 mbar CO adsorbed on SiO<sub>2</sub> are shown in Figure A2.3 (Appendix). At -150 °C, CO adsorbed on the OH groups of SiO<sub>2</sub> (2157 cm<sup>-1</sup>)<sup>[39-40]</sup> and on cations (2184 cm<sup>-1</sup>).<sup>[41-42]</sup> The band at 2135 cm<sup>-1</sup> is assigned to CO physically adsorbed on the surface of SiO<sub>2</sub>.<sup>[43-44]</sup> Stretching bands of CO adsorbed on Au or Pd nanoparticles (Figure 2.5i) above 2000 cm<sup>-1</sup> are attributed to linearly adsorbed CO, bands below 2000 cm<sup>-1</sup> to CO adsorbed in a bridged and threefold-hollow mode.<sup>[39, 45-46]</sup> On Au/SiO<sub>2</sub>, CO was only adsorbed linearly (2104 cm<sup>-1</sup>, Figure 2.5ai),<sup>[47-50]</sup> while on Pd, bands of linear and bridged bonded CO were observed at 2109 and 1991 cm<sup>-1</sup>, respectively (Figure 2.5bi).<sup>[48, 51-53]</sup>

The presence of KOAc on Au/SiO<sub>2</sub> (Figure 2.5aii) and on Pd/SiO<sub>2</sub> (Figure 2.5bii) led to a decrease of the wavenumbers of linearly adsorbed CO by 6 cm<sup>-1</sup> on Au and by 17 cm<sup>-1</sup> on Pd. The larger redshift of CO on Pd/KOAc/SiO<sub>2</sub> indicated a more pronounced electronic impact of KOAc on Pd than on Au. Alkali metal ions as well as neutral alkali metals were shown to act both as electron donors as they bear a positive charge,  $\delta^+$ , when they are adsorbed on a metal. In both cases, the CO frequency shifted to lower wavenumbers.<sup>[8, 10, 42, 54-59]</sup> In agreement with these experiments, we assign the downshift of  $\nu(\text{CO})$  on PdAu/KOAc compared to PdAu



to the presence of electron donating  $K^+$ .  $K^+$  increased the electron density on Pd and Au, enhancing the electron back donation from the metal into the non-bonding  $2\pi^*$  orbital of CO. This causes weakening of the CO bond reflected in the lower wavenumbers.<sup>[60-63]</sup> The intensity of the CO bands on Pd/SiO<sub>2</sub> and Au/SiO<sub>2</sub> were significantly lower in the presence of K, suggesting that K decreases the accessibility of Pd and Au for CO. On Pd/SiO<sub>2</sub> a redistribution from linear to bridged adsorbed CO was observed in the presence of the promoter, which is attributed to the formation of Pd-CO- $K^+$  (band at 1850 cm<sup>-1</sup>) from linear Pd-CO species.<sup>[10, 54, 59, 64-67]</sup> Bands of Pd-CO- $K^+$  and of bridged CO with a pronounced downshift may overlap in this region.

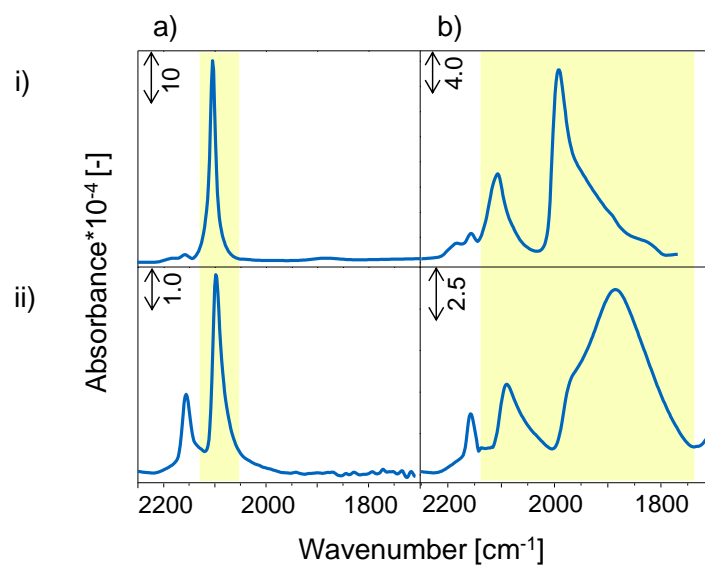


**Figure 2.5.** IR spectra of adsorbed CO at  $-150$  °C and 1.0 mbar partial pressure of CO on (i) unpromoted and (ii) KOAc promoted monometallic Au (a) and Pd (b).

While the experiments demonstrate qualitatively that K electronically influences the monometallic nanoparticles, a more detailed analysis requires exploring the changes also including the structural modifications induced by the promoter on bimetallic PdAu particles. The shift in the CO wavenumber as function of the surface PdAu geometry (ensemble effect)<sup>[48]</sup> is inevitably related to the electronic interaction between the two metals.<sup>[68-71]</sup> Alloying Pd with Au tends to shift the electron density toward the element with the larger fraction of empty valence states.<sup>[72]</sup> Lee et al. suggested that Au gains sp-type electrons and loses d-electrons whereas Pd loses sp-electrons and gains d-electrons.<sup>[73]</sup> As the reactivity is mainly determined by the d-orbitals, the increase in the electron density in Pd allows the stronger electron donation into the antibonding  $\pi^*$  orbitals of CO (shift of the CO stretching vibration to lower wavenumbers).<sup>[48]</sup> In contrast, the band of linearly adsorbed CO on Au in proximity to Pd shifts to higher wavenumbers, as the electron density in the d-bands of Au decreases by the interaction with Pd. Figure 2.6 schematically illustrates the adsorption of CO on Pd and Au in the different environments. It should be noted in passing that such electronic effects may be counteracted by a higher concentration of CO leading to an upward shift of the  $\nu(C=O)$  by CO dipole-dipole coupling. Dilution of Pd by Au reduces the probability of such dipole-dipole coupling.

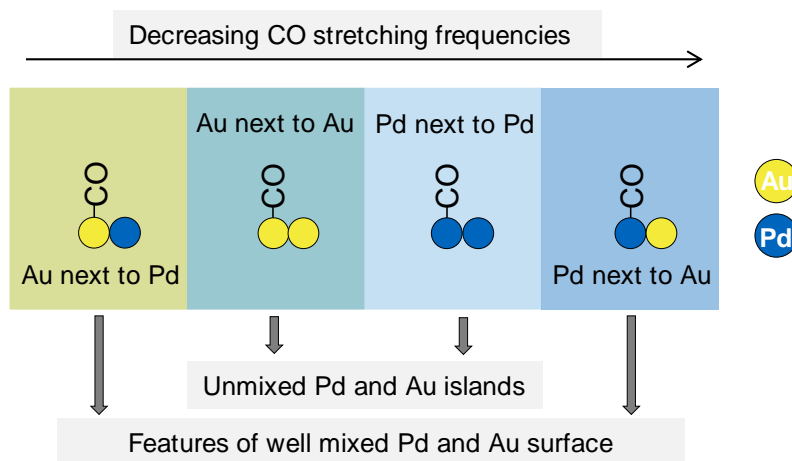


**Figure 2.6.** Linearly adsorbed CO on different PdAu environments.

The strong interaction of Pd with the acetate anion makes it likely that KOAc induces surface segregation in PdAu alloys. In absence of external factors it has been predicted<sup>[74]</sup> that Au segregates to the surface,<sup>[50, 75-79]</sup> because the surface free energy of Pd ( $2.043 \text{ J m}^{-2}$ )<sup>[80]</sup> is higher than that of Au ( $1.626 \text{ J m}^{-2}$ ).<sup>[81]</sup> However, the stronger interaction of Pd with the acetate anion is expected to revert this effect.

The relative intensities of the bands of linear and multiply bonded CO as well as their wavenumbers allow to characterize the degree of surface intermixing.<sup>[41]</sup> The probability of CO to adsorb in a multifold position is enhanced for larger Pd ensembles and, thus, the ratio of the band areas of linear to multifold adsorbed CO decreases. The surface concentrations as well as the fractions of linearly adsorbed CO (Table 2.2) were calculated from the integral areas of the bands using absorption coefficients  $\epsilon$  determined from the adsorption of CO on monometallic Au/SiO<sub>2</sub> and Pd/SiO<sub>2</sub>. In order to calculate  $\epsilon_{\text{linear}}(\text{Pd})$ , a ratio of  $\epsilon_{\text{linear}}/\epsilon_{\text{bridged}}$  of  $85 \cdot 10^7 \text{ cm mol}^{-1} / 3.3 \cdot 10^7 \text{ cm mol}^{-1}$  was assumed for Pd using absorption coefficients of Vannice et al.<sup>[45]</sup> (Appendix). The spectra of CO adsorbed on fresh and used as well as on parent and KOAc containing PdAu/SiO<sub>2</sub> are shown in Figure 2.7.

On the parent fresh catalyst (Figure 2.7ai), two bands for linearly bound CO on Au ( $2128$  and  $2106 \text{ cm}^{-1}$ )<sup>[44]</sup> and linearly bound CO on Pd ( $2084$  and  $2063 \text{ cm}^{-1}$ ) were observed. The band at  $2128 \text{ cm}^{-1}$  is attributed to CO on Au surrounded by Pd atoms (linear CO on “Au next to Pd”) and the band at  $2106 \text{ cm}^{-1}$  is assigned to CO linearly bound on Au in proximity to Au atoms (linear CO on “Au next to Au”). The band at  $2084 \text{ cm}^{-1}$  is associated with CO chemisorbed on larger Pd islands (linear CO on “Pd next to Pd”) and the band at  $2063 \text{ cm}^{-1}$  with linear CO adsorption on Pd surrounded by Au (linear CO on “Pd next to Au”).<sup>[82]</sup> Before reaction the surface of this catalyst (Figure 2.7ai) consisted mainly of larger Au and Pd domains as concluded from strong bands at  $2106 \text{ cm}^{-1}$  ( $8.7 \cdot 10^{-6} \text{ mol g}^{-1}$ , 33%) and  $2084 \text{ cm}^{-1}$  ( $12 \cdot 10^{-6} \text{ mol g}^{-1}$ , 45%). The intensities of the bands at  $2128$  and  $2063 \text{ cm}^{-1}$  (well-mixed PdAu surface) were low ( $2.9 \cdot 10^{-6} \text{ mol g}^{-1}$  (11%),  $3.0 \cdot 10^{-6} \text{ mol g}^{-1}$  (11%), respectively). The overall Pd/Au ratio of 1.28 indicates a slight Pd surface enrichment, which is attributed to a preferred stabilization of Pd via the interaction with H<sub>2</sub> during reduction.

The presence of KOAc caused the fraction of “Au next to Pd” and “Au next to Au” to decrease (from  $2.9 \cdot 10^{-6} \text{ mol g}^{-1}$  (11%) to  $0.9 \cdot 10^{-6} \text{ mol g}^{-1}$  (2%) and from  $8.7 \cdot 10^{-6} \text{ mol g}^{-1}$  (33%) to  $4.9 \cdot 10^{-6} \text{ mol g}^{-1}$  (12%), i.e., the surface concentration of Au decreased. The fraction of “Pd next to Au” increased in consequence significantly

from  $3.0 \cdot 10^{-6} \text{ mol g}^{-1}$  (11%) to  $18 \cdot 10^{-6} \text{ mol g}^{-1}$  (43%). The pronounced shift of the band for CO on “Pd next to Au” to  $2023 \text{ cm}^{-1}$  indicates that this change partially arises from CO adsorbed on the XRD amorphous Pd-KOAc species deposited on top of Au or mixed PdAu surfaces. Thus, the increase of this fraction cannot be directly assigned to the intermixing within a bimetallic particle. However, the surface concentration of “Pd next to Pd” increased from  $12 \cdot 10^{-6} \text{ mol g}^{-1}$  to  $18 \cdot 10^{-6} \text{ mol g}^{-1}$ , the overall surface Pd/Au ratio increased from 1.28 to 6.30 and the ratio of linear/bridged adsorbed CO decreased from 29.0 to 11.2 in presence of KOAc. Thus, Pd is concluded to migrate from the bulk to the surface.

XRD (Figure 2.3) indicates that the presence of KOAc removed some Pd from the alloy changing its nominal composition from Pd<sub>69</sub>Au<sub>31</sub> to Pd<sub>54</sub>Au<sub>46</sub> as well as leading to the formation of the Pd-KOAc adlayer. The high concentration of CO adsorbed on PdAu/KOAc/SiO<sub>2</sub> (Figure 2.7bi) is attributed to a much higher surface concentration of Pd, resulting from the segregation of Pd to the surface as well as from the presence of the acetate adlayer. The migration of Pd to the surface of the bimetallic particles accelerated the leaching of Pd and the associated reorganization of PdAu nanoparticles. The small fraction of Pd<sub>4</sub>Au<sub>96</sub> is attributed to excessive leaching in individual particles or to the formation of a core in a more complex particle.

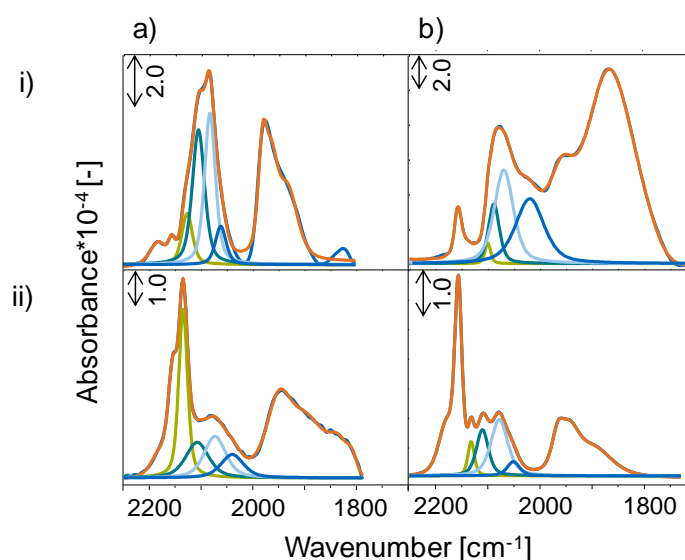


**Figure 2.7.** IR spectra of adsorbed CO at  $-150 \text{ }^{\circ}\text{C}$  and 1.0 mbar partial pressure of CO before (i) and washed after reaction (ii) on PdAu/SiO<sub>2</sub> (a) and PdAu/KOAc/SiO<sub>2</sub> (b). Green lines represent CO on Au and blue lines CO on Pd.

**Table 2.2.** Surface concentrations [ $10^{-6} \text{ mol/g}$ ] and corresponding fractions [%] in brackets of CO adsorbed on the catalysts before (B) and after (A) reaction.

Sample	Au next to Pd	Au next to Au	Pd next to Pd	Pd next to Au	linear/bridged CO	Pd/Au
	[ $10^{-6} \text{ mol/g}$ ] ([%])				[mol/g/mol/g]	[mol/g/mol/g]
PdAu/SiO <sub>2</sub> _B	2.9 (11)	8.7 (33)	12 (45)	3.0 (11)	29.0	1.28
PdAu/KOAc/SiO <sub>2</sub> _B	0.9 (2)	4.9 (12)	18 (43)	18 (43)	11.2	6.30
PdAu/SiO <sub>2</sub> _A	6.6 (36)	3.5 (19)	5.3 (28)	3.1 (17)	16.5	0.83
PdAu/KOAc/SiO <sub>2</sub> _A	0.6 (10)	1.6 (24)	3.6 (56)	0.7 (10)	20.5	1.97

On fresh and used PdAu/SiO<sub>2</sub> the fractions of unmixed “Au next to Au” decreased from  $8.7 \cdot 10^{-6} \text{ mol g}^{-1}$  (33%) to  $3.5 \cdot 10^{-6} \text{ mol g}^{-1}$  (19%) and “Pd next to Pd” decreased from  $12 \cdot 10^{-6} \text{ mol g}^{-1}$  (45%) to  $5.3 \cdot 10^{-6} \text{ mol g}^{-1}$  (28%) indicating a better intermixed, but overall Au-rich PdAu surface after reaction (Pd/Au ratio of 0.83). In accordance, the fractions of mixed “Au next to Pd” increased from  $2.9 \cdot 10^{-6} \text{ mol g}^{-1}$  (11%) to  $6.6 \cdot 10^{-6} \text{ mol g}^{-1}$  (36%), whereas the fraction of mixed “Pd next to Au” remained at  $\sim 3 \cdot 10^{-6} \text{ mol g}^{-1}$  (11%, 17%) on fresh and used PdAu/SiO<sub>2</sub> (Figure 2.7ai and 2.7aii). Assuming that “Pd next to Au” and “Au next to Pd” are neighbors in the same surface plane of the particle, both bands would have been expected to change in parallel. The absence of this observation guides us, therefore, to the conclusion that the outer layer of the bimetallic particles consists of mainly Au atoms, while Pd atoms are in a subsurface layer and, thus, not accessible for CO. It should be noted in passing that this observation agrees well with ion scattering results of Swartzfager et al.<sup>[83]</sup> Figure 2.8 shows an illustration of the hypothesized particle with an Au enriched surface and a Pd enriched subsurface layer.



**Figure 2.8.** Schematic intersection of a PdAu particle on spent PdAu/SiO<sub>2</sub> with an Au enriched surface and a Pd enriched subsurface layer.

In a related experiment, it was observed that on a used, unwashed PdAu/SiO<sub>2</sub> sample (Figure A2.4, Appendix) CO adsorption detects a lower Pd/Au ratio (0.62) than on the sample after the removal of acetic acid by washing (0.83). It is speculated that water induced surface segregation by strong interaction with Pd.

The Au surface enrichment is hypothesized to be the reason for the low activity of unpromoted PdAu/SiO<sub>2</sub>, as the generally proposed active site consists of two Pd atoms on a well-intermixed PdAu surface.<sup>[77, 84-85]</sup> The surface concentration of Pd on used PdAu/SiO<sub>2</sub> of 0.62 is too low for effectively coupling vinyl and acetate species considering that this reaction is the rate-determining step in VA synthesis. The initial high activity of PdAu/SiO<sub>2</sub> (Figure 2.2a) is exclusively related to the high Pd/Au surface ratio of 1.28 as rate enhancing factors like KOAc are absent and reactant concentrations remained constant. The drastic activity decrease is caused by Pd leaching lowering the Pd/Au surface ratio. This hinders the coupling of vinyl with acetate species but favor their decomposition to CO<sub>2</sub> and H<sub>2</sub>O, thus lowering the overall selectivity. The selectivity of industrial catalysts critically depend on the overall molar Pd/Au ratio and thus on the PdAu surface composition in equilibrium with leached Pd species.

In contrast, the presence of the KOAc promoter leads to an enrichment of Pd on PdAu/KOAc/SiO<sub>2</sub> (Pd/Au = 1.97) compared to unpromoted PdAu/SiO<sub>2</sub> (Pd/Au = 0.83) after reaction. The Pd/Au ratio of PdAu/KOAc/SiO<sub>2</sub> decreased from 6.30 before reaction to 1.97 after reaction, indicating that surface Pd leached into the acetic acid layer under reaction conditions. The low concentration of adsorbed CO on used PdAu/KOAc/SiO<sub>2</sub> (Figure 2.7bii) compared to used PdAu/SiO<sub>2</sub> (Figure 2.7aii) is attributed to the removal of the Pd-KOAc adlayer by washing.

The high activity of PdAu/KOAc/SiO<sub>2</sub> is attributed, in turn, to the fact that KOAc stabilizes a sufficient concentration of active Pd sites on the bimetallic PdAu surface. Interestingly, the high ratio of linear to bridged CO on PdAu/KOAc/SiO<sub>2</sub> (20.5) after reaction points to the presence of “optimized” Pd/Au ensembles (Figure 2.1). These ensembles reduce the probability of a direct combustion of adsorbed ethene or acetic acid, leading so to higher VA selectivity.

### 2.3.3. Formation of Reactive Pd Species in Presence and Absence of KOAc

After reaction PdAu/SiO<sub>2</sub>, PdAu/KOAc/SiO<sub>2</sub> and (Pd+Au)/KOAc/SiO<sub>2</sub> samples contained 64%, 53% and 92% of XRD amorphous Pd species. X-ray diffraction of fresh and used (Pd+Au)/KOAc/SiO<sub>2</sub> indicated an equilibrium between leached Pd<sup>2+</sup> (from Pd<sub>x</sub>Au<sub>y</sub>) and reincorporated Pd<sup>0</sup> (into Pd<sub>x</sub>Au<sub>y</sub>). As dissolved Pd<sup>2+</sup> complexes are generally accepted as active sites for the molecularly catalyzed VA synthesis,<sup>[86]</sup> the contribution of this route can at present not be excluded.

#### 2.3.3.1. Surface Structures in Presence and Absence of KOAc

In order to understand the presence of reactive Pd intermediates on Pd<sub>x</sub>Au<sub>y</sub> better and to study their interaction with KOAc during reaction, AcOH and AcOH/O<sub>2</sub> were adsorbed on Pd/SiO<sub>2</sub> and on PdAu/KOAc/SiO<sub>2</sub> under reaction conditions. The changes in the IR spectrum (1900–1300 cm<sup>-1</sup>) of Pd/SiO<sub>2</sub> after AcOH adsorption are shown in Figure 2.9a.

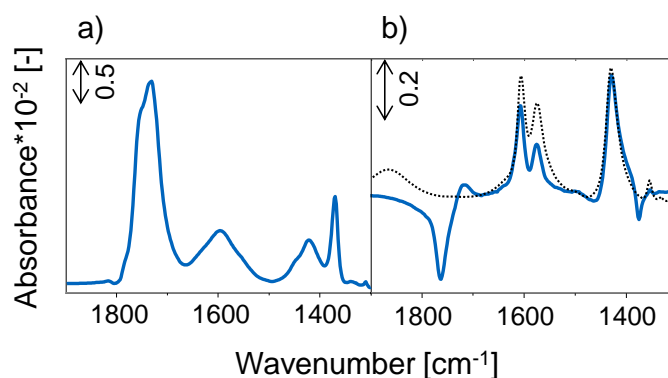


**Figure 2.9.** In situ IR spectra of Pd/SiO<sub>2</sub> (a) adsorbed with AcOH and (b) AcOH/O<sub>2</sub>. The black-dotted curve in (b) represents the spectrum of Pd(OAc)<sub>2</sub>/SiO<sub>2</sub>. Adsorption conditions: 16 mbar AcOH, 4.5 vol % O<sub>2</sub>, total flow of 20 mL/min; total pressure, 8.8 bar; temperature, 150 °C.

AcOH adsorbed in monomeric ( $\nu(\text{C}=\text{O})$  1767 cm<sup>-1</sup>) and dimeric form ( $\nu(\text{C}=\text{O})$  1737 cm<sup>-1</sup>) (Figure 2.10).<sup>[87-89]</sup>

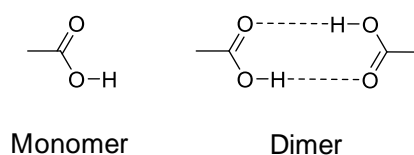


**Figure 2.10.** Structure of acetic acid monomer and dimer.

Small concentrations of acetic acid were converted into silyl-acetates by esterification of terminal Si-OH groups<sup>[90-91]</sup> as characterized by the asymmetric and symmetric carboxylate stretching vibrations at 1613 and 1586  $\text{cm}^{-1}$  ( $\nu_{\text{as}}(\text{COO})$ ) as well as at 1457 and 1434  $\text{cm}^{-1}$  ( $\nu_{\text{s}}(\text{COO})$ ). The band at 1380  $\text{cm}^{-1}$  is assigned to the symmetric  $\text{CH}_3$  bending vibration (Figure 2.9a).<sup>[87, 92]</sup> The presence of Pd acetate during AcOH adsorption on the fully reduced Pd/SiO<sub>2</sub> is excluded, because oxidizing reactants were absent.<sup>[12, 93-94]</sup>

The difference between the IR spectra of AcOH adsorbed in presence and absence of O<sub>2</sub> on Pd/SiO<sub>2</sub> is shown in Figure 2.9b in order to illustrate the changes on the catalyst surface during O<sub>2</sub> treatment in the presence of AcOH. The bands at 1610  $\text{cm}^{-1}$  and 1576  $\text{cm}^{-1}$  ( $\nu_{\text{as}}(\text{COO})$ ) and at 1432  $\text{cm}^{-1}$  ( $\nu_{\text{s}}(\text{COO})$ ) increased in intensity, while the  $\nu(\text{C}=\text{O})$  stretching vibration of AcOH at 1763  $\text{cm}^{-1}$  decreased. This decrease cannot be attributed to the combustion of AcOH with O<sub>2</sub>, because neither the formation of CO<sub>2</sub> nor the formation of carbonates was detected. Therefore, the decrease of  $\nu(\text{C}=\text{O})$  is attributed to the competitive adsorption of O<sub>2</sub> and to the formation of trimeric Pd<sub>3</sub>(OAc)<sub>6</sub><sup>[88, 95]</sup> (Figure 2.11a) and linear, dimeric (Pd<sub>2</sub>(OAc)<sub>4</sub>)<sup>[95]</sup> (Figure 2.11d) dissolved in the acetic acid layer. The equilibrium between Pd<sub>3</sub>(OAc)<sub>6</sub> and Pd<sub>2</sub>(OAc)<sub>4</sub> in AcOH favors the former.<sup>[95]</sup> The increase in the corresponding symmetric and asymmetric COO stretching vibrations agrees perfectly with those of the Pd(OAc)<sub>2</sub>/SiO<sub>2</sub> reference sample presented as black dotted curve in Figure 2.9b. However, acetate vibrations of Pd(OAc)<sub>2</sub>/SiO<sub>2</sub> disappeared upon heating to 150 °C due to decomposition in the absence of AcOH. This suggests that Pd<sub>3</sub>(OAc)<sub>6</sub>/Pd<sub>2</sub>(OAc)<sub>4</sub> are thermally stabilized only in presence of AcOH. The structure of trimeric Pd<sub>3</sub>(OAc)<sub>6</sub> is illustrated in Figure 2.11a<sup>[96]</sup> where the acetate ligands are bound in a bridging (B) mode (Figure 2.11b) to two Pd sites with a square planar configuration of Pd<sup>2+</sup> (d<sup>8</sup>). Figure 2.11c illustrates a terminal (T) acetate bound to Pd.

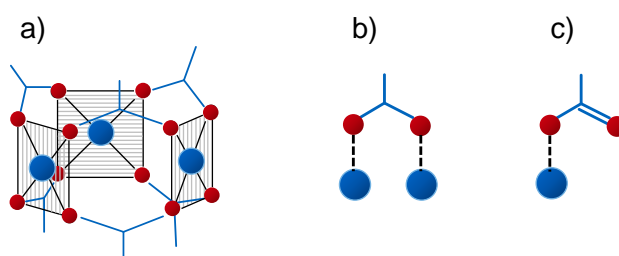


**Figure 2.11.** Molecular structure of a) trimeric Pd<sub>3</sub>(OAc)<sub>6</sub>, b) bridging (B) acetate on two Pd atoms and c) terminal (T) acetate on Pd. Blue balls represent Pd, red balls oxygen atoms.

The IR spectrum of PdAu/KOAc/SiO<sub>2</sub> during AcOH adsorption at 150 °C and 9 bar total pressure is shown in Figure 2.12a. The surface concentration of AcOH on this promoted catalyst ( $\nu(\text{C}=\text{O})$  1762, 1725  $\text{cm}^{-1}$ ) increased compared to Pd/SiO<sub>2</sub> (black dotted curve), which was caused by KOAc that retained additional AcOH. The high intensity of the  $\nu(\text{C}=\text{O})$  vibration located at 1725  $\text{cm}^{-1}$  suggested the formation of dimeric

KOAc(HOAc)<sub>n</sub> (n = 1, 2) species.<sup>[97]</sup> In addition, the presence of K<sup>+</sup> caused an overall conversion of AcOH to KOAc, demonstrated by the increasing intensity of acetate bands ( $\nu_{\text{as}}(\text{COO}) = 1500\text{-}1600\text{ cm}^{-1}$ ,  $\nu_{\text{s}}(\text{COO}) = 1400\text{-}1480\text{ cm}^{-1}$ ,<sup>[98]</sup> Figure 2.12a).

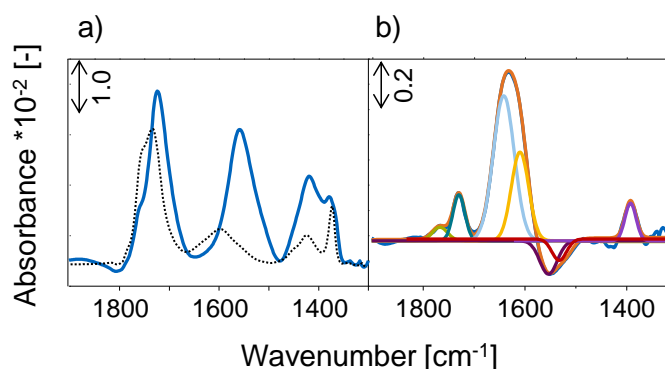
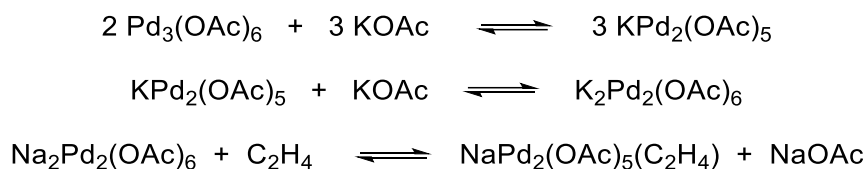


**Figure 2.12.** In situ IR spectra of PdAu/KOAc/SiO<sub>2</sub> adsorbed with (a) AcOH and (b) AcOH/O<sub>2</sub>. The black dotted curve in a) indicates AcOH on Pd/SiO<sub>2</sub>. 16 mbar AcOH, 4.5 vol % O<sub>2</sub>, total flow of 20 mL/min; total pressure, 8.8 bar; temperature, 150 °C.

The structural changes of the acetate species during exposure to the AcOH/O<sub>2</sub> mixture compared to pure AcOH are shown in Figure 2.12b. The bands at 1767 and 1730 cm<sup>-1</sup> result from  $\nu(\text{C}=\text{O})$  of AcOH monomers and dimers. It should be noted that Augustine et al.<sup>[88]</sup> assigned the band at 1730 cm<sup>-1</sup> to  $\nu(\text{C}=\text{O})$  of terminal acetate<sup>[16, 99]</sup> bound to surface Pd atoms<sup>[100]</sup> or adsorbed AcOH.<sup>[11, 101]</sup> The assignment to adsorbed AcOH appears unlikely, as the band at 1730 cm<sup>-1</sup> hardly changed its intensity after purging with N<sub>2</sub>. Thus, we conclude that terminal acetates are stabilized on Pd in Pd<sub>x</sub>Au<sub>y</sub> nanoparticles, which differ from the acetates in the molecular dissolved Pd<sub>3</sub>(OAc)<sub>6</sub> because the  $\nu_{\text{as}}(\text{COO})$  vibration of the bridging acetates in Pd<sub>3</sub>(OAc)<sub>6</sub> were found at 1610 cm<sup>-1</sup>.<sup>[88]</sup> The terminal acetate species at 1730 cm<sup>-1</sup> were not observed in the difference spectra of Pd/SiO<sub>2</sub> (Figure 2.9b), suggesting that KOAc favors the formation of these terminal acetates on PdAu. On PdAu/KOAc/SiO<sub>2</sub>, a band at 1635 cm<sup>-1</sup> appeared, in parallel to the decrease in intensity of the  $\nu_{\text{as}}(\text{COO})$  vibration of KOAc at 1575 cm<sup>-1</sup>.

Augustine et al.<sup>[88]</sup> observed a similar band at 1651 cm<sup>-1</sup> and assigned it to the  $\nu(\text{C}=\text{C})$  stretching vibrations in vinyl acetate, while the band was attributed to mixed “Li-Pd acetate” on a molecular Li-Pd acetate catalyst.<sup>[102]</sup> In the absence of ethene, the band at 1635 cm<sup>-1</sup> cannot be caused by  $\nu(\text{C}=\text{C})$  vibrations in our studies. We assigned it, therefore, to a combination of bands arising from terminal acetates<sup>[16]</sup> at 1642 cm<sup>-1</sup> and bridging acetates at 1610 cm<sup>-1</sup>. The contributions were quantified by fitting the band at 1635 cm<sup>-1</sup>. This ratio of terminal to bridging (“T/B”) acetates is characteristic for the different dimer species as K<sub>2</sub>Pd<sub>2</sub>(OAc)<sub>6</sub>, KPd<sub>2</sub>(OAc)<sub>5</sub> and Pd<sub>2</sub>(OAc)<sub>4</sub> exhibit ratios of 4/2, 2/3 and 0/4, respectively (Figure 2.13). The determined T/B ratio of 4/2 points to the formation of K<sub>2</sub>Pd<sub>2</sub>(OAc)<sub>6</sub> partly solved in the acetic acid layer. The presence of trimeric Pd<sub>3</sub>(OAc)<sub>6</sub> and dimeric Pd<sub>2</sub>(OAc)<sub>4</sub> was excluded as both do not contain K<sup>+</sup> cations and have only bridging acetates. The Pd<sub>3</sub>(OAc)<sub>6</sub> species formed were hypothesized to interact with KOAc<sup>[6, 88]</sup> and to be essentially converted to dimeric species by KOAc.<sup>[14, 16]</sup> Traces of unsaturated KPd<sub>2</sub>(OAc)<sub>5</sub> with a T/B ratio of 2/3 could not be excluded as it is in equilibrium with K<sub>2</sub>Pd<sub>2</sub>(OAc)<sub>6</sub> (Scheme 2.2).<sup>[103]</sup> Under the in situ conditions applied and

the excess of KOAc (overall Pd/K ratio of 1/4) present in the promoted catalyst, we expect, however, that the equilibrium favors  $\text{K}_2\text{Pd}_2(\text{OAc})_6$ . In agreement with this conclusion, studies of the homogeneous catalytic VA synthesis by palladium acetate in NaOAc/AcOH solution indicate  $\text{Na}_2\text{Pd}_2(\text{OAc})_6$  as active species that is converted to  $\text{NaPd}_2(\text{OAc})_5(\text{C}_2\text{H}_4)$  by attack of  $\text{C}_2\text{H}_4$  (Scheme 2.2) to finally form  $\text{Pd}^0$  and VA.<sup>[13, 15, 19]</sup>



**Scheme 2.2.** Equilibrium between  $\text{Pd}_3(\text{OAc})_6$ ,  $\text{KPd}_2(\text{OAc})_5$ ,  $\text{K}_2\text{Pd}_2(\text{OAc})_6$ .

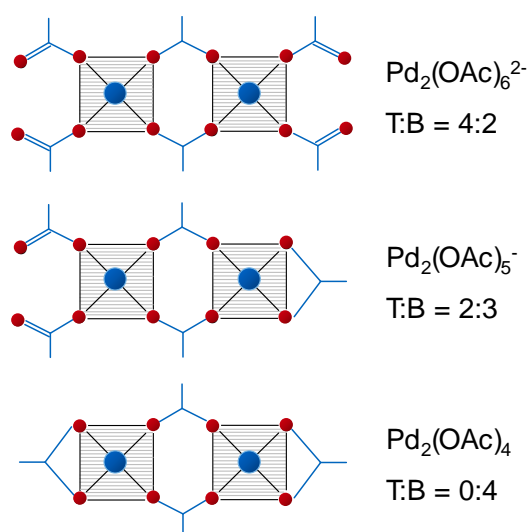


**Figure 2.13.** Dimeric palladium acetate species (T = terminal, B = bridging, bidentate acetate). Blue balls display Pd and red balls O atoms.

In summary, KOAc retains AcOH on the catalyst and favors formation of acetates, which are either transformed to terminal Pd acetates on PdAu nanoparticles surface (active sites in the pathways catalyzed by the solid surface) or to  $\text{Pd}_3(\text{OAc})_6$  to create dimeric  $\text{K}_2\text{Pd}_2(\text{OAc})_6$  partly solved in the AcOH layer. ( $\text{M}_2\text{Pd}_2(\text{OAc})_6$  as active site/complex in the pathways catalyzed by a molecular catalyst.<sup>[13-14]</sup>) The formation of homogeneous  $\text{K}_2\text{Pd}_2(\text{OAc})_6$  on the heterogeneous PdAu/KOAc catalyst and the presence of Pd- acetate esters on the  $\text{Pd}_x\text{Au}_y$  surface indicates a direct link between these two pathways of catalyzed VA synthesis. In consequence,  $\text{K}_2\text{Pd}_2(\text{OAc})_6$  is proposed to be the key intermediate in the reordering process of PdAu nanoparticles.

### 2.3.3.2. Exploring the Catalysts in the Working State

While the conditions used so far allowed the qualitative and quantitative analysis of the surface states of the active nanoparticles and molecular complexes, the additional presence of ethene is expected to affect the equilibria, requiring a closer analysis of this situation.



The IR spectrum of the (unwashed) K free PdAu/SiO<sub>2</sub> catalyst after reaction (SiO<sub>2</sub> support vibrations are subtracted) is shown in Figure 2.14a. The bands at 1785 and 1740 cm<sup>-1</sup> are typical  $\nu(\text{C}=\text{O})$  vibrations of AcOH monomers and dimers. Asymmetric and symmetric carboxylate stretching vibrations of bridging acetates in trimeric Pd<sub>3</sub>(OAc)<sub>6</sub> (Figure 2.11a) were observed at 1610 and 1436 cm<sup>-1</sup>. Additionally, the orange-brown color of the washing water of PdAu/SiO<sub>2</sub> after reaction points to the formation of Pd<sub>3</sub>(OAc)<sub>6</sub>. Thus, significant concentrations of Pd<sub>3</sub>(OAc)<sub>6</sub> were stable under the reducing influence of 60 vol% C<sub>2</sub>H<sub>4</sub> during reaction (150 °C and 9 bar total pressure). This agrees well with the fact that trimeric Pd<sub>3</sub>(OAc)<sub>6</sub> is one of the most stable forms of Pd(II) acetate in solution.<sup>[16, 95]</sup>

However, Pd(OAc)<sub>2</sub> impregnated on SiO<sub>2</sub> in absence of AcOH started to decompose at ~150 °C. Thus, the thermal and reductive stability of Pd<sub>3</sub>(OAc)<sub>6</sub> strongly depends on the presence and thickness of the acetic acid film, which we hypothesize to inhibit the reduction of Pd<sub>3</sub>(OAc)<sub>6</sub> to Pd<sup>0</sup>. To test this, PdAu/SiO<sub>2</sub> was quenched in C<sub>2</sub>H<sub>4</sub> instead of N<sub>2</sub> after VA synthesis. Indeed, the colorless washing water of this PdAu/SiO<sub>2</sub> catalyst after reaction contained black, dispersed Pd<sup>0</sup> particles from the reduction of Pd<sub>3</sub>(OAc)<sub>6</sub> by C<sub>2</sub>H<sub>4</sub> as soon as the protective AcOH layer was removed during quenching.

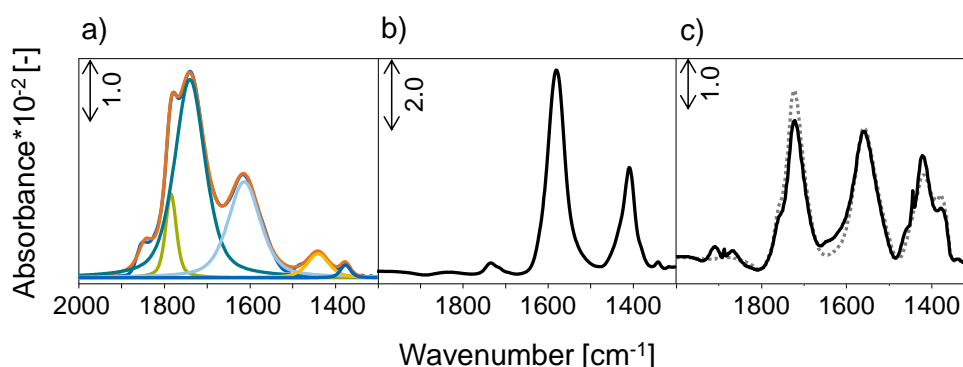


**Figure 2.14.** IR spectra of used, unwashed (a) PdAu/SiO<sub>2</sub>, (b) PdAu/KOAc/SiO<sub>2</sub> recorded at r.t. and (c) in situ IR spectra of PdAu/KOAc/SiO<sub>2</sub> adsorbed with AcOH (black dotted curve) and with AcOH/O<sub>2</sub>/C<sub>2</sub>H<sub>4</sub> (black curve). Adsorption conditions: 16 mbar AcOH, 4.5 vol % O<sub>2</sub>, 60 vol % C<sub>2</sub>H<sub>4</sub>; total flow of 20 mL/min; total pressure of 8.8 bar; temperature of 150 °C.

The IR spectrum of unwashed PdAu/KOAc/SiO<sub>2</sub> after reaction is shown in Figure 2.14b. In contrast to PdAu/SiO<sub>2</sub>, only KOAc vibrations ( $\nu_{\text{as}}(\text{COO})$  1575 cm<sup>-1</sup>,  $\nu_{\text{s}}(\text{COO})$  1411 cm<sup>-1</sup>) were observed, while bands of AcOH, Pd<sub>3</sub>(OAc)<sub>6</sub> or K<sub>2</sub>Pd<sub>2</sub>(OAc)<sub>6</sub> were not found. We conclude that AcOH desorbed completely during 2 h purging with N<sub>2</sub> at 150 °C. The absence of Pd<sub>3</sub>(OAc)<sub>6</sub> is reasonable as KOAc shifts the equilibrium (Scheme 2.1) to the side of K<sub>2</sub>Pd<sub>2</sub>(OAc)<sub>6</sub> as observed experimentally under working conditions for PdAu/KOAc/SiO<sub>2</sub> during AcOH/O<sub>2</sub> adsorption.

In order to study PdAu/KOAc/SiO<sub>2</sub> under reaction conditions, Figure 2.14 c compares the in situ IR spectra of PdAu/KOAc/SiO<sub>2</sub> adsorbed with AcOH (black dotted curve) and with AcOH/O<sub>2</sub>/C<sub>2</sub>H<sub>4</sub> (black curve). Bands for the CH<sub>2</sub> out of plane (1888 cm<sup>-1</sup>) and the CH<sub>2</sub> in plane (1445 cm<sup>-1</sup>) deformation vibrations of C<sub>2</sub>H<sub>4</sub> are present.<sup>103-104</sup> Asymmetric carboxylate stretch vibrations of terminal acetates at 1642 cm<sup>-1</sup> and small amounts

of bridging acetates at  $1611\text{ cm}^{-1}$  confirm the presence of far less  $\text{K}_2\text{Pd}_2(\text{OAc})_6$  species during reducing  $\text{AcOH}/\text{O}_2/\text{C}_2\text{H}_4$  treatment than in oxidizing  $\text{AcOH}/\text{O}_2$  (Figure 2.12b).

The reason for the absence of  $\text{K}_2\text{Pd}_2(\text{OAc})_6$  bands on  $\text{PdAu}/\text{KOAc}/\text{SiO}_2$  after reaction and the presence of  $\text{K}_2\text{Pd}_2(\text{OAc})_6$  during  $\text{AcOH}/\text{O}_2/\text{C}_2\text{H}_4$  to a lesser extent than during  $\text{AcOH}/\text{O}_2$  could be the facile reduction and decomposition of  $\text{K}_2\text{Pd}_2(\text{OAc})_6$  to  $\text{Pd}^0$ . Nakamura et al.<sup>[6]</sup> reported that Pd acetate with KOAc was easily reduced to Pd black by forming VA, while Pd acetate alone did not react. They concluded that KOAc weakens Pd-O bonds in Pd acetate,<sup>[6]</sup> which agrees with the present observation of the  $\text{K}_2\text{Pd}_2(\text{OAc})_6$  intermediate, while  $\text{Pd}_3(\text{OAc})_6$  was not formed. In fact, Pandey et al. suggested that bridging acetates in  $\text{Pd}_3(\text{OAc})_6$  are far less reactive towards olefins than the (labile) terminal acetates in dimeric  $\text{K}_2\text{Pd}_2(\text{OAc})_6$ .<sup>[13-14, 16]</sup>

In order to test the differences in reducibility of  $\text{K}_2\text{Pd}_2(\text{OAc})_6$  and  $\text{Pd}_3(\text{OAc})_6$ , silica supported  $\text{Pd}(\text{OAc})_2$  and  $\text{Pd}(\text{OAc})_2/\text{KOAc}$  were used as catalysts, following the formation of  $\text{Pd}^0$  particles by XRD (Figure A2.5, Appendix). The full width at half maximum of Pd reflections from  $\text{Pd}(\text{OAc})_2/\text{KOAc}$  was generally smaller than those of unpromoted  $\text{Pd}(\text{OAc})_2$ . The deduced formation of larger particles points to the lower stability of  $\text{K}_2\text{Pd}_2(\text{OAc})_6$  compared to  $\text{Pd}_3(\text{OAc})_6$ . Thus, we hypothesize that the addition of promoter acetates also increases the contribution of the molecularly catalyzed pathway of VA synthesis.<sup>[104]</sup>

### 2.3.4. Dynamic Reconstruction of KOAc Promoted and Unpromoted $\text{PdAu}/\text{SiO}_2$

Pd containing particles on fresh  $\text{PdAu}/\text{SiO}_2$  deplete in Pd by oxidative leaching of  $\text{Pd}_3(\text{OAc})_6$  into the acetic acid layer. This layer protects  $\text{Pd}_3(\text{OAc})_6$  from decomposition and reduction. Thus, reincorporation of  $\text{Pd}^0$  formed by reduction of  $\text{Pd}_3(\text{OAc})_6$  with ethene into  $\text{PdAu}$  particles is not favored.<sup>[6]</sup> Consequently, Au enriched  $\text{PdAu}$  particles are formed (Figure 2.15).

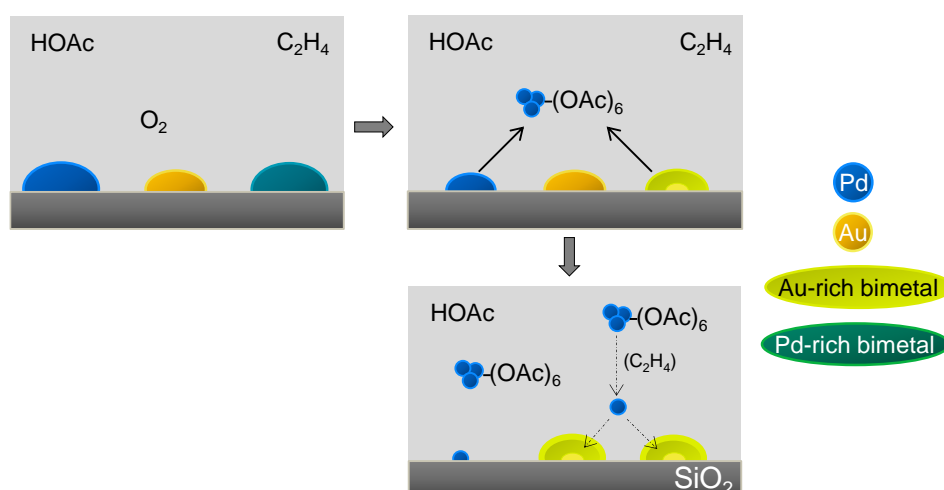


**Figure 2.15.** Proposed reordering mechanism of  $\text{PdAu}/\text{SiO}_2$  during VAS. Pd is represented in blue, Au in yellow and the bimetallic  $\text{PdAu}$  particles in green.

Fresh  $\text{PdAu}/\text{KOAc}/\text{SiO}_2$  contains Pd- and Au-rich and  $\text{Pd}_{54}\text{Au}_{46}$  bimetallic particles. KOAc adsorbed on  $\text{PdAu}$  particles leads to the migration of Pd from the bulk to the surface and finally to oxidative leaching of mixed

$K_2Pd_2(OAc)_6$ . In contrast to  $Pd_3(OAc)_6$ ,  $K_2Pd_2(OAc)_6$  is easily reduced by ethene to  $Pd^0$ , which either forms dispersed  $Pd^0$  clusters in AcOH or reincorporates into the PdAu particles to maintain the stable  $Pd_1Au_1$  bulk phase with a Pd-enriched PdAu surface (Figure 2.16).

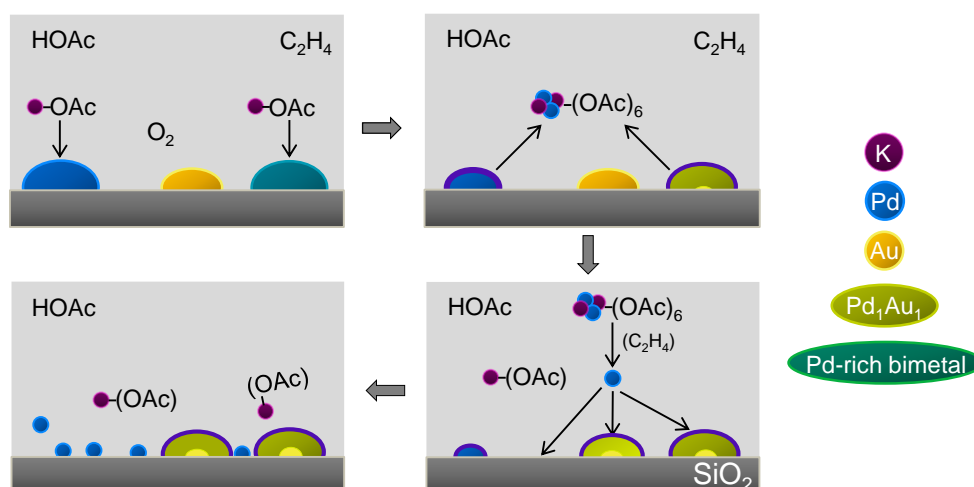


**Figure 2.16.** Proposed reordering mechanism for PdAu/KOAc/SiO<sub>2</sub> during VA synthesis. Pd is represented in blue, Au in yellow, K in violet and the bimetallic PdAu particles in green.

## 2.4. Conclusions

KOAc promotion of bimetallic PdAu/SiO<sub>2</sub> enhanced the activity by a factor of 10 and the selectivity by approximately 20 %. In the absence of KOAc, trimeric  $Pd_3(OAc)_6$  is oxidatively leached from the bimetallic particles into the AcOH layer. AcOH stabilized  $Pd_3(OAc)_6$  against reduction by ethene, thus lowering the probability for  $Pd^0$  to reincorporate into PdAu particles. Consequently,  $Pd_1Au_1$  enriched nanoparticles form the bulk of the supported particles. The low activity and selectivity of unpromoted PdAu/SiO<sub>2</sub> is attributed to the low Pd concentration on the Au rich bimetallic surfaces, favoring decomposition to CO<sub>2</sub> and H<sub>2</sub>O rather than VA formation.

Potassium acts as electronic promoter for Pd and Au and as agent to stabilize Pd on the surface of the bimetallic particles forming the active sites. Strong interactions between K and Pd led to the formation of dimeric  $K_2Pd_2(OAc)_6$  species, acting as organometallic catalyst in the condensed AcOH layer. KOAc transfers acetates to Pd, thereby increasing the acetate concentration for the rate-determining step to VA. The probability for ethene to adsorb and combust is so statistically lowered, increasing the selectivity VA.

## 2.5. Acknowledgements

Financial support by Wacker Chemie AG and fruitful discussions within the Wacker-Institut für Siliciumchemie is gratefully acknowledged. Xaver Hecht and Martin Neukamm are acknowledged for their experimental support.

**2.6. References**

- [1] Y. F. Han, J. H. Wang, D. Kumar, Z. Yan, D. W. Goodman, *J. Catal.* **2005**, *232*, 467-475.
- [2] G. Ertl, H. Knözinger, J. Weitkamp, *Handbook of Heterogeneous Catalysis, Vol. 5*, Wiley-VCH, Weinheim, Germany, **1997**.
- [3] M. Chen, D. Kumar, C.-W. Yi, D. W. Goodman, *Science* **2005**, *310*, 291-293.
- [4] M.-M. Pohl, J. Radnik, M. Schneider, U. Bentrup, D. Linke, A. Brückner, E. Ferguson, *J. Catal.* **2009**, *262*, 314-323.
- [5] S. Simson, A. Jentys, J. A. Lercher, *J. Phys. Chem. C* **2013**, *117*, 8161-8169.
- [6] S. Nakamura, T. Yasui, *J. Catal.* **1970**, *17*, 366-374.
- [7] S. Koukiou, M. Konsolakis, R. M. Lambert, I. V. Yentekakis, *Appl. Catal. B* **2007**, *76*, 101-106.
- [8] V. Pitchon, M. Guenin, H. Praliaud, *Appl. Catal.* **1990**, *63*, 333-343.
- [9] H. W. K. Tom, C. M. Mate, X. D. Zhu, J. E. Crowell, Y. R. Shen, G. A. Somorjai, *Surf. Sci.* **1986**, *172*, 466-476.
- [10] M. Gravelle-Rumeau-Maillot, V. Pitchon, G. A. Martin, H. Praliaud, *Appl. Catal. A* **1993**, *98*, 45-59.
- [11] E. A. Crathorne, D. Macgowan, S. R. Morris, A. P. Rawlinson, *J. Catal.* **1994**, *149*, 254-267.
- [12] R. G. Brown, J. M. Davidson, C. Triggs, *Am. Chem. Soc., Div. Petrol. Chem.* **1969**, *14*, B23-B28.
- [13] R. N. Pandey, P. M. Henry, *Canad. J. Chem.* **1975**, *53*, 1833-1841.
- [14] R. N. Pandey, P. M. Henry, *Canad. J. Chem.* **1974**, *52*, 1241-1247.
- [15] D. D. Kragten, R. A. van Santen, M. Neurock, J. J. Lerou, *J. Phys. Chem. A* **1999**, *103*, 2756-2765.
- [16] D. D. Kragten, R. A. van Santen, M. K. Crawford, W. D. Provine, J. J. Lerou, *Inorg. Chem.* **1999**, *38*, 331-339.
- [17] D. P. Bancroft, F. A. Cotton, L. R. Falvello, W. Schwotzer, *Polyhedron* **1988**, *7*, 615-621.
- [18] A. C. Skapski, M. L. Smart, *J. Chem. Soc., Chem. Commun.* **1970**, 658-659.
- [19] S. Winstein, J. McCaskie, H.-B. Lee, P. M. Henry, *J. Am. Chem. Soc.* **1976**, *98*, 6913-6918.
- [20] G. A. Somorjai, A. M. Contreras, M. Montano, R. M. Rioux, *Proc. Natl. Acad. Sci.* **2006**, *103*, 10577-10583.
- [21] H.-J. Eberle, R. Heidenreich, J. Weis, *Ger. DE 10 2006 058 800 A1 2008.06.19*, **2008**.
- [22] L. Vegard, *Z. Physik* **1921**, *5*, 17-26.
- [23] G. Mirth, F. Eder, J. A. Lercher, *Appl. Spectrosc.* **1994**, *48*, 194-197.
- [24] W. D. Provine, P. L. Mills, J. J. Lerou, *Stud. Surf. Sci. Catal.* **1996**, *101*, 191-200.
- [25] T. T. David, *Plat. Metals Rev.* **2004**, *48*, 169-172.
- [26] Y. F. Han, D. Kumar, D. W. Goodman, *J. Catal.* **2005**, *230*, 353-358.
- [27] P. S. Voskanyan, *Catal. Ind.* **2010**, *2*, 167-172.
- [28] S. N. Reifsnnyder, H. H. Lamb, *J. Phys. Chem. B* **1998**, *103*, 321-329.
- [29] R. J. Davis, M. Boudart, *J. Phys. Chem.* **1994**, *98*, 5471-5477.
- [30] N. Macleod, J. M. Keel, R. M. Lambert, *Appl. Catal. A* **2004**, *261*, 37-46.
- [31] Q. Smejkal, D. Linke, U. Bentrup, M. M. Pohl, H. Berndt, M. Baerns, A. Brückner, *Appl. Catal. A* **2004**, *268*, 67-76.

- [32] R. Pellegrini, G. Leofanti, G. Agostini, L. Bertinetti, S. Bertarione, E. Groppo, A. Zecchina, C. Lamberti, *J. Catal.* **2009**, *267*, 40-49.
- [33] E. G. Allison, G. C. Bond, *Catal. Rev.* **1972**, *7*, 233 - 289.
- [34] H. Okamoto, T. Massalski, *J. Phase Equilib.* **1985**, *6*, 229-235.
- [35] R. Oriani, W. K. Murphy, *Acta Metall.* **1962**, *10*, 879-885.
- [36] A. Wolf, F. Schüth, *Appl. Catal. A* **2002**, *226*, 1-13.
- [37] X. Liu, A. Wang, T. Zhang, D.-S. Su, C.-Y. Mou, *Catal. Today* **2011**, *160*, 103-108.
- [38] A. Wang, X. Y. Liu, C.-Y. Mou, T. Zhang, *J. Catal.* **2013**, *308*, 258-271.
- [39] W. K. Kuhn, J. Szanyi, D. W. Goodman, *Surf. Sci.* **1992**, *274*, L611-L618.
- [40] M. Mihaylov, K. Hadjiivanov, H. Knözinger, *Catal. Lett.* **2001**, *76*, 59-63.
- [41] T. Montanari, L. Castoldi, L. Lietti, G. Busca, *Appl. Catal. A* **2011**, *400*, 61-69.
- [42] T. Montanari, R. Matarrese, N. Artioli, G. Busca, *Appl. Catal. B* **2011**, *105*, 15-23.
- [43] T. P. Beebe, P. Gelin, J. T. Yates Jr, *Surf. Sci.* **1984**, *148*, 526-550.
- [44] M. Mihaylov, H. Knözinger, K. Hadjiivanov, B. C. Gates, *Chem. Ing. Tech.* **2007**, *79*, 795-806.
- [45] M. A. Vannice, S. Y. Wang, *J. Phys. Chem.* **1981**, *85*, 2543-2546.
- [46] R. P. Eischens, S. A. Francis, W. A. Pliskin, *J. Phys. Chem.* **1956**, *60*, 194-201.
- [47] J. Shen, J. Hill, R. Watwe, S. G. Podkolzin, J. A. Dumesic, *Catal. Lett.* **1999**, *60*, 1-9.
- [48] E. L. Kugler, M. Boudart, *J. Catal.* **1979**, *59*, 201-210.
- [49] D. C. Meier, D. W. Goodman, *J. Am. Chem. Soc.* **2004**, *126*, 1892-1899.
- [50] M. S. Chen, K. Luo, T. Wei, Z. Yan, D. Kumar, C. W. Yi, D. W. Goodman, *Catal. Today* **2006**, *117*, 37-45.
- [51] E. Ozensoy, D. Wayne Goodman, *Phys. Chem. Chem. Phys.* **2004**, *6*, 3765-3778.
- [52] T. Wei, J. Wang, D. W. Goodman, *J. Phys. Chem. C* **2007**, *111*, 8781-8788.
- [53] F. Gao, D. W. Goodman, *Chem. Soc. Rev.* **2012**, *41*, 8009-8020.
- [54] P. A. J. M. Angevaere, H. A. C. M. Hendrickx, V. Ponec, *J. Catal.* **1988**, *110*, 11-17.
- [55] N. D. Lang, A. R. Williams, *Phys. Rev. Lett.* **1976**, *37*, 212-215.
- [56] N. D. Lang, A. R. Williams, *Phys. Rev. B* **1978**, *18*, 616-636.
- [57] J. W. Gadzuk, *Surf. Sci.* **1967**, *6*, 133-158.
- [58] H. Praliaud, M. Primet, G.-A. Martin, *Applications of Surface Science* **1983**, *17*, 107-123.
- [59] L. F. Liotta, G. A. Martin, G. Deganello, *J. Catal.* **1996**, *164*, 322-333.
- [60] J. E. Crowell, E. L. Garfunkel, G. A. Somorjai, *Surf. Sci.* **1982**, *121*, 303-320.
- [61] G. Blyholder, *J. Phys. Chem.* **1964**, *68*, 2772-2777.
- [62] C. T. Campbell, D. W. Goodman, *Surf. Sci.* **1982**, *123*, 413-426.
- [63] E. L. Garfunkel, J. E. Crowell, G. A. Somorjai, *J. Phys. Chem.* **1982**, *86*, 310-313.
- [64] A. F. Gusovius, T. C. Watling, R. Prins, *Appl. Catal. A* **1999**, *188*, 187-199.
- [65] V. Pitchon, M. Primet, H. Praliaud, *Appl. Catal.* **1990**, *62*, 317-334.
- [66] K. J. Uram, L. Ng, M. Folman, J. T. Yates, *J. Chem. Phys.* **1986**, *84*, 2891-2895.
- [67] V. Dose, J. Rogozik, A. M. Bradshaw, K. C. Prince, *Surf. Sci.* **1987**, *179*, 90-100.
- [68] N. F. Mott, *Proc. Phys. Soc.* **1935**, *47*, 571-588.

- [69] P. Liu, J. K. Nørskov, *Phys. Chem. Chem. Phys.* **2001**, 3, 3814-3818.
- [70] A. Couper, D. D. Eley, *Discuss. Faraday Soc.* **1950**, 8, 172-184.
- [71] M. J. Kim, W. F. Flanagan, *Acta Metall.* **1967**, 15, 747-752.
- [72] J. A. Rodriguez, D. W. Goodman, *Science* **1992**, 257, 897-903.
- [73] Y.-S. Lee, Y. Jeon, Y.-M. Chung, K.-Y. Lim, C.-N. Whang, S.-J. Oh, *J. Korean Phys. Soc.* **2000**, 37, 451-455.
- [74] A. Christensen, A. V. Ruban, P. Stoltze, K. W. Jacobsen, H. L. Skriver, J. K. Nørskov, F. Besenbacher, *Phys. Rev. B* **1997**, 56, 5822-5834.
- [75] P. Varga, G. Hetzendorf, *Surf. Sci.* **1985**, 162, 544-549.
- [76] G. Maire, L. Hilaire, P. Legare, F. G. Gault, A. O'Conneide, *J. Catal.* **1976**, 44, 293-299.
- [77] K. Luo, T. Wei, C. W. Yi, S. Axnanda, D. W. Goodman, *J. Phys. Chem. B* **2005**, 109, 23517-23522.
- [78] C. W. Yi, K. Luo, T. Wei, D. W. Goodman, *J. Phys. Chem. B* **2005**, 109, 18535-18540.
- [79] S. J. Mejía-Rosales, C. Fernández-Navarro, E. Pérez-Tijerina, J. M. Montejano-Carrizales, M. José-Yacamán, *J. Phys. Chem. B* **2006**, 110, 12884-12889.
- [80] L. Z. Mezey, J. Giber, *Jpn. J. Appl. Phys.* **1982**, 21, 1569-1571.
- [81] R. Anton, H. Eggers, J. Veletas, *Thin Solid Films* **1993**, 226, 39-47.
- [82] D. Rainer, *J. Vac. Sci. Technol. A* **1997**, 15, 1653-1662.
- [83] D. G. Swartzfager, S. B. Ziemecki, M. J. Kelley, *J. Vac. Sci. Technol.* **1981**, 19, 185-191.
- [84] M. Chen, D. W. Goodman, *Chinese J. Catal.* **2008**, 29, 1178-1186.
- [85] D. Yuan, X. Gong, R. Wu, *J. Phys. Chem. C* **2008**, 112, 1539-1543.
- [86] I. E. Beck, E. V. Gusevskaya, A. G. Stepanov, V. A. Likholobov, *J. Mol. Catal.* **1992**, 73, 115-146.
- [87] W. Weltner, *J. Am. Chem. Soc.* **1955**, 77, 3941-3950.
- [88] S. M. Augustine, J. P. Blitz, *J. Catal.* **1993**, 142, 312-324.
- [89] L.-F. Liao, C.-F. Lien, J.-L. Lin, *Phys. Chem. Chem. Phys.* **2001**, 3, 3831-3837.
- [90] W. Hill, H. Miessner, G. Ohlmann, *J. Chem. Soc., Faraday Trans. 1* **1989**, 85, 691-697.
- [91] S. D. Jackson, G. J. Kelly, D. Lennon, *React. Kinet. Catal. Lett.* **2000**, 70, 207-212.
- [92] N. W. Alcock, V. M. Tracy, T. C. Waddington, *J. Chem. Soc., Dalton Trans.* **1976**, 2243-2246.
- [93] T. A. Stephenson, S. M. Morehouse, A. R. Powell, J. P. Heffer, G. Wilkinson, *J. Chem. Soc.* **1965**, 3632-3640.
- [94] K. Fujimoto, Y. Negami, T. Takahashi, T. Kunugi, *Ind. Eng. Chem. Prod. Res. Develop.* **1972**, 11, 303-308.
- [95] E. Stoyanov, *J. Struct. Chem.* **2000**, 41, 440-445.
- [96] A. F. Hollemann, N. Wiberg, *Lehrbuch der Anorganischen Chemie*, Walter de Gruyter, Berlin, New York, **1995**.
- [97] A. W. Davidson, W. H. McAllister, *J. Am. Chem. Soc.* **1930**, 52, 507-519.
- [98] K. Ito, H. J. Bernstein, *Can. J. Chem.* **1956**, 34, 170-178.
- [99] R. D. Haley, M. S. Tikhov, R. M. Lambert, *Catal. Lett.* **2001**, 76, 125-130.
- [100] Z. F. Pei, V. Ponec, *Appl. Surf. Sci.* **1996**, 103, 171-182.

- 
- [101] J. D. Kubicki, L. M. Schroeter, M. J. Itoh, B. N. Nguyen, S. E. Apitz, *Geochim. Cosmochim. Acta* **1999**, *63*, 2709-2725.
- [102] S. A. H. Zaidi, *Appl. Catal.* **1988**, *38*, 353-358.
- [103] S. Tamura, T. Yasui, *Shokubai (trans)* **1979**, *21*, 54.
- [104] R. van Helden, C. F. Kohll, D. Medema, G. Verberg, T. Jonkhoff, *Recl. Trav. Chim. Pays-Bas* **1968**, *87*, 961-991.

## 2.7. Appendix

### Transmission Electron Microscopy

TEM images were collected on a *JEM-2010-JEOL* microscope applying an acceleration voltage of 120 kV to electrons generated by a LaB<sub>6</sub> source. The resolution of the microscope is 0.2 nm. Before measurement, the samples were dispersed in ethanol and dropped on a copper-grid supported film.

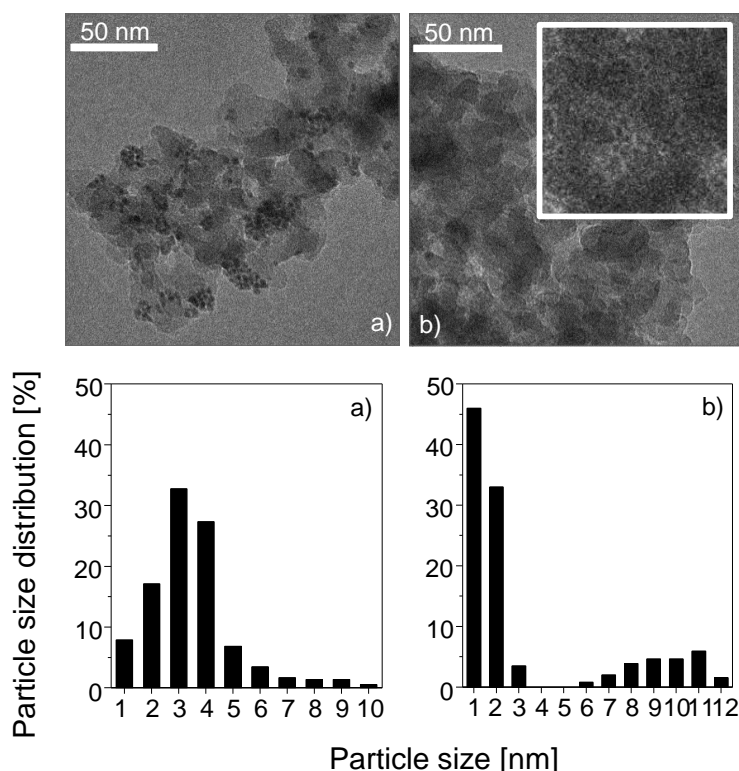


**Figure A2.1.** TEM images and particle size distribution of (a) fresh and (b) reacted (Pd+Au)/KOAc/SiO<sub>2</sub>.

The particle size distribution of fresh (Pd+Au)/KOAc/SiO<sub>2</sub> (Figure A2.1a) revealed an average particle size of ~3.5 nm. After reaction (Figure A2.1b), small particles in the range of 1-2 nm were found together with bigger agglomerates in the range of ~5 to 12 nm. The small particles are associated with leached and reduced Pd<sup>0</sup> clusters whereas the bigger particles are Au rich as indicated by XRD. A number of the large metal particles was encased within a low contrast shell, most likely consisting of acetate deposits.<sup>[1]</sup>

### Catalytic Result of (Pd+Au)/KOAc/SiO<sub>2</sub>

The catalytic activity normalized to the total concentration of Pd and the selectivity of PdAu/KOAc/SiO<sub>2</sub> and (Pd+Au)/KOAc/SiO<sub>2</sub> (Figure A2.2) are almost identical. The overall activity contains contributions of the activity of Pd in PdAu and from Pd<sup>2+</sup>, which is about 20% less active than Pd in PdAu. (Pd+Au)/KOAc/SiO<sub>2</sub> contains 91% dispersed Pd whereas PdAu/KOAc/SiO<sub>2</sub> contains only 53%. Therefore, for (Pd+Au)/KOAc/SiO<sub>2</sub>



dispersed Pd contributes more to the overall activity than on PdAu/KOAc/SiO<sub>2</sub>. On the other hand, the Au enriched PdAu particle surface (molar Pd/Au ratio on the surface of 1.1) on (Pd+Au)/KOAc/SiO<sub>2</sub> contributes less to the overall activity compared to PdAu/KOAc/SiO<sub>2</sub> (molar Pd/Au ratio on the surface of 2.0) both effects compensate and lead to the similar activity observed.

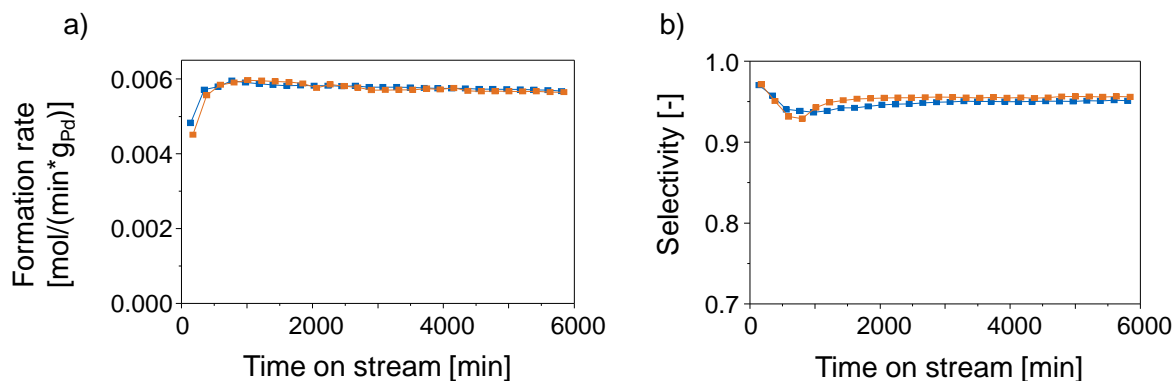


**Figure A2.2.** (a) Formation rates normalized to the total concentration of Pd and (b) selectivities for PdAu/KOAc/SiO<sub>2</sub> (blue) and (Pd+Au)/KOAc/SiO<sub>2</sub> (orange) with time on stream. Reaction conditions: 60 vol % C<sub>2</sub>H<sub>4</sub>, 13 vol % AcOH, 4.5 vol % O<sub>2</sub>, balance N<sub>2</sub>; total pressure, 8.8 bar; temperature, 150 °C.

### IR Spectroscopy of Adsorbed CO on Silica

At -150 °C, 1.0 mbar CO adsorbed on the silica support (Figure A2.3) by interacting with cations (2184 cm<sup>-1</sup>) and with the OH groups on silica (2157 cm<sup>-1</sup>).<sup>[2-3]</sup> Physically adsorbed CO appeared at 2135 cm<sup>-1</sup>.<sup>[4]</sup> The normalized absorbance (10<sup>-5</sup>) is about one order of magnitude lower than the absorbance on fresh and reacted samples (10<sup>-4</sup>).

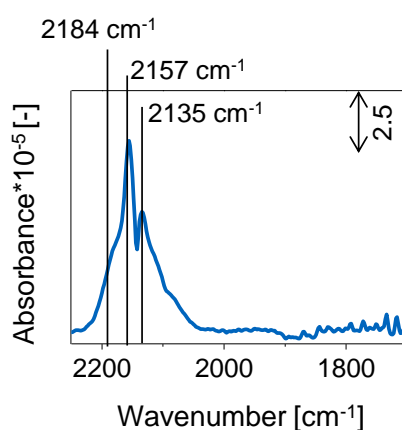


**Figure A2.3.** IR spectrum of 1.0 mbar CO adsorbed on SiO<sub>2</sub> at -150 °C.

## Calculation of the Absorption Coefficients $\varepsilon$ of CO on Au and Pd

*Lambert-Beer law:*  $A = \varepsilon \cdot c \cdot d$

$A$  = Absorbance (height) or integrated area [ $\text{cm}^{-1}$ ]

$\varepsilon$  = Absorption coefficient [ $\text{cm}^2 \text{mol}^{-1}$ ] (if IR band intensity is used) or [ $\text{cm mol}^{-1}$ ] (if IR band area [ $\text{cm}^{-1}$ ] is used)

$c$  = Concentration of the absorbing substance [ $\text{mol l}^{-1}$ ]

$d$  = Thickness [cm]

with  $c \cdot d = \frac{n_S}{S} = \text{const.}$

$n_S$  = Number of total Au or Pd surface atoms [mol]

$S$  = Surface of the wafer;  $S = r^2 \cdot \pi$ ,  $r$  = radius of the wafer [0.6 cm]

$$A = \varepsilon \cdot \frac{n_S}{S}$$

$$\varepsilon = A \cdot \frac{S}{n_S}$$

$$\varepsilon = A \cdot \frac{r^2 \cdot \pi}{n_S}$$

$$\varepsilon = A \cdot \frac{r^2 \cdot \pi}{\frac{n_S}{g_{\text{SiO}_2}} \cdot m_W}$$

$m_W$  = mass of the wafer [g]

$$n_S = \text{Number of total Au or Pd surface atoms; } n_{\text{Au}} = \frac{m_{\text{Au}}}{M_{\text{Au}}} \cdot \frac{g_{\text{SiO}_2}}{D} \quad n_{\text{Pd}} = \frac{m_{\text{Pd}}}{M_{\text{Pd}}} \cdot \frac{g_{\text{SiO}_2}}{D}$$

$$\frac{m_{\text{Au}}}{m_{\text{SiO}_2}} \text{ Concentration of Au on SiO}_2 \text{ [g/g]; } \quad \frac{m_{\text{Pd}}}{m_{\text{SiO}_2}} \text{ Concentration of Pd on SiO}_2 \text{ [g/g]}$$

$$M_{\text{Au}} = 197 \text{ g/mol; } \quad M_{\text{Pd}} = 106.4 \text{ g/mol}$$

$$D = \text{dispersion} \quad \left( D = \frac{n_S}{n_{\text{total}}} \right) \quad (\text{Dispersion derived from average particle size in TEM})$$

$$\varepsilon_{\text{Au}} = \frac{A \cdot r^2 \cdot \pi}{\frac{m_{\text{Au}}}{M_{\text{Au}}} \cdot \frac{g_{\text{SiO}_2}}{D} \cdot m_W}$$

$$\varepsilon_{\text{Pd}} = \frac{A \cdot r^2 \cdot \pi}{\frac{m_{\text{Pd}}}{M_{\text{Pd}}} \cdot \frac{g_{\text{SiO}_2}}{D} \cdot m_W}$$

*Calculation of the extinction coefficients of CO on Au ( $\varepsilon_{l,\text{Au}}$ )*

$$\varepsilon_{l,\text{Au}} = \frac{6.28 \text{ cm}^{-1} \cdot (0.6 \text{ cm})^2 \cdot \pi}{\frac{0.024 \text{ g}_{\text{Au}}}{\frac{g_{\text{SiO}_2}}{197 \text{ mol}} \cdot 0.26 \cdot 0.01606 \text{ g}}}$$

$$\varepsilon_{l,\text{Au}} = 1.40 \cdot 10^7 \text{ cm mol}^{-1}$$

*Calculation of the extinction coefficients of CO on Pd ( $\varepsilon_{l,\text{Pd}}$ ,  $\varepsilon_{b,\text{Pd}}$ )*

$$\varepsilon_{\text{Pd}} = \frac{A \cdot r^2 \cdot \pi}{\frac{m_{\text{Pd}}}{M_{\text{Pd}}} \cdot \frac{g_{\text{SiO}_2}}{D} \cdot m_W}$$

*Attention:* CO adsorbs in linear and bridged form on Pd atoms. (Equilibrium between linear and bridged CO depends on the partial pressure of CO.)

M.A. Vannice, S.Y. Wang, *The Journal of Physical Chemistry* 85 (1981) 2543-2546.<sup>[5]</sup>

$$\varepsilon_l = 3.3 \cdot 10^7 \text{ cm mol}^{-1} \quad \varepsilon_b = 85 \cdot 10^7 \text{ cm mol}^{-1}$$

*Calculation of  $\varepsilon_l$  and  $\varepsilon_b$*  (assuming  $\frac{\varepsilon_b}{\varepsilon_l} = \frac{85}{3.3}$  [5])

$$\frac{\varepsilon_b}{\varepsilon_l} = \frac{85}{3.3} \quad \varepsilon_b = \frac{85}{3.3} \cdot \varepsilon_l$$

$$n_S = n_l + 2 \cdot n_b \quad n_b = \frac{n_S - n_l}{2}$$

$n_l$  = Number of linearly adsorbed CO on Pd [mol]

$n_b$  = Number of bridged adsorbed CO on Pd [mol]

$$n_l = \frac{A_l \cdot S}{\varepsilon_l} \quad n_b = \frac{A_b \cdot S}{\varepsilon_b}$$

$$n_S = \frac{A_l \cdot S}{\varepsilon_l} + 2 \cdot \frac{A_b \cdot S}{\varepsilon_b} = \frac{A_l \cdot S}{\varepsilon_l} + 2 \cdot \frac{A_b \cdot S}{\varepsilon_l \cdot \frac{85}{3.3}}$$

$$n_S = \frac{(\frac{85}{3.3} A_l + 2 \cdot A_b) S}{\varepsilon_l \cdot \frac{85}{3.3}}$$

$$n_S = \frac{m_{Pd}}{\frac{g_{SiO_2}}{M_{Pd}}} \cdot D \cdot m_W = \frac{0.025 \text{ g}_{Pd}}{106.4 \frac{g}{mol}} \cdot 0.14 \cdot 0.01072 \text{ g} = 3.526 \cdot 10^{-7} \text{ mol}$$

$$\varepsilon_{l,Pd} = \frac{(\frac{85}{3.3} A_l + 2 \cdot A_b) r^2 \pi}{n_S \cdot \frac{85}{3.3}}$$

$$\varepsilon_{l,Pd} = \frac{(\frac{85}{3.3} \cdot 2.562 \text{ cm}^{-1} + 2 \cdot 8.27 \text{ cm}^{-1}) (0.6 \text{ cm})^2 \pi}{\frac{85}{3.3} \cdot 3.526 \cdot 10^{-7} \text{ mol}}$$

$$\varepsilon_{l,Pd} = 1.03 \cdot 10^7 \text{ cm mol}^{-1}$$

$$\varepsilon_{b,Pd} = \frac{85}{3.3} \cdot \varepsilon_{l,Pd}$$

$$\varepsilon_{b,Pd} = 2.65 \cdot 10^8 \text{ cm mol}^{-1}$$

$$\frac{\varepsilon_{l,Au}}{\varepsilon_{l,Pd}} = \frac{1.40}{1.03} = 1.36$$

## IR Spectroscopy of Adsorbed CO on Unwashed PdAu/SiO<sub>2</sub> After Reaction

As seen in Figure A2.4, the bright green band for CO linearly adsorbed on “Au next to Pd” dominated the spectrum compared to CO on “Au next to Au” (dark green), “Pd next to Pd” (bright blue) and “Pd next to Au” (blue). The lower Pd/Au ratio of 0.62 on unwashed compared to washed PdAu/SiO<sub>2</sub> after reaction of 0.83

indicated that the washing procedure leads to a slight overestimation of the Pd surface concentration, which is more pronounced on Au enriched PdAu particles.

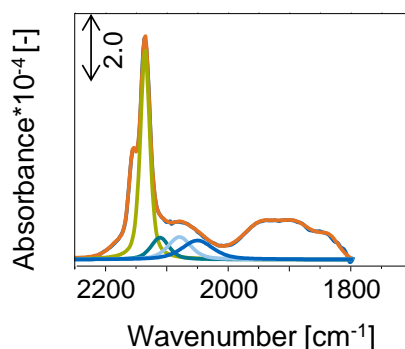


**Figure A2.4.** IR spectrum of 1.0 mbar CO adsorbed on reacted, unwashed PdAu/SiO<sub>2</sub>. Green lines represent CO on Au and blue lines CO on Pd at -150 °C.

### X-Ray Diffraction on KOAc Free and KOAc Promoted Pd(OAc)<sub>2</sub>/SiO<sub>2</sub> After Reaction

In order to estimate the reduction behavior of the reactive Pd<sub>3</sub>(OAc)<sub>6</sub> and K<sub>2</sub>Pd<sub>2</sub>(OAc)<sub>6</sub> intermediates, two model catalysts, Pd(OAc)<sub>2</sub>/SO<sub>2</sub> (Figure A2.5, blue) and Pd(OAc)<sub>2</sub>/KOAc/SiO<sub>2</sub> (Figure A2.5, orange) were studied by XRD after reaction. The general lower values for the full width at half maximum and the narrower Pd reflections revealed the formation of bigger Pd particles on Pd(OAc)<sub>2</sub>/KOAc/SiO<sub>2</sub>. We associate the bigger Pd particles to a lower reduction stability of K<sub>2</sub>Pd<sub>2</sub>(OAc)<sub>6</sub> compared to Pd<sub>3</sub>(OAc)<sub>6</sub>.

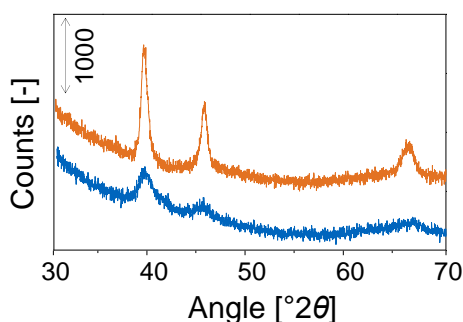


**Figure A2.5.** X-ray profile between 30 - 70 °2θ of Pd(OAc)<sub>2</sub>/SO<sub>2</sub> (blue) and Pd(OAc)<sub>2</sub>/KOAc/SiO<sub>2</sub> (orange) after reaction.

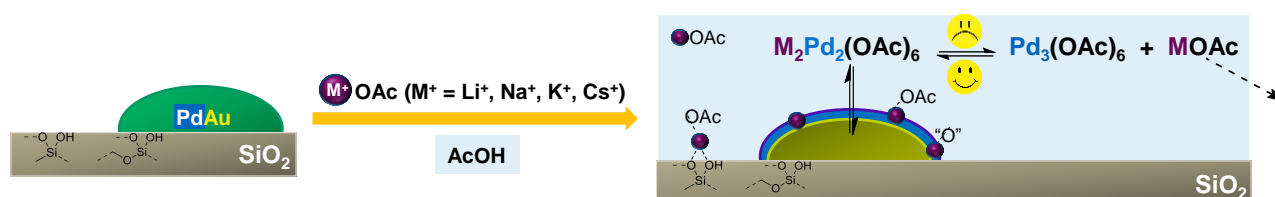
### References

- [1] N. Macleod, J. M. Keel, R. M. Lambert, *Appl. Catal. A* **2004**, 261, 37-46.
- [2] T. Montanari, L. Castoldi, L. Lietti, G. Busca, *Appl. Catal. A* **2011**, 400, 61-69.
- [3] T. Montanari, R. Matarrese, N. Artioli, G. Busca, *Appl. Catal. B* **2011**, 105, 15-23.
- [4] M. Mihaylov, H. Knözinger, K. Hadjiivanov, B. C. Gates, *Chem. Ing. Tech.* **2007**, 79, 795-806.
- [5] M. A. Vannice, S. Y. Wang, *J. Phys. Chem.* **1981**, 85, 2543-2546.

# Chapter 3

## Impact of Alkali Acetate Promoters on the Dynamic Ordering of PdAu catalysts during Vinyl Acetate Synthesis<sup>2</sup>

Fresh and used alkali acetate, MOAc ( $M^+ = \text{Li}^+, \text{Na}^+, \text{K}^+, \text{Cs}^+$ ), promoted PdAu catalysts were investigated to characterize the impact of  $M^+$  on the deactivation of PdAu during vinyl acetate (VA) formation from ethene and acetic acid. Dynamic reordering of PdAu towards an active  $\sim\text{Pd}_1\text{Au}_1$  phase, less active  $\text{M}_2\text{Pd}_2(\text{OAc})_6$  and inactive  $\text{Pd}_3(\text{OAc})_6$  complexes influenced by MOAc determines the overall activity. Thus, decreasing deactivation from LiOAc to CsOAc promoted PdAu is associated with the lower concentration of inactive  $\text{Pd}_3(\text{OAc})_6$  leached from active PdAu particles and with the lower loss of  $\text{Cs}^+$  compared to  $\text{Li}^+$  during reaction. CsOAc binds most efficiently to  $\text{Pd}_3(\text{OAc})_6$  and forms active  $\text{Cs}_2\text{Pd}_2(\text{OAc})_6$ , lowering the tendency to leach  $\text{Cs}^+$ . Reduction of Pd in  $\text{M}_2\text{Pd}_2(\text{OAc})_6$  to a mixed “Pd/ $M^+$ -O” adlayer on the bimetallic PdAu particles stabilized active  $\text{Pd}^0$  on the PdAu surface maintaining the catalyst activity. Thus, increasing “Pd/ $M^+$ -O” concentrations from LiOAc to CsOAc lower long term deactivation of PdAu.



<sup>2</sup> This chapter is based on the article of the same title as published in the Journal of Catalysis. Reprinted with permission from Elsevier.

### 3.1. Introduction

The complex interaction between Pd and Au in PdAu alloys leads to superior catalytic performance in many reactions. This is attributed to ligand (electronic) as well as ensemble (geometric) effects of the constituent alloy elements<sup>[1-2]</sup>. The ligand effect summarizes electronic effects between Pd and Au atoms that alter the strength of Pd-adsorbate bonds<sup>[3]</sup>. Ligand effects can, therefore, be viewed as electronic perturbations of Pd by Au, which generally increases the electron density in the Pd d-band<sup>[4]</sup>. The ensemble or dilution effect refers to structural modifications in the surface atom geometry to create hetero-nuclear bonds<sup>[3, 5-6]</sup>. Dilution of surface Pd atoms by the more weakly interacting Au modifies the arrangement of multi-atom sites required to better enable sorption in structure-sensitive reactions such as vinyl acetate synthesis (VAS)<sup>[3, 7-8]</sup>.

The catalytically active sites for VAS were identified as two Pd<sup>0</sup> atoms isolated by inactive Au atoms,<sup>[6, 9-11]</sup> such as Pd<sup>+</sup><sup>[12-14]</sup> or/and Pd<sup>2+</sup> species<sup>[13, 15-19]</sup>. The presence of solid Pd<sup>0</sup> and Pd<sup>+</sup>/Pd<sup>2+</sup> complexes were hypothesized to simultaneously contribute to the reaction within a supported liquid phase mechanism<sup>[20-21]</sup>. Oxidized Pd species (e.g. K<sub>2</sub>Pd<sub>2</sub>(OAc)<sub>6</sub><sup>[21]</sup>) may form during the dynamic reorganization of the PdAu bulk and surface structure<sup>[18-19, 21-22]</sup> being at least partly covered by a condensed liquid-like film of acetic acid/potassium acetate (KOAc) under operating conditions (150 °C, 9 bar)<sup>[16, 23]</sup>. The presence of K<sub>2</sub>Pd<sub>2</sub>(OAc)<sub>6</sub> points to a pathway catalyzed by a molecular organometallic species in addition to the reaction on the solid bimetallic PdAu particles. The overall activity is controlled by the concentration of Pd sites on the solid surface. The way the promoter interacts especially with the heterogeneous PdAu particles and its impact on the formation of less active Pd acetate species is crucial in order to understand the reordering and, thus, the deactivation of the catalysts.

Deactivation of supported Pd catalysts limits the lifetime of industrial catalysts (typically 8 months to 2 years)<sup>[24]</sup>. Deactivation was found to depend on the temperature as well as on the O<sub>2</sub> and acetic acid concentration<sup>[14-15]</sup>, while both ethylene concentration and initial GHSV have almost no influence<sup>[14]</sup>. PdC<sub>x</sub> formation from acetate and/or ethylene may also contribute to deactivation<sup>[25-31]</sup>. Diffusion of Au from the surface into the particle bulk<sup>[14]</sup> and formation of deposits on the catalyst surface<sup>[32]</sup> have been invoked as additional reasons for the deactivation. Abel et al.<sup>[15]</sup> had associated the formation of highly dispersed Pd acetate as transport species with sintering. In contrast, Han et al.<sup>[30-31]</sup> and Pohl et al.<sup>[18]</sup> observed hardly any sintering of the Pd particles during VAS. Thus, deactivation was explained by the Pd surface enrichment on PdAu particles and by the formation of water-soluble Pd acetate<sup>[13, 15, 17-18]</sup>.

In accordance with Samanos et al.<sup>[16]</sup> dispersed Pd particles have a significantly lower activity compared to Pd within the bimetallic PdAu particles, because the highly dispersed particles are completely embedded in the liquid AcOH layer and interact as consequence very weakly with ethene<sup>[16]</sup>. It is known that KOAc promoted PdAu catalysts suffer from gradual loss of KOAc, which is compensated by adding small amounts of KOAc to the feed stream in the industrial process<sup>[33]</sup>. As the rate crucially depends on the presence of KOAc<sup>[21, 34]</sup> the loss of the alkali ions is likely one of the reason for deactivation. Additionally, we have recently shown that the catalytic restructuring and, thus, the activity of PdAu catalysts strongly depends on the presence of the KOAc<sup>[21]</sup>. However, the effect of the different alkali acetate promoters on the PdAu reordering and on

deactivation is not understood. The present contribution addresses this gap and resolves the discrepancies regarding deactivation of PdAu in literature by systematically exploring the location and the interaction of the different alkali metal acetates with the active site Pd by elemental analysis, X-Ray diffraction, X-Ray absorption spectroscopy and infrared spectroscopy on fresh and used samples.

## 3.2. Experimental Section

### 3.2.1. Synthesis

PdAu/SiO<sub>2</sub> with a Pd/Au ratio of 2.0 was prepared via incipient wetness impregnation as described in patent DE102006058800A1<sup>[35]</sup>. H<sub>2</sub>AuCl<sub>4</sub> and PdCl<sub>2</sub> were dissolved in bidistilled water (1mL/1g support) and impregnated on SiO<sub>2</sub>. Precipitation with sodium carbonate and washing with ammonia solution (pH 8) was carried out to remove chloride ions from the precipitated metal salts. The PdAu/SiO<sub>2</sub> precursor catalysts were reduced in flowing H<sub>2</sub> (100 mL/min) at 300 °C for 1h (5 °C/min). The catalyst powder was freeze-dried under reduced pressure between the synthesis steps. The total noble metal loading was 1.5 wt% for Pd and Au. Portions of PdAu/SiO<sub>2</sub> were impregnated with equimolar amounts of Li-, Na-, K- or Cs-acetate (1.28 mmol/g catalyst) (“PdAu/MOAc/SiO<sub>2</sub>”).

### 3.2.2. Catalytic Reactions

Activity tests were performed in a 6-fold reactor setup at a temperature of 150 °C and a gas composition of 60 vol % C<sub>2</sub>H<sub>4</sub>, 13 vol % AcOH, 4.5 vol % O<sub>2</sub> in N<sub>2</sub> at 9 bar total pressure. The diluent SiC/catalyst ratio was 10/1 to maintain a constant temperature over the whole catalyst bed. The product stream was analyzed using a GC (model 2014 from Shimadzu) equipped with a Haysep Q and a molecular sieve column and a TCD detector. Deactivation was calculated from the maximum activity (~ 15 h time on stream) and the average activity level after 4500 minutes on stream.

### 3.2.3. Elemental Analysis

Contents of Pd and Au were determined by atomic absorption spectroscopy (AAS) using a Solaar M5 Dual Flame graphite furnace AAS (ThermoFisher). 50 mg of catalyst was dissolved in a mixture containing 48 % hydrofluoric acid and nitrohydrochloric acid.

The measured Pd concentration of washed samples after reaction is the sum of Pd in the PdAu bimetallic phase and Pd in the Pd/M<sup>+</sup>-O layer (Equation 1). The concentration of “Pd in the AcOH” layer (solved Pd acetate

species <sup>[17]</sup> or dispersed Pd<sup>0</sup>) was calculated from the difference between the initial and measured Pd loading (Equation 2).

$$\text{Pd}_{\text{measured by AAS}} = \text{Pd}_{(\text{PdAu})} + \text{Pd}_{(\text{Pd/M}^+-\text{O})} \quad (1)$$

$$\text{Pd}_{\text{total}} = \text{Pd}_{\text{measured by AAS}} + \text{Pd}_{(\text{acetic acid layer})} \quad (2)$$

$$\text{Pd}_{(\text{total})} = 1.30 \text{ wt\%}$$

### 3.2.4. IR Spectroscopy of Adsorbed CO

The IR spectra were recorded on a Vertex 70 spectrometer from Bruker Optics at a resolution of 4 cm<sup>-1</sup> collecting at least 100 scans. Samples were washed with bidistilled water (20 mL/100 mg catalyst) for 20 minutes to remove KOAc, AcOH and solved Pd<sup>2+</sup> species from the PdAu surface. Additionally, water-soluble Pd/M<sup>+</sup>-O compounds formed on the bimetallic particles were removed by washing with H<sub>2</sub>O for 24h. Samples were pressed into self-supporting wafers (~10 mg/cm<sup>2</sup>), activated in vacuum (~1.0 × 10<sup>-7</sup> mbar) at 300 °C for 1 h (heating rate of 5 °C/min), reduced in static H<sub>2</sub> (1000 mbar) and outgassed at 300 °C in vacuum for 30 min. The system was cooled to -150 °C with liquid N<sub>2</sub> and a spectrum of the activated sample was taken in 5 mbar He. After the removal of He, 1.0 mbar CO was adsorbed at -150 °C. Spectra were recorded every minute until the CO adsorption-desorption equilibrium was established.

Analysis of the spectra was carried out using the software Grams AI. Spectra were background corrected and subtracted from the background corrected spectrum of the activated sample to obtain the CO absorption bands. These difference spectra were normalized to the integrated area of Si-O overtones between 2107 and 1741 cm<sup>-1</sup> of the activated sample. Absorption bands were evaluated by band fitting applying a mixed 50/50 Gaussian-Lorentzian function.

### 3.2.5. X-Ray Absorption Spectroscopy

#### *Pd-K and Au-L<sub>3</sub> edge*

X-Ray absorption spectroscopy was measured at HASYLAB, DESY, Hamburg/Germany, on the beamlines X1 and C. During the experiments, the storage ring operated at an electron energy of 4.5 GeV and an average current of 100 mA. Spectra were recorded in transmission mode at the Pd-K edge ( $E_0 = 24350$  eV, Si(311) crystals) and Au-L<sub>3</sub> edge ( $E_0 = 11919$  eV, Si(111) crystals). The alignment of the second monochromator crystal was set to 60 % of the maximum intensity to minimize the intensity of higher order reflections. The samples were pressed into self-supporting wafers with weights of a total absorbance of 2.0 to optimize the signal to noise ratio. The samples were heated to 300 °C with 5 °C/min in H<sub>2</sub> (100 mL/min), reduced at 300 °C for 1h and flushed with 150 mL/min He before cooling to -150 °C to record 2-3 XAS spectra per sample.



EXAFS data were processed and analyzed with IFEFFIT, Athena and Artemis<sup>[36]</sup>. The scattering contributions of the pre- and post-edge were removed from the X-ray absorption spectra by a third-order polynomial function. The oscillations were weighted by  $k^2$  and Fourier transformed within the limits  $k = 2.1-12 \text{ \AA}^{-1}$  for the Pd K edge and  $k = 2.8-12 \text{ \AA}^{-1}$  for the Au L<sub>3</sub> edge. The amplitude  $S_o^2$ , was derived from EXAFS data analysis of known references with known coordination numbers and was fixed during analysis ( $S_o^2$  was found to be 0.9 for Au and 1.0 for Pd). The multiple-edge fitting was carried out with following constraints.

$$N_{\text{AuPd}} = N_{\text{PdAu}} x_{\text{Pd}} / x_{\text{Au}} \quad (3)$$

$$d_{\text{AuPd}} = d_{\text{PdAu}} \quad (4)$$

$$\sigma_{\text{AuPd}} = \sigma_{\text{PdAu}} \quad (5)$$

### Cs-L<sub>3</sub> edge

EXAFS at the Cs-L<sub>3</sub> edge (5012 eV) was performed at HASYLAB, DESY, Hamburg/Germany, on the beamline A1. The spectra of the self-supporting wafers were collected in transmission mode during flushing with helium (150 mL/min) at 77 K after activation and reduction in H<sub>2</sub> (100 mL/min) at 300 °C for 1h. The location of cesium on PdAu/CsOAc/SiO<sub>2</sub> was investigated on fresh and used, (washed) samples in order to distinguish between incorporated and physically adsorbed Cs<sup>+</sup>. Cs<sup>+</sup> incorporated in the outer surface of the metallic particles is likely not to be removed via washing with water and thus, possible metallic Pd and Au neighbors should be visible in spectra of used, washed samples. Pure CsOAc and CsOAc impregnated on SiO<sub>2</sub> were measured as reference.

FEFF calculations for CsOAc were performed using the structural data for CsOAc published by Lossin et al.<sup>[37]</sup> XAS data processing and EXAFS analysis were performed using IFEFFIT with the Horae package<sup>[36]</sup>. The oscillations were weighted by  $k^1$  and  $k^3$  to emphasize contributions of light and heavy scatterers. Fourier transformation was carried out within the limits  $k = 2.35 - 7.00 \text{ \AA}^{-1}$ . The amplitude reduction factor  $S_o^2$  was fixed during analysis at 1.1. Pd neighbors were estimated using first shell analysis.

## 3.3. Results and Discussion

### 3.3.1. Deactivation Behavior of PdAu/MOAc/SiO<sub>2</sub> (M<sup>+</sup> = Li<sup>+</sup>, Na<sup>+</sup>, K<sup>+</sup>, Cs<sup>+</sup>)

Figure 3.1 illustrates the formation rates for VA over PdAu/MOAc/SiO<sub>2</sub> (M<sup>+</sup> = Li<sup>+</sup>, Na<sup>+</sup>, K<sup>+</sup>, Cs<sup>+</sup>) with time on stream. The length of the initial induction period to build up full activity decreased with increasing alkali metal radius from M<sup>+</sup> = Li<sup>+</sup> (1100 min), Na<sup>+</sup> (900 min), K<sup>+</sup> (770 min) to Cs<sup>+</sup> (740 min). During this induction period, the Pd<sub>x</sub>Au<sub>y</sub> particles on the catalysts undergo severe reordering as well as leaching of Pd<sup>2+</sup> species<sup>[17-19]</sup>. Larger alkali metal cations of the promoters enhanced the formation of Pd-acetate species and, therefore, the reorganization of bimetallic PdAu towards a more active catalyst. It should be noted in passing that PdAu/LiOAc/SiO<sub>2</sub> had a 10 % lower maximum activity (~5.2 mmol/min\*g<sub>Pd</sub>) than Na<sup>+</sup>, K<sup>+</sup> and Cs<sup>+</sup> promoted

PdAu/SiO<sub>2</sub> (~5.7 mmol/min\*g<sub>Pd</sub>). Furthermore, the catalytic activity of PdAu/LiOAc/SiO<sub>2</sub> decreased continuously until 4500 min time on stream and then dropped markedly accompanied by a drastic selectivity loss (Appendix, Figure A3.1). The deactivation of PdAu/LiOAc/SiO<sub>2</sub> (Figure 3.1, blue curve) showed two regimes, presumably reflecting the two roles of MOAc during reaction, i.e., (i) transfer of acetates to Pd on solid PdAu and (ii) reduction of leached M<sub>2</sub>Pd<sub>2</sub>(OAc)<sub>6</sub> to Pd<sup>0</sup> that partly reincorporates into PdAu to maintain the active Pd<sub>1</sub>Au<sub>1</sub> phase [21]. Deactivation in Regime I is hypothesized to reflect the pronounced but constant loss of Li<sup>+</sup> and, thus, the insufficient transfer of acetates to the active site Pd on PdAu. In Regime II, the LiOAc concentration dropped presumably below a minimum loading necessary to stabilize a critical Pd monomer concentration on the PdAu surface. Evidence for the significant loss of LiOAc as well as the deactivation is provided in Table 3.1. Generally, the larger the radius of the alkali promoter, the lower the promoter loss and the lower the deactivation of PdAu.

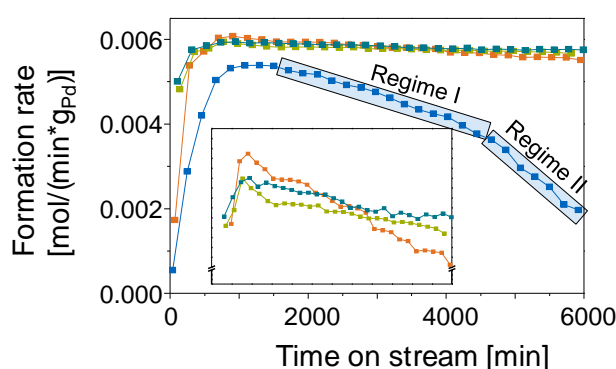


**Figure 3.1.** Formation rates with time on stream normalized to the total Pd concentration for PdAu/MOAc/SiO<sub>2</sub>. M = Li (blue), Na (red), K (bright green), Cs (dark green). Reaction conditions: 60 vol % C<sub>2</sub>H<sub>4</sub>, 13 vol % AcOH, 4.5 vol % O<sub>2</sub>, balance N<sub>2</sub>; total pressure, 8.8 bar; temperature, 150 °C.

**Table 3.1.** Loss of alkali metal concentration and deactivation of PdAu/MOAc/SiO<sub>2</sub> (M<sup>+</sup> = Li<sup>+</sup>, Na<sup>+</sup>, K<sup>+</sup>, Cs<sup>+</sup>) after 4500 min time on stream.

PdAu/MOAc/SiO <sub>2</sub> ; M <sup>+</sup> =	Deactivation [(mol/min*gPd)/min]*10 <sup>-7</sup>	Loss of alkali metal [%]
Li <sup>+</sup>	4.6	52.9
Na <sup>+</sup>	1.0	27.7
K <sup>+</sup>	0.4	7.3
Cs <sup>+</sup>	0.3	3.2

Having shown that deactivation of PdAu on PdAu/MOAc/SiO<sub>2</sub> (M<sup>+</sup> = Li<sup>+</sup>, Na<sup>+</sup>, K<sup>+</sup>, Cs<sup>+</sup>) is unequivocally linked to the nature of the alkali promoter, the question arises how the promoter interacts with active PdAu and influences PdAu reordering under reaction conditions.

### 3.3.2. Impact of the Pd Surface Concentration on Deactivation of PdAu

#### 3.3.2.1. Pd Surface Enrichment on PdAu/MOAc/SiO<sub>2</sub> (M<sup>+</sup> = Li<sup>+</sup>, Na<sup>+</sup>, K<sup>+</sup>, Cs<sup>+</sup>) during Reaction

The interaction of the different alkali metals with PdAu during reaction was studied by IR spectroscopy of adsorbed CO at -150 °C on PdAu/MOAc/SiO<sub>2</sub> (M<sup>+</sup> = Li<sup>+</sup>, Na<sup>+</sup>, K<sup>+</sup>, Cs<sup>+</sup>) (Figure 3.2). After reaction, the samples were washed with deionized water (40 mL/0.2 mg catalyst) for 20 minutes to remove the MOAc/AcOH layer formed during reaction. The washing water contained Pd and KOAc, while Au was not detected by chemical analysis. It has been established previously that this procedure does not alter the underlying metal particle [19]. CO adsorbs at -150 °C on trace cations (2184 cm<sup>-1</sup>), surface hydroxyl groups (2157 cm<sup>-1</sup>) and alkali cations (2145 cm<sup>-1</sup>) of SiO<sub>2</sub> [38-42]. The band at 2135 cm<sup>-1</sup> is assigned to physically adsorbed CO [39, 43-44]. In the IR spectra of adsorbed CO on washed PdAu/MOAc/SiO<sub>2</sub> catalysts after reaction (Figure 3.2) the intensity of the CO band at 2157 cm<sup>-1</sup> decreased from M<sup>+</sup> = Li<sup>+</sup> to Cs<sup>+</sup> due to the gradually increasing inaccessibility of the SiOH groups. Blocking OH groups by strongly adsorbed organic oligomers or low polymers of VA [14, 18] can be excluded, as they would have been decomposed during the activation/reduction treatment at 300 °C prior to CO adsorption. The promoter cations were removed by washing and therefore, insoluble Pd<sup>0</sup> species are concluded to cause blocking of the OH groups for adsorption of CO. Hence, not only the formation of Pd acetate species, but also the concentration of dispersed Pd<sup>0</sup> increased from Li<sup>+</sup> to Cs<sup>+</sup>.

Bands with wavenumbers between 2135-2000 cm<sup>-1</sup> are generally assigned to CO linearly adsorbed on Pd (2109 cm<sup>-1</sup> [4, 7, 45-46]) or on Au (2104 cm<sup>-1</sup> [7, 47-49]), while bands with wavenumbers below 2000 cm<sup>-1</sup> are caused by CO adsorbed in a bridged and threefold-hollow mode on Pd [38, 50-51]. We concentrate here on the analysis of linear CO adsorption as the concentration of multifold bonded CO on contiguous Pd sites is negligibly small due to the ratio of absorption coefficients  $\epsilon_{\text{linear}}/\epsilon_{\text{bridged}}$  of  $85 \cdot 10^7 \text{ cm mol}^{-1}/3.3 \cdot 10^7 \text{ cm mol}^{-1} \approx 26$  [50].

On bimetallic PdAu catalysts, the broad band assigned to linearly adsorbed CO consists of four contributions. For PdAu/LiOAc/SiO<sub>2</sub> (Figure 3.2a) the band at 2135 cm<sup>-1</sup> (bright green) was attributed to CO on Au surrounded by Pd atoms (linear CO on “Au next to Pd”) and the band at 2105 cm<sup>-1</sup> (dark green) was assigned to CO linearly bonded on Au in proximity to Au atoms (linear CO on “Au next to Au”). The linear adsorption of CO on Pd led to a band at 2069 cm<sup>-1</sup> (bright blue) assigned to CO chemisorbed on larger Pd islands (linear CO on “Pd next to Pd”) and to a band at 2040 cm<sup>-1</sup> (blue) ascribed to linear CO adsorption on Pd surrounded by Au (linear CO on “Pd next to Au”) [5, 19, 21]. The shift in the band position for CO on the bimetallic PdAu surface can be explained by the interaction between Pd and Au [52]. In PdAu alloys, the empty states in the Pd d-band are filled with s electrons from Au. With increasing concentrations of Au atoms in contact with Pd the electron density on Pd increases and consequently, Pd in contact to Au can donate more electron density into the antibonding  $\pi^*$  orbital of CO leading to a decrease in the CO bond strength and to a lower wavenumber of the CO band. In contrast, the band for CO linearly adsorbed on Au in proximity to Pd shifted to higher wavenumbers as the electron density in the d-band of Au decreases by the contact with Pd [7, 53]. Beside the electronic interaction between Pd and Au, the dilution of Au in Pd may influence the wavenumbers of the CO stretching bands, as the wavenumber of  $\nu(\text{C}=\text{O})$  increases with surface coverage due to increased CO dipole-

dipole coupling. Thus, the decrease of the wavenumber of  $\nu(\text{C}=\text{O})$  was tentatively attributed to dilution of Pd domains with Au reducing so CO dipole interactions<sup>[54]</sup>. However, as the wavenumber of the band of CO on Au close to Pd at  $\sim 2130\text{ cm}^{-1}$  increased in comparison to CO on monometallic Au/SiO<sub>2</sub> at  $2104\text{ cm}^{-1}$ , dipole interactions between the adsorbed CO molecules are unlikely.

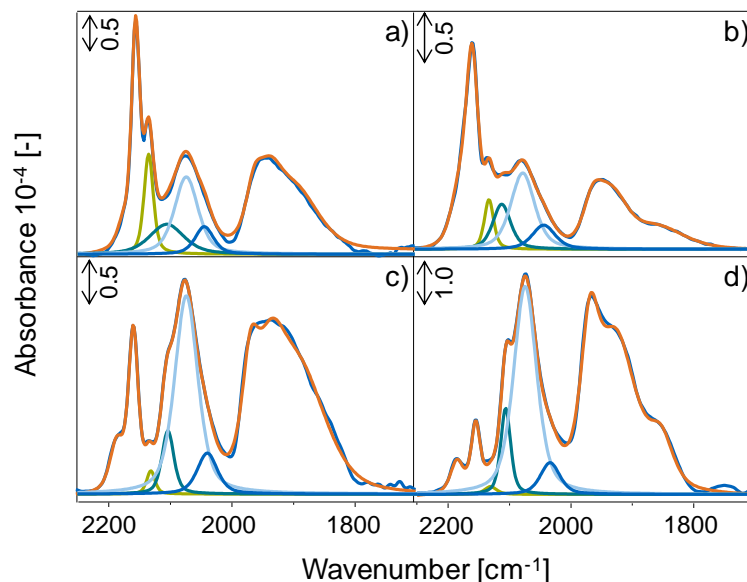


**Figure 3.2.** IR spectra of adsorbed CO at  $-150\text{ }^{\circ}\text{C}$  and 1 mbar partial pressure of CO on spent PdAu/SiO<sub>2</sub> promoted with (a) LiOAc, (b) NaOAc, (c) KOAc and (d) CsOAc, washed for 20min. Green lines represent CO adsorbed on Au and blue lines CO adsorbed on Pd.

The relative intensities of the bands of linear to multifold CO adsorption as well as the exact band positions reflect the degree of surface intermixing<sup>[40]</sup>. The probability of CO to adsorb in a multifold position is enhanced for larger Pd ensembles and, thus, the ratio of the intensities of linear to multifold adsorbed CO decreases.

When qualitatively comparing the PdAu surface composition of used PdAu/MOAc/SiO<sub>2</sub> ( $\text{M}^+ = \text{Li}^+, \text{Na}^+, \text{K}^+, \text{Cs}^+$ ) in Figure 3.2, the (relative) concentration of Pd on the surface increased from  $\text{M}^+ = \text{Li}^+$  to  $\text{Cs}^+$ . The surface concentrations of Pd and Au determined from the absorption coefficients  $\epsilon$  for the respective CO stretching vibrations<sup>[21, 50]</sup> are summarized in Table 3.2. The fractions “Au next to Pd” and “Pd next to Au” indicative for bimetallic well-mixed PdAu surfaces decreased with increasing promoter radius from 19 % to 1 % and from 18 % to 10 %, respectively and concomitantly, the fraction of “Pd next to Pd” in larger Pd ensembles increased from 44 % to 78 %. The increase in the Pd/Au surface ratio from 1.6 to 7.6 underline a pronounced migration and improved stabilization of Pd on the bimetallic surface by the bigger alkali metal promoters, which is concluded to be caused by the decreasing bond strength between  $\text{M}^+$  and acetate from  $\text{Li}^+$  to  $\text{Cs}^+$ . Thus, acetate covalently bonded to  $\text{Li}^+$  exerts less adsorptive strength on Pd of PdAu in contrast to the acetate from ionic CsOAc species.

**Table 3.2.** Surface concentrations [ $10^{-6}$  mol/g] and corresponding fractions [%] in brackets of CO adsorbed on PdAu/MOAc/SiO<sub>2</sub> after reaction (washed for 20 min).

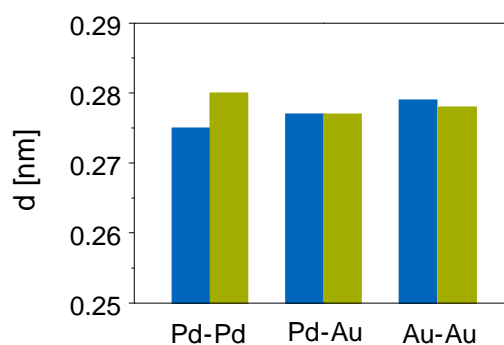
PdAu/MOAc/SiO <sub>2</sub> M <sup>+</sup> =	Au next	Au next	Pd next	Pd next	linear/bridged	Pd/Au
	to Pd	to Au	to Pd	to Au	CO	
	[10 <sup>-6</sup> mol/g] ([%])				[mol/g/mol/g]	[mol/g/mol/g]
Li <sup>+</sup>	1.6 (19)	1.6 (20)	3.7 (44)	1.5 (18)	20.8	1.6
Na <sup>+</sup>	0.5 (10)	0.9 (18)	2.8 (55)	0.8 (17)	25.7	2.5
K <sup>+</sup>	0.2 (2)	1.0 (9)	7.9 (75)	1.4 (14)	15.0	7.6
Cs <sup>+</sup>	0.2 (1)	2.2 (10)	16 (78)	2.1 (10)	16.3	7.6

Having established a direct link between the Pd surface concentration and the promoter species we explore in the next step the nature of the promoter interaction in close contact to the Pd enriched PdAu surface.

### 3.3.2.2. Interaction of the Promoter with the Pd Enriched Surface of PdAu

#### a) X-Ray Absorption Spectroscopy at the Pd-K and Au-L<sub>3</sub> edge

The coordination of the promoter on the PdAu particles during reaction has been studied by EXAFS at the Pd-K and Au-L<sub>3</sub> edges on the bimetallic PdAu/KOAc/SiO<sub>2</sub> catalysts before and after reaction. The metal-metal distances and the corresponding coordination numbers are summarized in ref [19]. EXAFS showed an increase in the Pd-Pd distance of  $\sim 0.055$  Å (from 2.75 Å to 2.80 Å) but no increase in the Au-Au (2.79 Å) or Au-Pd (2.77 Å) distances between fresh (Figure 3.3, blue) and used PdAu/KOAc/SiO<sub>2</sub> catalysts (Figure 3.3, green). Thus, the Pd-Pd distance adopted the Au-Au distance on used samples indicating the enrichment of Pd on the surface of the bimetallic PdAu particles. Strong interactions of Pd with the KOAc resulted in the formation of a mixed Pd<sup>0</sup>/K<sup>+</sup> adlayer on top of the PdAu particles and on SiO<sub>2</sub>. An alternative explanation for the long Pd-Pd distances, i.e., the formation of PdC<sub>x</sub> from decomposed acetates was excluded because the samples were reduced in situ at 300 °C before EXAFS measurements, a treatment which would convert PdC<sub>x</sub> formed during VA synthesis to metallic Pd<sup>[55]</sup>. Sárkány et al. [56] and Akita et al. [57] reported a similar lattice expansion of an epitaxially grown Pd lattice (4-9 Pd layers) on Au<sub>core</sub>Pd<sub>shell</sub> particles, attributing it to the perturbation by the underlying Au core [58].

**Figure 3.3.** Pd-Pd, Pd-Au and Au-Au bond lengths in PdAu/KOAc/SiO<sub>2</sub> before (blue) and after reaction (green).

## b) X-Ray Absorption Spectroscopy at the Cs-L<sub>3</sub> edge

To explore further the nature of the Pd/M<sup>+</sup> adlayer on PdAu, the state and environment of Cs<sup>+</sup> was probed by XAFS at the Cs-L<sub>3</sub> edge on PdAu/CsOAc/SiO<sub>2</sub>. Measurements on the K- and L-edges of potassium are not feasible due to their low energies. Furthermore, if Cs<sup>+</sup> with an ionic radius of ~2.0 Å was located in the Pd adlayer, the smaller promoter ions like Li<sup>+</sup>, Na<sup>+</sup> and K<sup>+</sup> are expected to act similar with Pd. Figure A3.2 in the Appendix shows the EXAFS functions  $\chi(k)$  and the fit results of (a) fresh, (b) used and (c) used, washed PdAu/CsOAc/SiO<sub>2</sub>, weighted by i)  $k^1$  and ii) by  $k^3$ .

XAS on fresh and used but unwashed PdAu/CsOAc/SiO<sub>2</sub> varied only subtly in the oxygen environment of Cs<sup>+</sup>. Due to the excess of CsOAc and the volume-averaged information obtained by XAS, the contributions for the support and the metallic particle could not be differentiated. Analysis of washed PdAu/CsOAc/SiO<sub>2</sub> after reaction differed significantly from CsOAc<sup>[37]</sup>. Two oxygen neighbors of Cs<sup>+</sup> with  $r_{\text{Cs}^+-\text{O}}$  of 3.115 and 3.124 Å at a total coordination number of 4.5 were observed, which indicates that Cs<sup>+</sup> and O are in close contact as the closest Cs<sup>+</sup>-O distance is 3.02 Å ( $= r_{\text{Cs}^+} + r_{\text{O}} = 1.62 + 1.40$ )<sup>[59]</sup>. The formation of a Cs<sub>2</sub>O phase can be excluded as  $r_{\text{Cs}^+-\text{O}}$  in Cs<sub>2</sub>O (CsOH·H<sub>2</sub>O) of 3.43 Å<sup>[60]</sup> is much larger than the obtained values.

The number of Pd neighbors is  $N_{\text{Cs}^+-\text{Pd}} = 1.4 \pm 1.0$  at a distance  $r_{\text{Cs}^+-\text{Pd}}$  in the range of 2.4 to 3.1 Å. As the signal was very weak, the error was rather large, but the presence of Pd backscattering contributions could be clearly confirmed. In order to preserve the electroneutrality of the mixed Pd/Cs<sup>+</sup> adlayer, Cs<sup>+</sup> has to be in close contact to oxygen atoms, e.g., in form of acetate ions on the outermost surface. This is supported by the fact that both, Cs<sup>+</sup>-O and Cs<sup>+</sup>-Pd contributions were observed for washed PdAu/CsOAc/SiO<sub>2</sub> after reaction. The average Pd-Pd and Pd-Cs<sup>+</sup> distance of ~2.83 Å is slightly larger than the average Pd-Pd and Pd-K<sup>+</sup> distance of ~2.80 Å on PdAu/KOAc/SiO<sub>2</sub> after reaction. The larger distance is explained with the larger ionic radius of Cs<sup>+</sup> compared to K<sup>+</sup>. Assuming a substitution of Pd by Cs<sup>+</sup> in the fcc metal structure, a much larger Pd-Cs<sup>+</sup> distance of ~3.2 Å would be expected on the basis of metallic  $r_{\text{Pd}}$  (1.39 Å) and ionic  $r_{\text{Cs}^+}$  (1.81 Å) radii. The distances determined are an average for the outer surface, where the alkaline ion is located, and for the promoter-free bulk particle, which should not change. The fact that Cs<sup>+</sup> is detectable by XAS and that the CsOAc structure was not observed for washed PdAu/CsOAc/SiO<sub>2</sub> after reaction suggests the formation of a mixed Pd/Cs<sup>+</sup>-O adlayer on the PdAu particles during reaction.

### 3.3.3. Stability of the Pd/M<sup>+</sup>-O Adlayer on PdAu/MOAc/SiO<sub>2</sub> (M<sup>+</sup> = Li<sup>+</sup>, Na<sup>+</sup>, K<sup>+</sup>, Cs<sup>+</sup>)

Having established the existence of a mixed Pd/M<sup>+</sup>-O layer as shell on the PdAu bulk particles for M<sup>+</sup> = K<sup>+</sup> and Cs<sup>+</sup>, we extend the investigation to the stability of Pd/M<sup>+</sup>-O for M<sup>+</sup> = Li<sup>+</sup>, Na<sup>+</sup>, K<sup>+</sup>, Cs<sup>+</sup> using IR spectroscopy of adsorbed CO at -150 °C. Assuming that Pd/M<sup>+</sup>-O is less soluble in water than the MOAc/AcOH layer in contrast to the completely insoluble bimetallic PdAu core, 20 minutes washing removed adsorbed MOAc/AcOH and Pd<sup>2+</sup> species whereas Pd<sup>0</sup> from Pd/M<sup>+</sup>-O can be only removed after 24 h washing.

Figure A3.3 reflects the IR spectra of adsorbed CO at  $-150\text{ }^{\circ}\text{C}$  on PdAu/MOAc/SiO<sub>2</sub> washed for 24 h and Table A3.1 in the Appendix the corresponding surface concentrations of CO.

Figure 3.4 illustrates the difference in Pd surface concentration of samples washed for 20 min (blue) and 24 h (orange) as green bars, which allow comparing the relative concentrations of the Pd/M<sup>+</sup>-O adlayer as function of the cations. The concentration of the Pd/M<sup>+</sup>-O layer (green bar) increased from LiOAc to CsOAc promoted PdAu/SiO<sub>2</sub>. The relation between higher Pd/M<sup>+</sup>-O concentrations deposited on PdAu and the higher Pd surface concentrations on PdAu surfaces indicates the existence of an equilibrium between Pd in Pd/M<sup>+</sup>-O and on PdAu under reaction conditions.

The generally higher Pd surface concentration of LiOAc compared to NaOAc promoted PdAu/SiO<sub>2</sub> (Figure 3.4) might result from slightly smaller PdAu particles on PdAu/LiOAc/SiO<sub>2</sub> than on the other samples. As LiOAc was significantly leached during reaction (Table 3.1), less particle sintering induced by the promoter maintained smaller PdAu particles and led to higher CO band intensities.

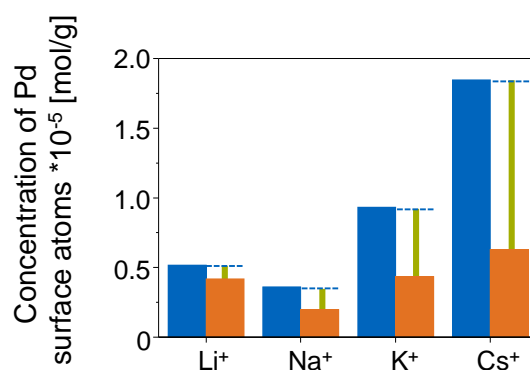


**Figure 3.4.** Surface concentrations of Pd in contact to Pd [mol/g] for spent Li-, Na-, K- and Cs-acetate promoted PdAu/SiO<sub>2</sub> washed for 20 min (blue) and 24 h (orange). Calculated from the band areas of CO linearly adsorbed on Pd (blue) with the molar absorption coefficients of CO on Pd/SiO<sub>2</sub>.<sup>[21]</sup>

The increasing concentration of Pd/M<sup>+</sup>-O from Li<sup>+</sup> to Cs<sup>+</sup> was confirmed by AAS of Pd in used PdAu/MOAc/SiO<sub>2</sub> samples washed for 20 min (Table 3.3).

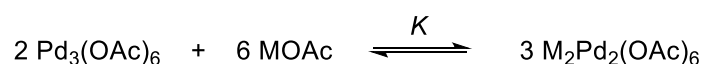
**Table 3.3.** Pd concentrations [wt%] in PdAu/MOAc/SiO<sub>2</sub> (M<sup>+</sup> = Li<sup>+</sup>, Na<sup>+</sup>, K<sup>+</sup>, Cs<sup>+</sup>) after 20 min washing and in the AcOH layer.

PdAu/MOAc/SiO <sub>2</sub> ; M <sup>+</sup> =	Pd concentration [wt%]	
	Pd in PdAu and in adlayer	Pd in AcOH (inactive for VAS)
Li <sup>+</sup>	1.03	0.27
Na <sup>+</sup>	1.15	0.15
K <sup>+</sup>	1.20	0.10
Cs <sup>+</sup>	1.28	0.02

Both, the AAS results (Table 3.3) and IR spectra (Figure 3.4) strongly suggest increasing concentrations of Pd/M<sup>+</sup>-O and decreasing concentrations of “Pd in AcOH” (Pd<sub>3</sub>(OAc)<sub>6</sub>) from M<sup>+</sup> = Li<sup>+</sup> to Cs<sup>+</sup>.

The conclusion that the nature of the promoter metal determines the distribution of Pd in PdAu, Pd/M<sup>+</sup>-O and in the AcOH layer (Pd<sup>2+</sup>/Pd<sup>0</sup>) allowed us to hypothesize that the Pd acetate species present are linked by equilibria influenced by MOAc. The key to rationalize activity and deactivation of PdAu is an understanding of the genesis and reduction of Pd<sup>2+</sup> species in dependence of the type of cation in MOAc.

The existence of a dimeric K<sub>2</sub>Pd<sub>2</sub>(OAc)<sub>6</sub><sup>[21]</sup>, dimeric Na<sub>2</sub>Pd<sub>2</sub>(OAc)<sub>6</sub><sup>[61]</sup> and a “lithium-palladium acetate complex”<sup>[62]</sup> were suggested previously. We show here that these complexes are formed with all alkali metal acetates by the reaction of trimeric Pd<sub>3</sub>(OAc)<sub>6</sub> species with MOAc (Scheme 3.1)<sup>[63]</sup> (Figure A3.4, Appendix).



**Scheme 3.1.** Conversion of trimeric Pd<sub>3</sub>(OAc)<sub>6</sub> to dimeric M<sub>2</sub>Pd<sub>2</sub>(OAc)<sub>6</sub> with MOAc.

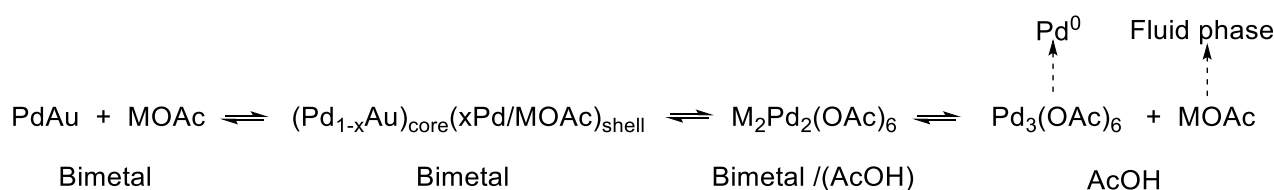
The equilibrium constant *K* between (inactive) trimeric Pd<sub>3</sub>(OAc)<sub>6</sub> and (active) dimeric M<sub>2</sub>Pd<sub>2</sub>(OAc)<sub>6</sub> is proportional to the solvation energy of the alkali metal cation M<sup>+</sup><sup>[64]</sup>. The equilibrium constant *K* and the solvation energy of M<sup>+</sup> increase in parallel with the increasing hydration enthalpy from Li<sup>+</sup> to Cs<sup>+</sup><sup>[65-66]</sup>. Consequently, the highest M<sub>2</sub>Pd<sub>2</sub>(OAc)<sub>6</sub> concentrations can be expected for CsOAc<sup>[64-65]</sup>. Thus, the washing water of used PdAu/MOAc/SiO<sub>2</sub> was colorless (M<sub>2</sub>Pd<sub>2</sub>(OAc)<sub>6</sub>) when Cs<sup>+</sup> was used and orange brown due to Pd<sub>3</sub>(OAc)<sub>6</sub> for M<sup>+</sup> = Li<sup>+</sup>. As expected, the concentration of soluble Pd<sub>3</sub>(OAc)<sub>6</sub> (“Pd in AcOH”) decreased from M<sup>+</sup> = Li<sup>+</sup> to Cs<sup>+</sup> (Table 3.3).

The dimeric M<sub>2</sub>Pd<sub>2</sub>(OAc)<sub>6</sub> is distributed between the surface of solid PdAu and the AcOH layer<sup>[20]</sup> depending on its solubility in AcOH which decreases with increasing *K* (from Li<sup>+</sup> to Cs<sup>+</sup>). Li<sub>2</sub>Pd<sub>2</sub>(OAc)<sub>6</sub> is expected to be present in both phases, while the solubility of Na<sub>2</sub>Pd<sub>2</sub>(OAc)<sub>6</sub> was found to be limited<sup>[67]</sup>. Thus, M<sub>2</sub>Pd<sub>2</sub>(OAc)<sub>6</sub> (M<sup>+</sup> = K<sup>+</sup>, Cs<sup>+</sup>) are hypothesized to be mainly located around the bimetallic PdAu core under reaction conditions. M<sub>2</sub>Pd<sub>2</sub>(OAc)<sub>6</sub> was easily reduced by C<sub>2</sub>H<sub>4</sub> to Pd/M<sup>+</sup>-O, which can be seen as precursor for the incorporation of Pd<sup>0</sup> into bimetallic PdAu. The higher the Pd/M<sup>+</sup>-O concentration (especially for M<sup>+</sup> = K<sup>+</sup>, Cs<sup>+</sup>), the higher the Pd surface concentration on PdAu/MOAc/SiO<sub>2</sub> as observed by IR spectroscopy of adsorbed CO (Figure 3.4).

Increasing equilibrium constants *K* from Li<sup>+</sup> to Cs<sup>+</sup> lower the concentrations of MOAc in AcOH and thus, reduce the probability for MOAc to leach into the fluid phase (Table 3.1).

Scheme 3.2 summarizes the reaction pathway of Pd from the bimetallic core to the particle surface and into AcOH by oxidative solvation and finally the release of MOAc from AcOH into the fluid phase. The formation of Pd<sup>0</sup> is not in equilibrium with Pd<sub>3</sub>(OAc)<sub>6</sub> as the reduction of Pd<sup>2+</sup> proceeds via an irreversible β-H elimination within the homogeneous pathway to VA<sup>[16]</sup>.





**Scheme 3.2.** Proposed network for the overall reordering process of PdAu/MOAc/SiO<sub>2</sub> during reaction.

### 3.3.4. Deactivation of PdAu/MOAc/SiO<sub>2</sub> (M<sup>+</sup> = Li<sup>+</sup>, Na<sup>+</sup>, K<sup>+</sup>, Cs<sup>+</sup>)

On the basis of Scheme 3.2, reordering of PdAu with MOAc towards (Pd<sub>1-x</sub>Au)<sub>core</sub>(xPd/MOAc)<sub>shell</sub> is essential for reaching the maximum activity level in the first hours of time-on-stream. Subsequent deactivation resulted from leaching of less active M<sub>2</sub>Pd<sub>2</sub>(OAc)<sub>6</sub><sup>[16]</sup> and almost inactive Pd<sub>3</sub>(OAc)<sub>6</sub><sup>[12]</sup> into the acetic acid film. Pd/M<sup>+</sup>-O formed from reduction of M<sub>2</sub>Pd<sub>2</sub>(OAc)<sub>6</sub> stabilizes Pd on the PdAu surface and maintains the activity of the bimetallic PdAu particles. Thus, deactivation is linked to the concentration of Pd<sub>3</sub>(OAc)<sub>6</sub> (“Pd in AcOH”) (Figure 3.5b) for Na<sup>+</sup>, K<sup>+</sup> and Cs<sup>+</sup> acetate promoted PdAu/SiO<sub>2</sub>, because Pd<sub>3</sub>(OAc)<sub>6</sub> is inactive in the pathway to VA. According to Scheme 3.2, deactivation (Table 3.1) also correlates with the promoter loss (Figure 3.5a) implying that the promoter is essential to maintain maximum activity levels. However, PdAu/LiOAc/SiO<sub>2</sub> deactivated much faster than expected from the loss of Li<sup>+</sup> or the Pd<sub>3</sub>(OAc)<sub>6</sub> concentration. After the LiOAc loading decreased below a minimum level, a Pd depleted PdAu surface was observed (Figure 3.2a). Together with the limited transfer of acetates/AcOH from Li<sup>+</sup> to Pd on PdAu (Figure A3.4bi, Appendix) this was concluded to be the main reason for the strong deactivation<sup>[21]</sup>.

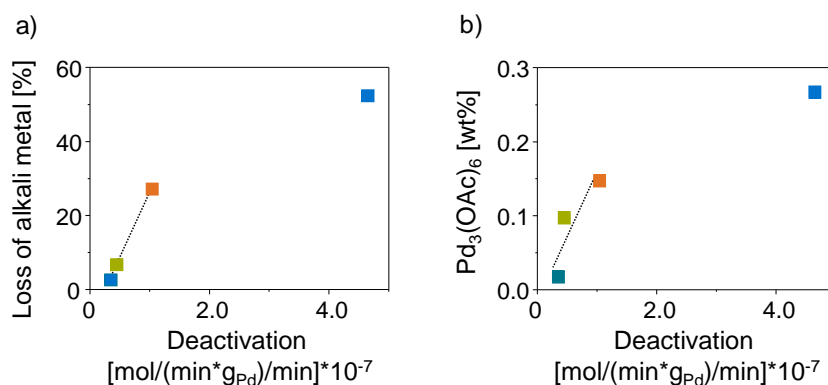


**Figure 3.5.** Correlation between (a) the loss of MOAc [%], (b) the concentration of Pd<sub>3</sub>(OAc)<sub>6</sub> [wt%] and deactivation [(mol/min\*gPd)/min] for Li<sup>+</sup> (blue), Na<sup>+</sup> (orange), K<sup>+</sup> (bright green) and Cs<sup>+</sup> (green) promoted PdAu/SiO<sub>2</sub>.

## 3.4. Conclusions

Deactivation of alkali acetate MOAc (M<sup>+</sup> = Li<sup>+</sup>, Na<sup>+</sup>, K<sup>+</sup>, Cs<sup>+</sup>) promoted PdAu/SiO<sub>2</sub> catalysts increased with smaller M<sup>+</sup> cations during vinyl acetate synthesis. MOAc forms a heterogeneous, mixed “Pd/M<sup>+</sup>-O” layer on

top of the PdAu particles and a homogeneous (active) complex  $M_2Pd_2(OAc)_6$  in equilibrium with (inactive)  $Pd_3(OAc)_6/MOAc$ . The presence of CsOAc in  $Cs_2Pd_2(OAc)_6$  and “Pd/Cs<sup>+</sup>-O” prevents CsOAc to leach into the fluid phase. In contrast LiOAc converts less inactive  $Pd_3(OAc)_6$  to  $Li_2Pd_2(OAc)_6$ , which increased the probability for LiOAc to leach from the acetic acid layer. The loss of  $M^+$  as well as the concentration of inactive  $Pd_3(OAc)_6$  species on PdAu/MOAc/SiO<sub>2</sub> ( $M^+ = Na^+, K^+, Cs^+$ ) are shown to cause deactivation. Intense deactivation of PdAu/LiOAc/SiO<sub>2</sub> is due to the dramatic decrease in LiOAc content to transfer sufficient acetates and acetic acid to the PdAu surface and to maintain a minimum of Pd on the active and selective bimetallic surface in contrast to promotion by Na<sup>+</sup>, K<sup>+</sup>, and Cs<sup>+</sup>.

### 3.5. References

- [1] P. Liu, J. K. Nørskov, *Phys. Chem. Chem. Phys.* **2001**, *3*, 3814-3818.
- [2] A. E. Baber, H. L. Tierney, E. C. H. Sykes, *ACS Nano* **2010**, *4*, 1637-1645.
- [3] S. N. Reifsnnyder, H. H. Lamb, *J. Phys. Chem. B* **1998**, *103*, 321-329.
- [4] F. Gao, D. W. Goodman, *Chem. Soc. Rev.* **2012**, *41*, 8009-8020.
- [5] D. Rainer, *J. Vac. Sci. Technol. A* **1997**, *15*, 1653-1662.
- [6] M. Chen, D. Kumar, C.-W. Yi, D. W. Goodman, *Science* **2005**, *310*, 291-293.
- [7] E. L. Kugler, M. Boudart, *J. Catal.* **1979**, *59*, 201-210.
- [8] C. J. Baddeley, R. M. Ormerod, A. W. Stephenson, R. M. Lambert, *J. Phys. Chem.* **1995**, *99*, 5146-5151.
- [9] D. Kumar, M. S. Chen, D. W. Goodman, *Catal. Today* **2007**, *123*, 77-85.
- [10] M. n. García-Mota, N. r. López, *J. Am. Chem. Soc.* **2008**, *130*, 14406-14407.
- [11] D. Yuan, X. Gong, R. Wu, *J. Phys. Chem. C* **2008**, *112*, 1539-1543.
- [12] S. Nakamura, T. Yasui, *J. Catal.* **1970**, *17*, 366-374.
- [13] S. Nakamura, T. Yasui, *J. Catal.* **1971**, *23*, 315-320.
- [14] Q. Smejkal, D. Linke, U. Bentrup, M. M. Pohl, H. Berndt, M. Baerns, A. Brückner, *Appl. Catal. A* **2004**, *268*, 67-76.
- [15] R. Abel, G. Prauser, H. Tiltscher, *Chem. Eng. Technol.* **1994**, *17*, 112-118.
- [16] B. Samanos, P. Boutry, R. Montarnal, *J. Catal.* **1971**, *23*, 19-30.
- [17] N. Macleod, J. M. Keel, R. M. Lambert, *Appl. Catal. A* **2004**, *261*, 37-46.
- [18] M.-M. Pohl, J. Radnik, M. Schneider, U. Bentrup, D. Linke, A. Brückner, E. Ferguson, *J. Catal.* **2009**, *262*, 314-323.
- [19] S. Simson, A. Jentys, J. A. Lercher, *J. Phys. Chem. C* **2013**, *117*, 8161-8169.
- [20] C. R. Reilly, J. J. Lerou, *Catal. Today* **1998**, *41*, 433-441.
- [21] E. K. Hanrieder, A. Jentys, J. A. Lercher, *ACS Catal.* **2015**, 5776-5786.
- [22] L. Prati, A. Villa, F. Porta, D. Wang, D. Su, *Catal. Today* **2007**, *122*, 386-390.
- [23] E. A. Crathorne, D. Macgowan, S. R. Morris, A. P. Rawlinson, *J. Catal.* **1994**, *149*, 254-267.
- [24] M. L. Luyben, B. D. Tyréus, *Comp. Chem. Eng.* **1998**, *22*, 867-877.
- [25] M. Bowker, C. Morgan, *Catal. Lett.* **2004**, *98*, 67-67.
- [26] A. H. Zaidi, *Appl. Catal.* **1987**, *30*, 131-140.
- [27] S. B. Ziemecki, G. A. Jones, D. G. Swartzfager, R. L. Harlow, J. Faber, *J. Am. Chem. Soc.* **1985**, *107*, 4547-4548.
- [28] D. Kumar, Y. Han, M. Chen, D. Goodman, *Catal. Lett.* **2006**, *106*, 1-5.
- [29] D. Kumar, Y. F. Han, D. Goodman, *Top. Catal.* **2007**, *46*, 169-174.
- [30] Y. F. Han, D. Kumar, D. W. Goodman, *J. Catal.* **2005**, *230*, 353-358.
- [31] Y. F. Han, J. H. Wang, D. Kumar, Z. Yan, D. W. Goodman, *J. Catal.* **2005**, *232*, 467-475.
- [32] A. Rabl, A. Renken, *Chem. Ing. Tech.* **1986**, *58*, 434-435.

- [33] G. Ertl, H. Knözinger, J. Weitkamp, *Handbook of Heterogeneous Catalysis, Vol. 5*, Wiley-VCH, Weinheim, Germany, **1997**.
- [34] W. D. Provine, P. L. Mills, J. J. Lerou, *Stud. Surf. Sci. Catal.* **1996**, *101*, 191-200.
- [35] H.-J. Eberle, R. Heidenreich, J. Weis, *Ger. DE 10 2006 058 800 A1 2008.06.19*, **2008**.
- [36] B. Ravel, M. Newville, *J. Synchrotron Rad.* **2005**, *12*, 537-541.
- [37] A. Lossin, G. Meyer, *Z. Anorg. Allg. Chem.* **1993**, *619*, 1462-1464.
- [38] W. K. Kuhn, J. Szanyi, D. W. Goodman, *Surf. Sci.* **1992**, *274*, L611-L618.
- [39] K. Hadjiivanov, J. Lamotte, J.-C. Lavalley, *Langmuir* **1997**, *13*, 3374-3381.
- [40] T. Montanari, L. Castoldi, L. Lietti, G. Busca, *Appl. Catal. A* **2011**, *400*, 61-69.
- [41] T. Montanari, R. Matarrese, N. Artioli, G. Busca, *Appl. Catal. B* **2011**, *105*, 15-23.
- [42] C. Bisio, P. Massiani, K. Fajerweg, L. Sordelli, L. Stievano, E. R. Silva, S. Coluccia, G. Martra, *Microp. Mesop. Materials* **2006**, *90*, 175-187.
- [43] T. P. Beebe, P. Gelin, J. T. Yates Jr, *Surf. Sci.* **1984**, *148*, 526-550.
- [44] M. Mihaylov, K. Hadjiivanov, H. Knözinger, *Catal. Lett.* **2001**, *76*, 59-63.
- [45] E. Ozensoy, D. Wayne Goodman, *Phys. Chem. Chem. Phys.* **2004**, *6*, 3765-3778.
- [46] T. Wei, J. Wang, D. W. Goodman, *J. Phys. Chem. C* **2007**, *111*, 8781-8788.
- [47] J. Shen, J. Hill, R. Watwe, S. G. Podkolzin, J. A. Dumesic, *Catal. Lett.* **1999**, *60*, 1-9.
- [48] D. C. Meier, D. W. Goodman, *J. Am. Chem. Soc.* **2004**, *126*, 1892-1899.
- [49] M. S. Chen, K. Luo, T. Wei, Z. Yan, D. Kumar, C. W. Yi, D. W. Goodman, *Catal. Today* **2006**, *117*, 37-45.
- [50] M. A. Vannice, S. Y. Wang, *J. Phys. Chem.* **1981**, *85*, 2543-2546.
- [51] R. P. Eischens, S. A. Francis, W. A. Pliskin, *J. Phys. Chem.* **1956**, *60*, 194-201.
- [52] N. F. Mott, *Proc. Phys. Soc.* **1935**, *47*, 571-588.
- [53] Y.-S. Lee, Y. Jeon, Y.-M. Chung, K.-Y. Lim, C.-N. Whang, S.-J. Oh, *J. Korean Phys. Soc.* **2000**, *37*, 451-455.
- [54] F. Stoop, F. J. C. M. Toolenaar, V. Ponec, *J. Catal.* **1982**, *73*, 50-56.
- [55] M. Bonarowska, A. Malinowski, W. Juszczak, Z. Karpiński, *Appl. Catal. B* **2001**, *30*, 187-193.
- [56] A. Sárkány, O. Geszti, G. Sáfrán, *Appl. Catal. A* **2008**, *350*, 157-163.
- [57] T. Akita, T. Hiroki, S. Tanaka, T. Kojima, M. Kohyama, A. Iwase, F. Hori, *Catal. Today* **2008**, *131*, 90-97.
- [58] A. F. Lee, C. J. Baddeley, C. Hardacre, R. M. Ormerod, R. M. Lambert, G. Schmid, H. West, *J. Phys. Chem.* **1995**, *99*, 6096-6102.
- [59] F. Beniere, N. Bertru, C. R. A. Catlow, M. Cole, J. Simonet, L. Angely, *J. Phys. Chem. Solids* **1992**, *53*, 449-457.
- [60] H. Jacobs, B. Harbrecht, *Z Kristall.* **1981**, *156*, 58-62.
- [61] S. Winstein, J. McCaskie, H.-B. Lee, P. M. Henry, *J. Am. Chem. Soc.* **1976**, *98*, 6913-6918.
- [62] S. A. H. Zaidi, *Appl. Catal.* **1988**, *38*, 353-358.
- [63] R. N. Pandey, P. M. Henry, *Canad. J. Chem* **1974**, *52*, 1241-1247.

- 
- [64] D. D. Kragten, R. A. van Santen, M. K. Crawford, W. D. Provine, J. J. Lerou, *Inorg. Chem.* **1999**, *38*, 331-339.
- [65] [http://www.chem.tamu.edu/rgroup/dunbar/Teaching/CHEM362/Lecture\\_33.pdf](http://www.chem.tamu.edu/rgroup/dunbar/Teaching/CHEM362/Lecture_33.pdf).
- [66] W. G. Van Der Sluys, *J. Chem. Educ.* **2001**, *78*, 111-115.
- [67] R. N. Pandey, P. M. Henry, *Canad. J. Chem.* **1975**, *53*, 1833-1841.

## 3.6. Appendix

Selectivity Behavior of PdAu/MOAc/SiO<sub>2</sub> (M<sup>+</sup> = Li<sup>+</sup>, Na<sup>+</sup>, K<sup>+</sup>, Cs<sup>+</sup>)

After a selectivity decrease during the induction period, the selectivity of PdAu/MOAc/SiO<sub>2</sub> (M<sup>+</sup> = Li<sup>+</sup>, Na<sup>+</sup>, K<sup>+</sup>, Cs<sup>+</sup>) subtly increased to ~95%. The high selectivity of PdAu/LiOAc/SiO<sub>2</sub> is attributed to the lower activity level compared with PdAu/MOAc/SiO<sub>2</sub> (M<sup>+</sup> = Na<sup>+</sup>, K<sup>+</sup>, Cs<sup>+</sup>). After 4500 min time on stream, the selectivity markedly decreased at the time when the activity dropped as well.

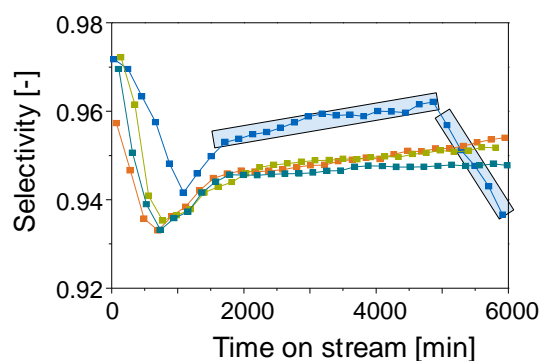


**Figure A3.1.** Selectivity with time on stream for PdAu/MOAc/SiO<sub>2</sub>; M<sup>+</sup> = Li<sup>+</sup> (blue), Na<sup>+</sup> (red), K<sup>+</sup> (bright green), Cs<sup>+</sup> (dark green). Reaction conditions: 60 vol % C<sub>2</sub>H<sub>4</sub>, 13 vol % AcOH, 4.5 vol % O<sub>2</sub>, balance N<sub>2</sub>; total pressure, 8.8 bar; temperature, 150 °C.

## EXAFS Fit Results

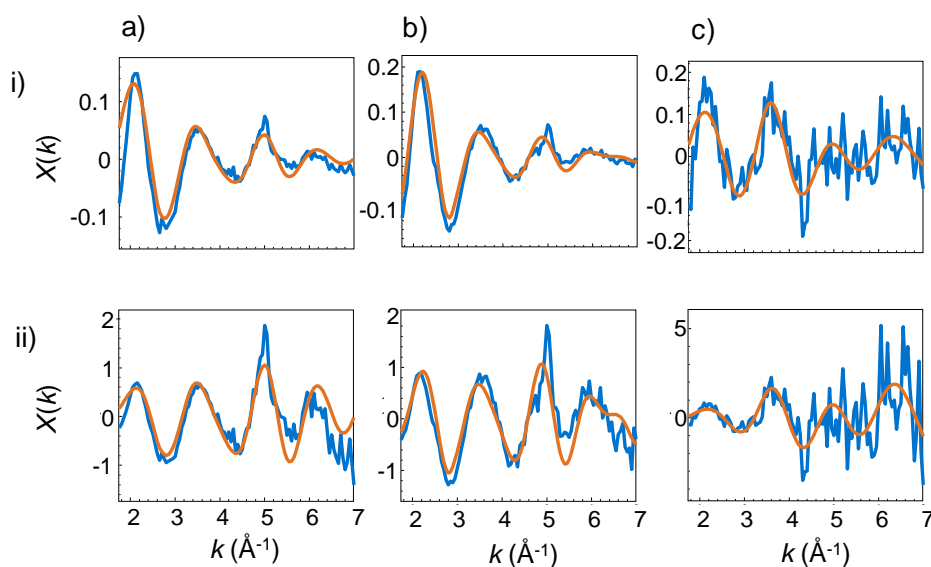


**Figure A3.2.** EXAFS function  $\chi(k)$  (blue) and fit result (orange) of a) fresh PdAu/CsOAc, b) reacted PdAu/CsOAc and c) washed, reacted PdAu/CsOAc weighted by i)  $k^1$  and ii) by  $k^3$ .

### IR Spectroscopy of Adsorbed CO on PdAu/MOAc/SiO<sub>2</sub> (M<sup>+</sup> = Li<sup>+</sup>, Na<sup>+</sup>, K<sup>+</sup>, Cs<sup>+</sup>) Washed for 24h

Figure A3.3 displays the IR spectra of adsorbed CO on spent PdAu/MOAc/SiO<sub>2</sub> (M<sup>+</sup> = Li<sup>+</sup>, Na<sup>+</sup>, K<sup>+</sup>, Cs<sup>+</sup>) which were washed for 24h in order to completely remove dispersed Pd from the catalytically active PdAu surface. Table A3.1 summarizes the corresponding surface concentrations [10<sup>-6</sup> mol/g] and fractions [%] of the different Au and Pd species. The individual concentrations were calculated with absorption coefficients  $\epsilon$  determined on monometallic Au/SiO<sub>2</sub> and Pd/SiO<sub>2</sub> samples<sup>[1]</sup> assuming a ratio of  $\epsilon_{\text{linear}}/\epsilon_{\text{bridged}} \approx 25.8$  for Pd.<sup>[2]</sup> The fractions for well-mixed PdAu surfaces (“Au next to Pd” and “Pd next to Au”) decreased from 14 % to 11 % and from 19 % to 5 % when going from M<sup>+</sup> = Li<sup>+</sup> to Cs<sup>+</sup>. In contrast, the surface concentration, the fraction of Pd in larger ensembles (“Pd next to Pd”) and the surface Pd/Au ratio increased markedly reflecting a pronounced stabilization of Pd on the PdAu surface from Li<sup>+</sup> to Cs<sup>+</sup>.

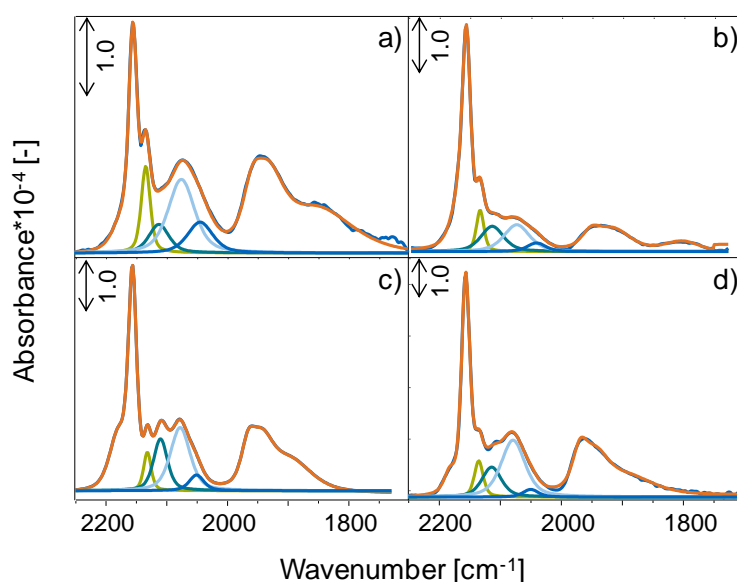


**Figure A3.3.** IR spectra of adsorbed CO (1 mbar) at -150 °C on reactively restructured PdAu/MOAc/SiO<sub>2</sub> (M<sup>+</sup> = Li<sup>+</sup> (a), Na<sup>+</sup> (b), K<sup>+</sup> (c) and Cs<sup>+</sup> (d) after 24h washing. Green lines represent CO on Au and blue lines CO on Pd.

**Table A3.1.** Surface concentrations [10<sup>-6</sup> mol/g] and corresponding fractions [%] in brackets of CO adsorbed on PdAu/MOAc/SiO<sub>2</sub> after reaction (washed for 24 h).

PdAu/MOAc/SiO <sub>2</sub> M <sup>+</sup> =	Au next to Pd	Au next to Au	Pd next to Pd	Pd next to Au	linear/bridged CO	Pd/Au
	[10 <sup>-6</sup> mol/g] ([%])				[mol/g/mol/g]	[mol/g/mol/g]
Li <sup>+</sup>	1.0 (14)	1.8 (26)	2.9 (41)	1.3 (19)	16.7	1.5
Na <sup>+</sup>	0.6 (10)	1.0 (28)	1.6 (45)	0.4 (11)	35.6	1.3
K <sup>+</sup>	0.6 (10)	1.6 (24)	3.6 (56)	0.7 (10)	20.5	2.0
Cs <sup>+</sup>	1.0 (11)	1.7 (20)	5.5 (63)	0.5 (5)	23.3	2.2

### In Situ IR Spectroscopy of PdAu/MOAc/SiO<sub>2</sub> (M<sup>+</sup> = Li<sup>+</sup>, Cs<sup>+</sup>)

Infrared spectra of the samples in continuous reactant flow were collected with a resolution of 4 cm<sup>-1</sup> on a Thermo Fisher Nexus. The samples were pressed into self-supporting wafers (10 mg/cm<sup>2</sup>), cut in half and placed in a flow IR cell designed by Mirth et al.<sup>[3]</sup> The cell could be vertically moved to measure either the IR spectra of the wafer or of the gas phase present inside the cell through the empty section in the upper half to be able to subtract the contributions of the gas phase (which is significant at a pressure of 9 bar) from the spectra of the adsorbed species measured. Prior to adsorption, samples were reduced and activated at 250 °C (heating rate 5 °C/min) in H<sub>2</sub> followed by N<sub>2</sub>. The adsorption of the reactants, acetic acid and oxygen was carried out at 150 °C and 9 bar total pressure. Acetic acid (16 mbar) was added using a temperature controlled saturator (40 °C, 7.1 mL/min N<sub>2</sub>). The oxygen flow (0.9 mL/min) is mixed into the N<sub>2</sub> carrier gas stream (12 mL/min) via a mass flow controller (Total flow of 20 mL/min).

Figure A3.4 represents the difference IR spectra of PdAu/MOAc/SiO<sub>2</sub> (M<sup>+</sup> = Li<sup>+</sup>, Cs<sup>+</sup>) during AcOH (a) and AcOH/O<sub>2</sub> (b) treatment. AcOH adsorption (Figure A3.4a) leads to a broad  $\nu(\text{C}=\text{O})$  band of the different AcOH adsorption species: monomers (~1767 cm<sup>-1</sup>), dimers (1737 cm<sup>-1</sup>) and AcOH in contact to M<sup>+</sup> (1719 cm<sup>-1</sup>). Additionally,  $\nu_{\text{as}}(\text{COO})$  and  $\nu_{\text{s}}(\text{COO})$  of acetates in MOAc appeared between 1650-1500 cm<sup>-1</sup> and 1470-1400 cm<sup>-1</sup> whereas CH<sub>3</sub> deformation modes were located at 1380 cm<sup>-1</sup>. The changes upon AcOH/O<sub>2</sub> compared to AcOH sorption (Figure A3.4b) indicated the presence of terminal acetates bound to the PdAu surface at 1735 cm<sup>-1</sup> on PdAu/CsOAc/SiO<sub>2</sub> (Figure A3.4bii). The decrease of  $\nu(\text{C}=\text{O})$  of terminal acetates at ~1735 cm<sup>-1</sup> that are supposed to be intermediates in the heterogeneous pathway to VA, may be one reason for the general low activity of PdAu/LiOAc/SiO<sub>2</sub> (Figure A3.4bi). Additionally, the shift of  $\nu(\text{C}=\text{O})$  from 1735 cm<sup>-1</sup> (Li) to 1720 cm<sup>-1</sup> (Cs) suggest weakening of the carbonyl group in AcOH by eventual interactions with M<sup>+</sup> of MOAc. The decrease of LiOAc (1574/1448 cm<sup>-1</sup>) and CsOAc (1551 cm<sup>-1</sup>) vibrations and the simultaneous increase in acetate vibrations at 1656/1624 cm<sup>-1</sup> for LiOAc and at 1631/1601 cm<sup>-1</sup> for CsOAc revealed the formation of dimeric M<sub>x</sub>Pd<sub>y</sub>(OAc)<sub>z</sub> species.<sup>[1]</sup> The acetate carboxylate stretch vibrations are shifted to lower wavenumbers from LiOAc to CsOAc promoted PdAu/SiO<sub>2</sub>. As the ratio in band area of terminal to bridging acetates (T/B) is ~4/2, the formation of dimeric M<sub>2</sub>Pd<sub>2</sub>(OAc)<sub>6</sub> for M<sup>+</sup> = Li<sup>+</sup>, Cs<sup>+</sup> on both catalysts is proposed like for the case of K<sub>2</sub>Pd<sub>2</sub>(OAc)<sub>6</sub>.



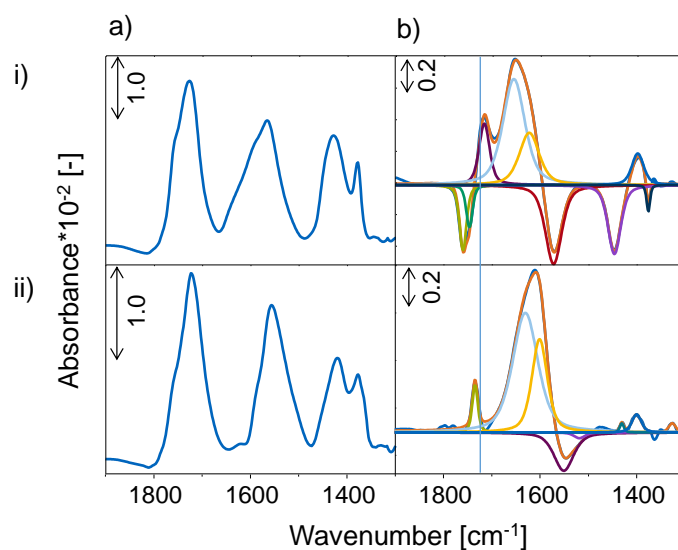


**Figure A3.4.** In situ IR difference spectra of i) PdAu/LiOAc/SiO<sub>2</sub> and ii) PdAu/CsOAc/SiO<sub>2</sub> adsorbed with (a) AcOH and (b) AcOH/O<sub>2</sub>. 16 mbar AcOH, 4.5 vol % O<sub>2</sub>, total flow of 20 mL/min; total pressure, 8.8 bar; temperature, 150 °C.

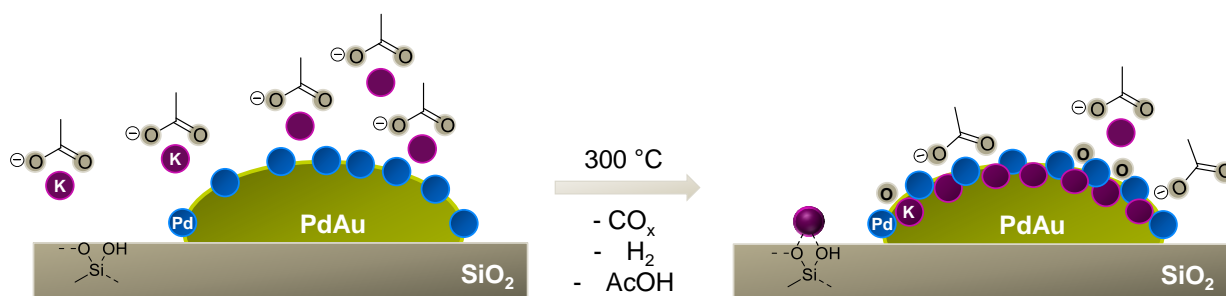
## References

- [1] E. K. Hanrieder, A. Jentys, J. A. Lercher, *ACS Catal.* **2015**, 5776-5786.
- [2] M. A. Vannice, S. Y. Wang, *J. Phys. Chem.* **1981**, 85, 2543-2546.
- [3] G. Mirth, J. A. Lercher, *J. Catal.* **1991**, 132, 244-252.

# Chapter 4

## Interaction of Alkali Acetates with PdAu<sup>3</sup>

The temperature dependence of the interaction of PdAu alloy particles with alkali acetate promoters (MOAc; M<sup>+</sup> = Li<sup>+</sup>, Na<sup>+</sup>, K<sup>+</sup>, Cs<sup>+</sup>) was studied by X-ray absorption and infrared spectroscopy as well as in situ X-ray diffraction. Alkali acetate promotion on PdAu particles results in irreversible enlargements of the Pd-Pd distances upon heating compared to the promoter free PdAu/SiO<sub>2</sub> catalyst. The promoter induces the migration of Pd to the particle surface and the formation of a mixed Pd/M<sup>+</sup>-O layer on the surface of the bimetallic PdAu particles, which alters catalytic reactions by electronically and geometrically modifying the PdAu surface.



<sup>3</sup> This chapter is based on the article of the same title ready for submission.

## 4.1. Introduction

Bimetallic alloy catalysts have attracted significant attention as the presence of a second metal allows to subtly modify activity and selectivity.<sup>[1-3]</sup> Metal combinations exhibiting a continuous range of solubility such as Pd and Au,<sup>[4]</sup> where both elements have similar electronegativity, metal radii and number of valence electrons have been found to be particularly rewarding.<sup>[5]</sup> Formation heats of PdAu alloys are exothermic over the entire composition range, pointing to attractive interactions between the alloy constituents and of a tendency to form long range ordered phases<sup>[6]</sup> such as Au<sub>3</sub>Pd (stable up to ~850 °C), Au<sub>1</sub>Pd<sub>1</sub> (stable up to ~100 °C) and AuPd<sub>3</sub> (stable up to ~870 °C).<sup>[7-8]</sup> Lattice parameters of these bimetallic phases follow Vegard's law and vary from 0.389 nm to 0.406 nm as a function of the composition for PdAu particles with a small negative deviation of 0.0004 nm at about 30 at-% Pd.<sup>[9]</sup>

However, the Pd/Au composition of the bulk and the catalytically active surface can differ markedly<sup>[4, 10]</sup> due to differences in surface free energies of Pd (2.043 J/m<sup>2</sup>)<sup>[11]</sup> and Au (1.626 J/m<sup>2</sup>).<sup>[12]</sup> Au preferentially decorates the surface in PdAu particles upon heating in vacuum,<sup>[13]</sup> however, we have recently shown that the presence of potassium acetate (KOAc) on PdAu, the trend reverses to surface segregation of Pd under reaction conditions of vinyl acetate (VA) synthesis.<sup>[14-15]</sup> This is induced by the stronger interaction of KOAc.<sup>[14, 16-17]</sup>

The activity and selectivity of the structure sensitive VA synthesis reaction are determined by the relative arrangement of active Pd monomers suitably spaced by inert Au atoms on the solid surface.<sup>[18]</sup> Thus, the rate-enhancing effect of KOAc in VA synthesis is attributed to a geometric reordering effect in PdAu particles. It is unclear, however, whether such local reordering induced on PdAu by KOAc exists also under “non-reactive” conditions and which impact the nature of the alkali metal has on this process. The influence on the metal-metal distances is also unclear at present. With the aim of answering these questions, we systematically studied the impact of the promoter metal nature on the local environment of Pd and Au using a combination of bulk and surface sensitive techniques and to explore the impact on activity and selectivity for the structure sensitive VA synthesis.

## 4.2. Experimental

### 4.2.1. Synthesis

PdAu/SiO<sub>2</sub> with an atomic Pd/Au ratio of 2.0 was prepared via incipient wetness impregnation.<sup>[19]</sup> HAuCl<sub>4</sub> and PdCl<sub>2</sub> were dissolved in bidistilled water (1mL/1g support) and impregnated on SiO<sub>2</sub> (HDK<sup>®</sup>). Precipitation with sodium carbonate and washing with ammonia solution (pH 8) was carried out to remove chloride ions from the precipitated metal salts. The PdAu/SiO<sub>2</sub> precursors were reduced in flowing H<sub>2</sub> (100 mL/min) at 300 °C for 1h (5 °C/min). The Pd and Au metal loading was 1.5 wt% each for all catalysts. The monometallic references Pd/SiO<sub>2</sub> and Au/SiO<sub>2</sub> were synthesized with a metal loading of 3 wt% in the same way. Li<sup>+</sup>, Na<sup>+</sup>, K<sup>+</sup> and Cs<sup>+</sup> were added as acetates to PdAu/SiO<sub>2</sub>, Pd/SiO<sub>2</sub> and Au/SiO<sub>2</sub>. For the K<sup>+</sup> containing catalysts,

different counter ions were used including acetate (KOAc), hydroxide (KOH), carbonate ( $K_2CO_3$ ) and oxalate ( $K_2C_2O_4$ ), while maintaining a constant potassium concentration of 1.28 mmol/g catalyst.

#### 4.2.2. Elemental Analysis

Potassium, palladium and gold contents were determined by atomic absorption spectroscopy (AAS). For this, 50 mg of catalyst was dissolved in a mixture containing 48 % hydrofluoric acid and nitro-hydrochloric acid. The spectrometer used was a Solaar M5 Dual Flame graphite furnace AAS (ThermoFisher).

#### 4.2.3. X-Ray Powder Diffraction

X-Ray powder diffraction measurements were conducted on a Philips X'Pert Pro PW 3040/60 system in Bragg-Brentano geometry ( $0-2\theta$ -goniometer) using Cu  $K_\alpha$  radiation (0.154056 nm) generated at 45 kV and 40 mA and a solid state detector (X'Celerator). In situ experiments were carried out in an Anton Paar HTK 1200 cell under flowing gas atmosphere ( $N_2$ ,  $H_2$ , synthetic air). The XRD patterns were measured in a  $2\theta$  range of  $5^\circ-70^\circ$  with a step size of  $0.019^\circ/s$ . Samples were annealed at  $140^\circ C$  or  $300^\circ C$  and cooled to ambient temperature with a heating and cooling rate of  $3^\circ C/min$ . The two temperature programs are shown in Figure A4.1, Appendix. The XRD patterns obtained were analyzed with High Score Plus (PANalytical) and compared to Au and Pd references from the Crystallographic Open Database (COD). Alloy compositions were calculated by applying fitted peak positions to Vegard's law.<sup>[20]</sup>

#### 4.2.4. IR Spectroscopy of Adsorbed CO

The IR spectra were recorded on a Vertex 70 spectrometer from Bruker Optics at a resolution of  $4\text{ cm}^{-1}$  collecting 100 scans. Samples were pressed into self-supporting wafers ( $\sim 10\text{ mg/cm}^2$ ), activated in vacuum ( $\sim 1.0 \times 10^{-7}\text{ mbar}$ ) and reduced in static  $H_2$  (1000 mbar) at  $300^\circ C$  for 1 h with a heating rate of  $5^\circ C/min$ . The samples were outgassed at  $300^\circ C$  in vacuum for 30 min to remove Pd hydrides before the temperature was decreased either to  $100^\circ C$  or to  $-150^\circ C$  in 5 mbar He (added to improve the thermal conductivity) to record a spectrum of the activated sample. 1.0 mbar CO was introduced and spectra were recorded until the CO adsorption-desorption equilibrium was established.

Analysis of the spectra was carried out using the software Grams AI. The spectra were background corrected and subtracted from the background corrected spectrum of the activated sample to isolate the infrared bands of adsorbed CO. These subtracted spectra were normalized to the integrated area of Si-O overtones between  $2107$  and  $1741\text{ cm}^{-1}$  of the activated sample. The intensities of the CO absorption bands were evaluated by fitting with a mixed 50/50 Gaussian-Lorentzian function.

#### 4.2.5. X-Ray Absorption Spectroscopy at the Pd-K and Au-L<sub>3</sub>-edge

X-Ray absorption spectra were measured at HASYLAB (DESY, Hamburg/Germany) on the beamlines X1 and C (electron energy of 4.5 GeV, average current of 100 mA). Spectra were recorded in transmission mode at the Pd-K edge ( $E_0 = 24350$  eV) using Si(311) crystals and Au-L<sub>3</sub> edge ( $E_0 = 11919$  eV) using Si(111) crystals. The samples were pressed into self-supporting wafers with weights to obtain a total absorbance of 2.0 to optimize the signal to noise ratio. The samples were activated at 300 °C with 5 °C/min in He (100 mL/min), reduced at 300 °C for 1h in H<sub>2</sub> and flushed with 150 mL/min He before cooling to liquid nitrogen temperature to record 2-3 spectra per sample.

EXAFS data were processed with IFEFFIT, Athena and Artemis.<sup>[21]</sup> The scattering contributions of the pre- and post-edge were removed by a third-order polynomial function. The oscillations were weighted by  $k^2$  and Fourier transformed within the limits  $k = 2.1-12 \text{ \AA}^{-1}$  for the Pd-K edge and  $k = 2.8-12 \text{ \AA}^{-1}$  for the Au-L<sub>3</sub> edge. The EXAFS functions from PdAu/LiOAc/SiO<sub>2</sub> are compared to PdAu/SiO<sub>2</sub> in Figure A4.2, Appendix.

The amplitude reduction factor  $S_o^2$  was determined for bulk references and set to 0.9 for Au and 1.0 for Pd during analysis. Multiple-edge fitting was carried out with following constraints.

$$N_{\text{AuPd}} = N_{\text{PdAu}} x_{\text{Pd}} / x_{\text{Au}} \quad (1)$$

$$r_{\text{AuPd}} = r_{\text{PdAu}} \quad (2)$$

$$\sigma_{\text{AuPd}} = \sigma_{\text{PdAu}} \quad (3)$$

$x$  being the molar fraction of the element in the bimetallic sample. The contribution of incorporated alkali metal ions in PdAu particles was evaluated applying first shell analysis.

### 4.3. Results and Discussion

#### 4.3.1. Pd Surface Enrichment on PdAu Particles Induced by MOAc ( $M^+ = \text{Li}^+, \text{Na}^+, \text{K}^+, \text{Cs}^+$ )

Electronic and geometric effects of MOAc promotor ( $M^+ = \text{Li}^+, \text{Na}^+, \text{K}^+$  and  $\text{Cs}^+$ ) on surface properties of the PdAu particles were studied by the adsorption of CO at -150 °C on PdAu/MOAc/SiO<sub>2</sub> followed by IR spectroscopy. Bands for CO adsorbed on OH groups of SiO<sub>2</sub> at 2157 cm<sup>-1</sup> [22-23] and with trace concentrations of cations at 2184 cm<sup>-1</sup> [24-25] were observed. The stretching frequency  $\nu(\text{C}=\text{O})$  of physisorbed CO appeared at 2135 cm<sup>-1</sup>. [26-27] CO adsorbed on Au atoms in a linear mode at 2104 cm<sup>-1</sup>, [2, 28-30] while on Pd atoms, both linear and bridged adsorption modes were observed at 2109 cm<sup>-1</sup> and 1991 cm<sup>-1</sup>, respectively. [29, 31-33]

On bimetallic PdAu surfaces the broad band between 2135-2000 cm<sup>-1</sup> consists of two contributions for CO linearly bound to Au (2128/2106 cm<sup>-1</sup>) and of two bands for CO linearly bound to Pd (2084/2063 cm<sup>-1</sup>). The band at 2128 cm<sup>-1</sup> is attributed to CO on Au atoms surrounded by Pd (linear CO on ‘‘Au next to Pd’’) and the band at 2106 cm<sup>-1</sup> is assigned to CO linearly bound on Au atoms in proximity to other Au atoms (linear CO

on “Au next to Au”). The band at  $2084\text{ cm}^{-1}$  is attributed to CO chemisorbed on larger Pd islands (linear CO on “Pd next to Pd”) and the band at  $2063\text{ cm}^{-1}$  to linearly adsorbed CO on Pd atoms surrounded by Au (linear CO on “Pd next to Au”).<sup>[34]</sup>

Alloying of Pd with Au shifts electron density towards the element with the larger fraction of empty valence states.<sup>[35]</sup> Lee et al. suggested that Au gains sp-type electrons and loses d-electrons, whereas Pd loses sp-electrons and gains d-electrons.<sup>[36]</sup> The increase in the electron density in the d-states of Pd leads to a stronger electron (back-)donation into the antibonding  $\pi^*$  orbitals of CO, which shifts the CO stretching vibration to lower wavenumbers.<sup>[29]</sup> In contrast, the band of linearly adsorbed CO on Au in proximity to Pd appeared at higher wavenumbers, as the electron density in the d-bands of Au decreases by the interaction with Pd.<sup>[14]</sup>

Figure 4.1 presents the IR spectra of CO adsorbed on PdAu/MOAc/SiO<sub>2</sub> ( $M^+ = \text{Li}^+, \text{Na}^+, \text{K}^+, \text{Cs}^+$ ) at  $-150\text{ }^\circ\text{C}$ .

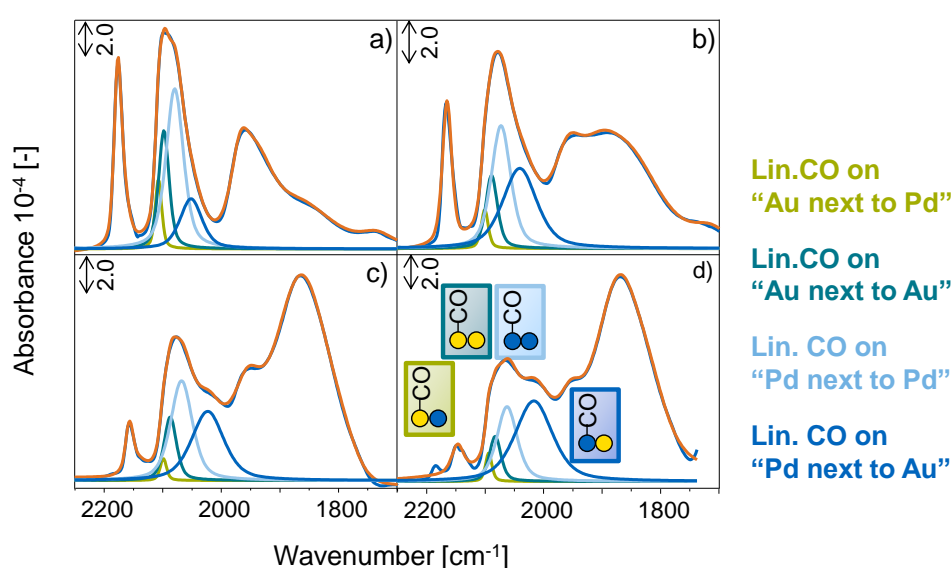


**Figure 4.1.** IR spectra of 1.0 mbar CO adsorbed on PdAu/SiO<sub>2</sub> promoted with (a) LiOAc, (b) NaOAc, (c) KOAc and (d) CsOAc at  $-150\text{ }^\circ\text{C}$ . Green lines represent linearly adsorbed CO on Au, blue lines CO on Pd.

The presence of MOAc on PdAu led (i) to a shift of the stretching frequencies assigned to linear and bridged CO to lower wavenumbers, (ii) to a broadening of linear and bridged bands of adsorbed CO, (iii) to a preferential adsorption of CO on bridged rather than on linear sites and (iv) to a change in the relative band areas of linearly adsorbed CO on Au and Pd. These changes increased with increasing alkali metal radius from  $\text{Li}^+, \text{Na}^+, \text{K}^+$  to  $\text{Cs}^+$ .

The gradual downshift (Figure 4.2) of the linear and bridged CO bands from  $\text{Li}^+$  to  $\text{Cs}^+$  promoted PdAu resulted from the electron donating effect of the promoter towards the metal d-orbitals. This leads to an enhanced back donation from Pd and Au into the  $2\pi^*$  antibonding orbitals of CO, which strengthens the metal-carbon bond but weakens the carbon-oxygen bond.<sup>[37-42]</sup>

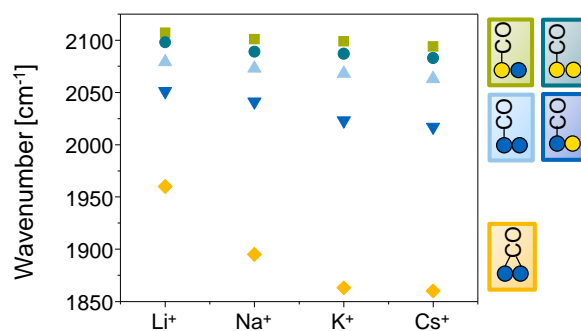


**Figure 4.2.** IR band positions [cm<sup>-1</sup>] of linearly and bridged adsorbed CO in dependence of the promoter  $M^+$  in PdAu/MOAc/SiO<sub>2</sub> ( $M^+ = \text{Li}^+, \text{Na}^+, \text{K}^+, \text{Cs}^+$ ).

The electron-donating character increased from Li<sup>+</sup> (hard) to Cs<sup>+</sup> (soft).  $M^+$  species are considered to produce a long-range electronic effect mediated by the substrate, which is effective over several interatomic distances.<sup>[40]</sup> These electronic effects of MOAc on PdAu can interfere with the intermolecular dipole-dipole coupling of CO, which leads to an increase in the wavenumber of  $\nu(\text{C}=\text{O})$  vibration with increasing surface coverage.<sup>[43]</sup> Therefore, an alternative explanation for the decrease in the frequency of the CO stretching vibration could be related to the reduction of the concentration Pd adsorption sites for CO by the presence of K<sup>+</sup> and thus the extent of dipole-dipole coupling.<sup>[44]</sup> The electron-donating alkali metals  $M^+$  increase the binding energy of reactive molecules to the metal by enhancing back donation, leading, e.g., to a higher heat of adsorption of CO.<sup>[37-38, 41]</sup> Therefore, we attribute the shift of the CO stretching vibration to electronic effects resulting from the interaction with MOAc, while (geometric) CO dipole interactions do not play a role for band positions.

The increased widths at half height of the CO band is attributed to an enhanced surface heterogeneity induced by the presence of MOAc, which resulted in an enhanced disorder in adsorbed CO overlayer. The continuous shift of CO bands results from the varying distances between CO to  $M^+$ . The shorter the distance between CO and  $M^+$ , the larger the CO band shift.

The preferential adsorption of CO in bridged rather than linear form and the change in integral intensity of linearly adsorbed CO on Au and Pd indicates a MOAc induced enrichment of Pd on the bimetallic PdAu surface. The increasing Pd enrichment from Li<sup>+</sup> to Cs<sup>+</sup> can be seen from the decreasing concentration of CO adsorbed on Au than on Pd as well as the decreasing ratio between linear/bridged adsorbed CO and the increasing overall Pd/Au ratio derived from IR spectra. Table 4.1 compiles the surface concentrations [10<sup>-6</sup> mol/g] and fractions [%] for CO adsorbed on PdAu/MOAc/SiO<sub>2</sub> calculated from absorption coefficients of CO on pure Au and Pd.<sup>[14]</sup>

**Table 4.1.** Surface concentrations [ $10^{-6}$  mol/g] and corresponding fractions [%] in brackets of CO adsorbed on PdAu/MOAc/SiO<sub>2</sub> after reaction (washed for 20 min).

PdAu/MOAc/SiO <sub>2</sub>	Au next to Pd	Au next to Au	Pd next to Pd	Pd next to Au	linear/bridged CO	Pd/Au
M <sup>+</sup> =	[10 <sup>-6</sup> mol/g] ([%])				[mol/g/mol/g]	[mol/g/mol/g]
Li <sup>+</sup>	3.0 (6)	8.3 (18)	25 (54)	9.8 (21)	20.3	3.1
Na <sup>+</sup>	1.9 (4)	5.9 (14)	20 (47)	15 (35)	14.5	4.5
K <sup>+</sup>	0.9 (2)	4.9 (12)	18 (43)	18 (44)	11.2	6.3
Cs <sup>+</sup>	1.1 (3)	3.2 (8)	13 (30)	24 (59)	11.8	8.5

The fractions of Au on PdAu, i.e., “Au next to Pd” and “Au next to Au” decreased from 6 % to 3 % and from 18 % to 8 %, respectively, with increasing main quantum number of the promoter. At the same time, the fraction of “Pd next to Pd” decreased from 54 % to 30 %, while that of “Pd next to Au” strongly increased from 21 % to 59 % from Li<sup>+</sup> to Cs<sup>+</sup>. The significant increase of the band for CO on “Pd next to Au” is accompanied by a decrease of “Au next to Pd”. These bands are complementary and thus, they should show an opposite trend. The large shift in band position of “Pd next to Au” and to lower wavelengths indicated that these Pd domains were in contact with MOAc. Due to these significant band shifts the bands assigned to “Pd next to Pd” and “Pd next to Au” were overlapping. The overall linear/bridged CO as well as the Pd/Au surface ratio was calculated with absorption coefficients<sup>[14]</sup> from the adsorption of CO on monometallic Au/SiO<sub>2</sub> and Pd/SiO<sub>2</sub>. It decreased from 20.3 to 11.8 while the overall surface Pd/Au ratio increased from 3.1 to 8.5 when going from Li- to CsOAc. Acetates covalently bound to Li<sup>+</sup> show a lower strength of interaction with Pd in PdAu than acetates from CsOAc. The effect of acetate ions on PdAu and thus, the Pd surface enrichment increased towards CsOAc.

Having shown that MOAc induced PdAu particle reordering towards a pronounced Pd surface enrichment (increasing from Li to Cs acetate) under “non-reactive” heating, we investigate in the next step if the promoter has also an influence on the metal-metal distances.

#### 4.3.2. Interaction of MOAc (M<sup>+</sup> = Li<sup>+</sup>, Na<sup>+</sup>, K<sup>+</sup>, Cs<sup>+</sup>) with Pd on PdAu

The influence of LiOAc on the structure of the bimetallic PdAu particles was further studied by EXAFS. Table 4.2 shows the metal-metal distances  $r$  and the coordination numbers  $N$  in PdAu/SiO<sub>2</sub> compared to PdAu/LiOAc/SiO<sub>2</sub> determined by multiple edge fitting with first shell analysis of Pd/Li<sup>+</sup> and Au/Li<sup>+</sup> contributions.

The addition of LiOAc to PdAu/SiO<sub>2</sub> extended the Pd-Pd distances compared to PdAu/SiO<sub>2</sub>. The total coordination numbers for Pd ( $N_{PdM} = N_{PdPd} + N_{PdAu}$ ) and for Au ( $N_{AuM} = N_{AuPd} + N_{AuAu}$ ) allow to distinguish a core-shell particle from one with a random alloy structure. In presence of a Pd enriched surface,  $N_{PdM}$  will be smaller than  $N_{AuM}$  because surface atoms have fewer neighbors than atoms in the core. On the other hand in a



random alloy structure  $N_{\text{PdM}}$  is close to  $N_{\text{AuM}}$ .<sup>[33]</sup> The presence of Pd<sub>1</sub>Au<sub>1</sub> phases can be concluded from a 2:1 ratio between  $N_{\text{Pd-Pd}}$  and  $N_{\text{Pd-Au}}$  (the same applies for the coordination numbers of Au).<sup>[16]</sup> For the samples studied, the total coordination numbers for Pd (~10) were lower than that of Au (~12), which indicates that Au occupied with preference sites in the core of the particles, while Pd atoms were located with preference on the surface. With the addition of LiOAc  $N_{\text{PdPd}}$  decreased from 7.9 to 7.1 indicating an enhanced surface segregation of Pd in presence of the promotor.

For (PdAu)<sub>core</sub>Pd<sub>shell</sub> structures, the Pd atoms in the shell adopt the bond length of the Au atoms in the core up to a thickness of the shell of ~1 nm.<sup>[33, 45]</sup> On PdAu/LiOAc/SiO<sub>2</sub> the Pd–Pd distance was significantly longer by ~0.05 Å (2.75–2.80 Å) compared to the distances PdAu/SiO<sub>2</sub>, whereas mixed interatomic Pd-Au and Au-Pd distances only slightly increased from 2.77 to 2.78 Å. The Pd lattice expansion after LiOAc impregnation suggests the formation of a Pd/Li<sup>+</sup> mixed adlayer on the PdAu alloy particle.<sup>[16]</sup> First shell analysis of the EXAFS of the promoted sample indicated a Pd/Li<sup>+</sup> distance of 2.14 Å, which is reasonable on the basis of Pd and Li<sup>+</sup> radii ( $r_{\text{Pd}} = 1.39$  Å,  $r_{\text{Li}^+} = 0.75$  Å). The small coordination number  $N_{\text{Pd/Li}^+}$  of 0.8, which averaged over all Pd atoms present in the sample, additionally underlined that the Pd/Li<sup>+</sup> adlayer is formed as a thin shell on the alloy particle core.

The fit of the EXAFS oscillations improved significantly by including Pd/Li<sup>+</sup> contributions, while Au/Li<sup>+</sup> interactions were excluded as first shell analysis yielded nonrealistic parameters (i.e. unacceptable distances and partly negative coordination numbers).

**Table 4.2.** Interatomic metal distances and coordination numbers in PdAu/SiO<sub>2</sub> and PdAu/LiOAc/SiO<sub>2</sub>.

Sample	Au-Pd		Au-Au		Pd-Au		Pd-Pd		Pd-M <sup>+</sup>	
	$r/\text{Å}$	$N$	$r/\text{Å}$	$N$	$r/\text{Å}$	$N$	$r/\text{Å}$	$N$	$r/\text{Å}$	$N$
PdAu/SiO <sub>2</sub>	2.77	4.5	2.80	7.3	2.77	2.2	2.75	7.9	-	-
PdAu/LiOAc/SiO <sub>2</sub>	2.78	4.8	2.79	7.2	2.78	2.4	2.80	7.1	2.14	0.8

The changes in the interatomic Pd distances upon promoter impregnation and activation were first studied by XRD using the KOAc as model and then expanded to the other alkali acetates. The in situ XRD measured in N<sub>2</sub> flow in presence and absence of KOAc on mono- and on bimetallic catalysts is shown Figure 4.3. The Pd(111) and Pd<sub>x</sub>Au<sub>y</sub>(111) reflexes were observed between 36 and 42 °2θ for (a) PdAu/KOAc/SiO<sub>2</sub>, (b) PdAu/SiO<sub>2</sub>, (c) Au/KOAc/SiO<sub>2</sub> and (d) Pd/KOAc/SiO<sub>2</sub>. On fresh PdAu/KOAc/SiO<sub>2</sub> catalysts. Au- and Pd-rich (Pd<sub>0</sub>Au<sub>100</sub>, Pd<sub>89</sub>Au<sub>11</sub>) as well as bimetallic particles composed of Pd<sub>54</sub>Au<sub>46</sub> were observed (Figure 4.3a).<sup>[14]</sup> While heating to 300 °C the Pd(111) reflex shifted from 40.0° to 39.3 °2θ between 150 to 200°C and further to 39.1 °2θ at 250 °C. The total shift of Pd(111) by Δθ = -0.9° to lower angles was irreversible upon cooling to room temperature. This KOAc induced shift in the Pd(111) reflex can be related to the enlargement of the Pd-Pd bond distance of ~0.055 Å, which is in good agreement with the increase in the Pd-Pd bond distance observed by EXAFS (~0.05 Å).

Temperature induced miscibility effects on bimetallic PdAu particles are independent of the presence of KOAc (Figure 4.3b). The absence of a shift of the Au(111) peak in PdAu/KOAc/SiO<sub>2</sub> as well as in monometallic

Au/KOAc (Figure 4.3c) confirmed that KOAc adsorption had no influence on the Au-Au distance, while in monometallic Pd/KOAc/SiO<sub>2</sub> the Pd(111) diffraction peak shifted to lower angles by -1 ° (Figure 4.3d). The asymmetric shape of the Pd(111) reflection after cooling to 50 °C indicated the presence of two overlapping contributions at 39.26° and 40.05 °2θ corresponding to Pd-Pd distance enlargements of 0.055 Å and 0.002 Å. Consequently, in situ XRD results confirm the presence of a Pd/K<sup>+</sup> shell on Pd or PdAu implying that Pd migrates from the particle bulk to the alloy surface upon KOAc loading.

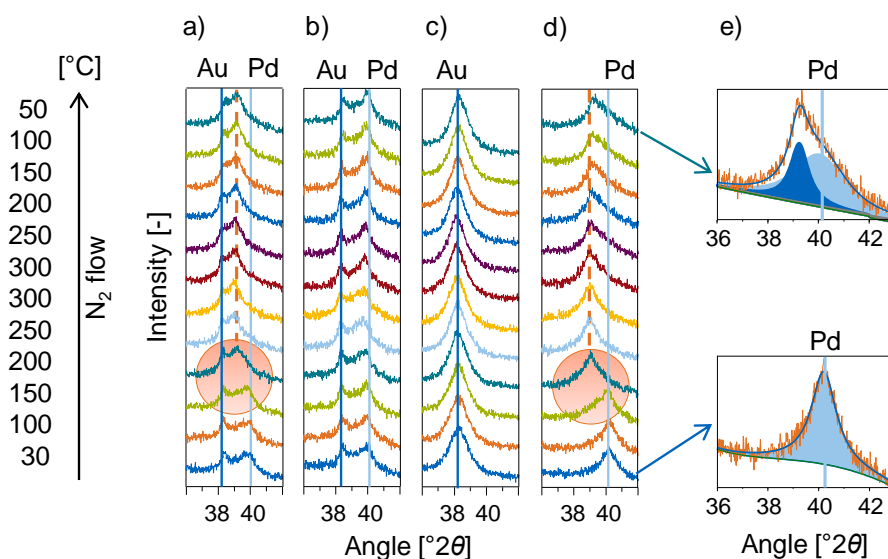


**Figure 4.3.** In situ XRD profiles of Pd<sub>x</sub>Au<sub>y</sub>(111) for (a) PdAu/KOAc/SiO<sub>2</sub> (b) PdAu/SiO<sub>2</sub>, (c) Au/KOAc/SiO<sub>2</sub> and (d) Pd/KOAc/SiO<sub>2</sub> in flowing N<sub>2</sub>. The bimetallic phase is located between those of the pure metals: Au(111) (2θ = 38.3°, blue line) and Pd(111) (2θ = 40.1°, bright blue line).

The next part addresses the question whether the Pd-Pd distance depends on the size of the promoter ions by comparing Li-, Na-, K- and Cs-acetate promoted PdAu/SiO<sub>2</sub> (Figure A4.3, Appendix). In order to detect the starting temperature of Pd-Pd bond expansion, the temperature was increased from 100 °C to 140 °C with steps of 10 °C allowing the system to equilibrate for 2 h at each temperature.

The position of the Pd(111) peak was independent on the type of promoter. However, the temperature of the Pd-Pd bond expansion decreased from 120 °C for PdAu/LiOAc/SiO<sub>2</sub> to 110 °C for Na-, K- and Cs-OAc impregnated PdAu/SiO<sub>2</sub>. This indicates that the formation of the Pd/M<sup>+</sup> adlayer is accompanied by acetate decomposition to CO<sub>x</sub> and H<sub>2</sub> catalyzed by Pd.<sup>[46]</sup> To test this hypothesis, the K<sup>+</sup> counter ion was varied from acetate to (non-decomposable) OH<sup>-</sup>, CO<sub>3</sub><sup>2-</sup>, C<sub>2</sub>O<sub>4</sub><sup>2-</sup>. The Pd-Pd bond enlargement increased in the order OH<sup>-</sup> < CO<sub>3</sub><sup>2-</sup> < C<sub>2</sub>O<sub>4</sub><sup>2-</sup> < OAc<sup>-</sup> (Figure A4.4b, Appendix) underlining that Pd/M<sup>+</sup> formation is induced by counter ion transformation..

Summarizing, IR, XAS and in situ XRD showed the temperature and counter ion dependent, but alkali cation radius independent formation of a Pd/M<sup>+</sup> adlayer on PdAu alloy particles. The formation of PdC<sub>x</sub>, Pd hydride or Pd oxide species, which result in a similar Pd(111) peak shift<sup>[47-50]</sup>, was excluded by additional in situ XRD experiments in Figure A4.5, Appendix. So only M<sup>+</sup> from MOAc (M<sup>+</sup> = Li<sup>+</sup>, Na<sup>+</sup>, K<sup>+</sup>, Cs<sup>+</sup>) induced the Pd-Pd bond enlargement. The fact that the Pd-Pd distance does not change as a function of the cation suggests that

these cations form a surface layer on top of Pd inducing widening of the Pd-Pd distance in analogy to the widening of M-M distances increase upon H adsorption on metal nanoparticles.

### 4.3.3. Chemical Nature of the Pd/M<sup>+</sup> Adlayer

Having shown that the migration of Pd to the PdAu particle surface and the formation of a mixed Pd/M<sup>+</sup> (M<sup>+</sup> = Li<sup>+</sup>, Na<sup>+</sup>, K<sup>+</sup>, Cs<sup>+</sup>) shell on the bimetallic PdAu core is induced by the presence of alkali acetates, the chemical nature of this adlayer will be discussed in the next step.

Four locations of M<sup>+</sup> on PdAu/MOAc/SiO<sub>2</sub> can be considered, i.e., (i) physisorbed MOAc species, (ii) interactions of M<sup>+</sup> with the silica support,<sup>[51]</sup> (iii) interaction of M<sup>+</sup> on the Pd/M<sup>+</sup> adlayer (Figure 4.4) and (iv) binding of M<sup>+</sup> within the Pd/M<sup>+</sup> adlayer (see supporting information, section “In situ Spectroscopy”).

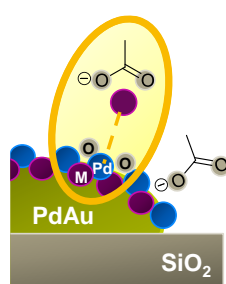


**Figure 4.4.** Interaction of M<sup>+</sup> (violet) with the Pd/M<sup>+</sup> adlayer (blue/violet).

The samples were washed with water in order to differentiate the strength of interaction. It is expected that physisorbed MOAc species are easily removed by washing, while more strongly interacting M<sup>+</sup> ions on SiO<sub>2</sub> and on/in Pd/M<sup>+</sup> have higher stability. Thus, these components would be still detected after washing by chemical analysis of the washed KOAc/SiO<sub>2</sub> (concentration of K<sup>+</sup> in SiO<sub>2</sub>) and PdAu/KOAc/SiO<sub>2</sub> samples (concentration of K<sup>+</sup> in SiO<sub>2</sub> and Pd/M<sup>+</sup>) (Table 4.3). While the samples initially contained identical K<sup>+</sup> concentrations (~4.6 wt%), 0.208 wt% K<sup>+</sup> remained on washed KOAc/SiO<sub>2</sub> and a significant higher K<sup>+</sup> concentration (0.330 wt%) was found on washed PdAu/KOAc/SiO<sub>2</sub>.

**Table 4.3.** Potassium concentrations on unwashed and washed KOAc/SiO<sub>2</sub> and PdAu/KOAc/SiO<sub>2</sub> after annealing to 300 °C.

Sample	Potassium concentration [wt%]	
	Unwashed sample	Washed sample
KOAc/SiO <sub>2</sub>	4.64	0.208
PdAu/KOAc/SiO <sub>2</sub>	4.61	0.330

The difference in K<sup>+</sup> concentrations on both washed samples (0.122 wt% ) allows to determine the K<sup>+</sup> concentration at or within the Pd/K<sup>+</sup> adlayer. With a dispersion of 24% (average PdAu particle size of 3.6 nm),

a Pd/Au molar surface ratio of 6.3 (from IR of adsorbed CO<sup>[14]</sup>) and a total Pd loading of 1.4 wt%, about  $2.7 \times 10^{-5}$  mol Pd/g is located on the surface of the bimetallic particles. The agreement with the concentration of K<sup>+</sup> in Pd/K<sup>+</sup> ( $3.1 \times 10^{-5}$  mol K<sup>+</sup>/g) indicates the formation of a Pd/K<sup>+</sup> monolayer with a ratio between K<sup>+</sup> and Pd surface atoms of  $\sim 1$ .

Having established the composition of Pd/K<sup>+</sup> as monolayer, its chemical nature was studied in more detail. To preserve the electroneutrality M<sup>+</sup> is expected to be in contact to oxygen species either in form of acetate or its oxidic decomposition products. In order to check for oxygen counter ions of K<sup>+</sup> in Pd/K<sup>+</sup>, IR spectra of CO adsorbed on activated PdAu/KOAc/SiO<sub>2</sub> and PdAu/KOH/SiO<sub>2</sub> at 100 °C were compared (Figure 4.5a and b). KOH, which partly forms K<sub>2</sub>CO<sub>3</sub> in air, is stable in oxidic form on the catalyst surface during activation at 300 °C and, thus, the electronic influence of K<sup>+</sup> and O species on Pd can be observed by comparing the IR spectra of CO adsorbed on PdAu/KOH/SiO<sub>2</sub> and on PdAu/KOAc/SiO<sub>2</sub> at 100 °C. At this temperature, CO adsorbs only on Pd surface atoms in the bimetallic PdAu particles (Figure A4.6, Appendix). Both spectra in Figure 4.5 exhibited five CO bands between 2150 and 1600 cm<sup>-1</sup> (Table 4.4). Linearly adsorbed CO on Pd sites has stretching frequencies of 2055 and  $\sim 2007$  cm<sup>-1</sup>. Bridged adsorbed CO on two neighboring Pd species appeared at 1937 cm<sup>-1</sup> and the two CO bands at  $\sim 1832$  and  $\sim 1780$  cm<sup>-1</sup> are attributed to threefold bridged adsorbed CO. Similar positions of the CO bands on both samples point to the formation of K<sup>+</sup>-oxide species from KOAc during temperature treatment. The shift of the band for threefold bridged CO species to higher wavenumbers on PdAu/KOH/SiO<sub>2</sub> (1837 and 1788 cm<sup>-1</sup>) compared to PdAu/KOAc/SiO<sub>2</sub> (1829 and 1773 cm<sup>-1</sup>) can be attributed to local CO-K<sup>+</sup> interactions with KOH. This indicates that K<sup>+</sup> from KOH remains accessible for CO adsorption and is not “incorporated” into the Pd enriched PdAu surface. In contrast, K<sup>+</sup> from KOAc formed a mixed Pd/K<sup>+</sup> layer on PdAu. The lower ratio between linear and multifold adsorbed CO and the lower total Pd surface concentration (Table 4.4) on PdAu/KOH/SiO<sub>2</sub> compared with PdAu/KOAc/SiO<sub>2</sub> indicates that KOH covered and blocks the PdAu surface, whereas K<sup>+</sup> from KOAc was incorporated in the outer Pd layer of PdAu and generated the Pd/K<sup>+</sup>-O adlayer.

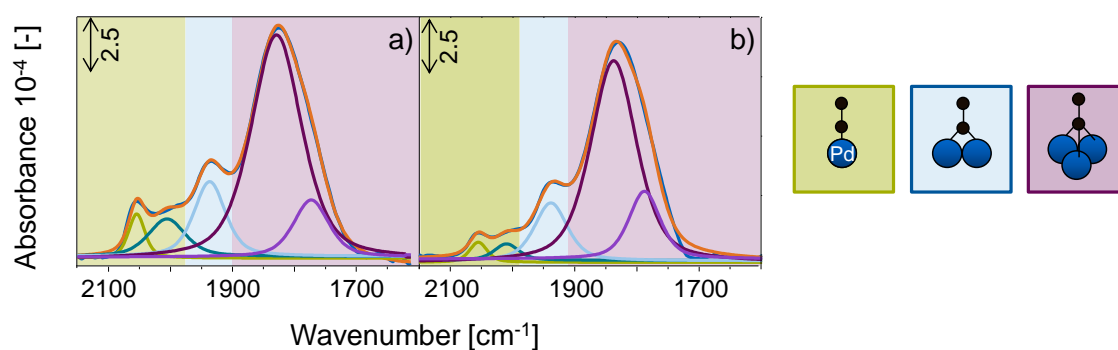


**Figure 4.5.** IR spectra of 1.0 mbar CO adsorbed on (a) PdAu/KOAc/SiO<sub>2</sub> and on (b) PdAu/KOH/SiO<sub>2</sub> at 100 °C. Green bands are due to linearly adsorbed CO, the bright blue band is assigned to bridged adsorbed CO and violet bands to threefold hollow adsorbed CO.

**Table 4.4.** CO band positions, molar ratio of linear/bridged adsorbed CO ratio and total concentration of surface Pd sites on PdAu/KOAc/SiO<sub>2</sub> and PdAu/KOH/SiO<sub>2</sub> calculated from absorption coefficients of CO on Pd.<sup>[14]</sup>

PdAu/x/SiO <sub>2</sub>	Band positions [cm <sup>-1</sup> ]				Concentration of Pd [10 <sup>-5</sup> mol/g]
	Linear	Bridged	Threefold bridged	Linear/multifold	
KOAc	2055, 2006	1937	1829, 1773	3.5	2.3
KOH	2055, 2009	1938	1837, 1788	1.5	1.0

#### 4.4. Conclusions

The promoters MOAc ( $M^+ = Li^+, Na^+, K^+, Cs^+$ ) on PdAu/SiO<sub>2</sub> are located on the bimetallic particles as well as on the support. On SiO<sub>2</sub>, MOAc forms M<sup>+</sup>-silicates, while on the metal particles it induces the segregation of Pd to the surface of PdAu thereby generating a Pd/M<sup>+</sup>-oxide adlayer during annealing. The formation of the Pd/K<sup>+</sup>-oxide monolayer shell on PdAu particles exerts electronic and geometric changes in the catalysts accompanied by decomposition of acetates and leads to an increase in Pd-Pd bond length. These differences are characterized by two effects on Pd at the outermost layer. Those Pd atoms, which are pulled out beyond the K<sup>+</sup> layer and form a “mixed” layer are located at irregular intervals (and do not contribute to the larger regular Pd-Pd distances). Those Pd atoms enriched at the surface of the PdAu particle have an enhanced distance independent of the nature of the alkali cation, pointing to an unspecific interaction with the outer surface layer. Both Pd will contribute to catalysis, but with a rate significantly lower than the PdAu alloy. For VA synthesis, however, the surface ensembles of Pd modified by KOAc limit side reactions and confine the reactants in small regions. Additionally the weakening of the interaction of the reactants with the metal sites enhances reaction selectivities and activities in the structure sensitive VA synthesis reaction.

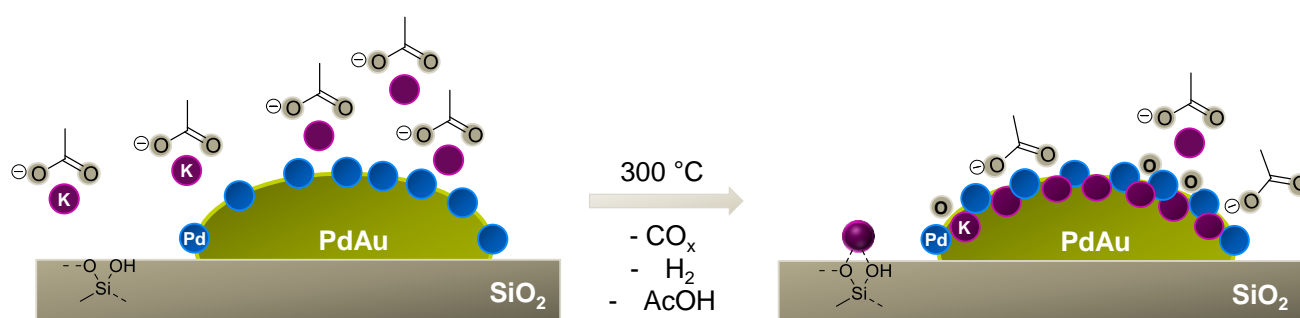


**Figure 4.6.** Formation of the Pd/K<sup>+</sup>-oxide adlayer on PdAu/KOAc/SiO<sub>2</sub> during activation and AcOH adsorption.

## 4.5. References

- [1] M. Chen, D. W. Goodman, *Chinese J. Catal.* **2008**, *29*, 1178-1186.
- [2] M. S. Chen, K. Luo, T. Wei, Z. Yan, D. Kumar, C. W. Yi, D. W. Goodman, *Catal. Today* **2006**, *117*, 37-45.
- [3] A. E. Baber, H. L. Tierney, E. C. H. Sykes, *ACS Nano* **2010**, *4*, 1637-1645.
- [4] E. G. Allison, G. C. Bond, *Catal. Rev.* **1972**, *7*, 233 - 289.
- [5] H. P. Myers, L. Wallden, B. Karlsson, *Philosoph. Magazine* **1968**, *18*, 725-744.
- [6] D. Kumar, M. S. Chen, D. W. Goodman, *Catal. Today* **2007**, *123*, 77-85.
- [7] H. Okamoto, T. Massalski, *J. Phase Equilib.* **1985**, *6*, 229-235.
- [8] R. Elliott, F. Shunk, *J. Phase Equilib.* **1982**, *2*, 482-484.
- [9] A. Maeland, T. B. Flanagan, *Canad. J. Phys.* **1964**, *42*, 2364-2366.
- [10] W. M. H. Sachtler, P. Van Der Plank, *Surf. Sci.* **1969**, *18*, 62-79.
- [11] L. Z. Mezey, J. Giber, *Jpn. J. Appl. Phys.* **1982**, *21*, 1569-1571.
- [12] R. Anton, H. Eggers, J. Veletas, *Thin Solid Films* **1993**, *226*, 39-47.
- [13] C. W. Yi, K. Luo, T. Wei, D. W. Goodman, *J. Phys. Chem. B* **2005**, *109*, 18535-18540.
- [14] E. K. Hanrieder, A. Jentys, J. A. Lercher, *ACS Catalysis* **2015**, 5776-5786.
- [15] E. K. Hanrieder, A. Jentys, J. A. Lercher, *J. Catal.* **2016**, *333*, 71-77.
- [16] S. Simson, A. Jentys, J. A. Lercher, *J. Phys. Chem. C* **2013**, *117*, 8161-8169.
- [17] S. Simson, A. Jentys, J. A. Lercher, *J. Phys. Chem. C* **2015**, *119*, 2471-2482.
- [18] M. Chen, D. Kumar, C.-W. Yi, D. W. Goodman, *Science* **2005**, *310*, 291-293.
- [19] H.-J. Eberle, R. Heidenreich, J. Weis, *Ger. DE 10 2006 058 800 A1 2008.06.19*, **2008**.
- [20] L. Vegard, *Z. Physik* **1921**, *5*, 17-26.
- [21] B. Ravel, M. Newville, *J. Synchrotron Rad.* **2005**, *12*, 537-541.
- [22] W. K. Kuhn, J. Szanyi, D. W. Goodman, *Surf. Sci.* **1992**, *274*, L611-L618.
- [23] M. Mihaylov, K. Hadjiivanov, H. Knözinger, *Catal. Lett.* **2001**, *76*, 59-63.
- [24] T. Montanari, L. Castoldi, L. Lietti, G. Busca, *Appl. Catal. A* **2011**, *400*, 61-69.
- [25] T. Montanari, R. Matarrese, N. Artioli, G. Busca, *Appl. Catal. B* **2011**, *105*, 15-23.
- [26] T. P. Beebe, P. Gelin, J. T. Yates Jr, *Surf. Sci.* **1984**, *148*, 526-550.
- [27] M. Mihaylov, H. Knözinger, K. Hadjiivanov, B. C. Gates, *Chem. Ing. Tech.* **2007**, *79*, 795-806.
- [28] J. Shen, J. Hill, R. Watwe, S. G. Podkolzin, J. A. Dumesic, *Catal. Lett.* **1999**, *60*, 1-9.
- [29] E. L. Kugler, M. Boudart, *J. Catal.* **1979**, *59*, 201-210.
- [30] D. C. Meier, D. W. Goodman, *J. Am. Chem. Soc.* **2004**, *126*, 1892-1899.
- [31] E. Ozensoy, D. Wayne Goodman, *Phys. Chem. Chem. Phys.* **2004**, *6*, 3765-3778.
- [32] T. Wei, J. Wang, D. W. Goodman, *J. Phys. Chem. C* **2007**, *111*, 8781-8788.
- [33] F. Gao, D. W. Goodman, *Chem. Soc. Rev.* **2012**, *41*, 8009-8020.
- [34] D. Rainer, *J. Vac. Sci. Technol. A* **1997**, *15*, 1653-1662.
- [35] J. A. Rodriguez, D. W. Goodman, *Science* **1992**, *257*, 897-903.

- [36] Y.-S. Lee, Y. Jeon, Y.-M. Chung, K.-Y. Lim, C.-N. Whang, S.-J. Oh, *J. Korean Phys. Soc.* **2000**, *37*, 451-455.
- [37] C. T. Campbell, D. W. Goodman, *Surf. Sci.* **1982**, *123*, 413-426.
- [38] J. E. Crowell, E. L. Garfunkel, G. A. Somorjai, *Surf. Sci.* **1982**, *121*, 303-320.
- [39] J. E. Crowell, G. A. Somorjai, *Appl. Surf. Sci.* **1984**, *19*, 73-91.
- [40] E. L. Garfunkel, M. H. Farias, G. A. Somorjai, *J. Am. Chem. Soc.* **1985**, *107*, 349-353.
- [41] E. L. Garfunkel, J. E. Crowell, G. A. Somorjai, *J. Phys. Chem.* **1982**, *86*, 310-313.
- [42] E. L. Garfunkel, G. A. Somorjai, *Surf. Sci.* **1982**, *115*, 441-454.
- [43] A. F. Gusovius, T. C. Watling, R. Prins, *Appl. Catal. A* **1999**, *188*, 187-199.
- [44] F. Stoop, F. J. C. M. Toolenaar, V. Ponc, *J. Catal.* **1982**, *73*, 50-56.
- [45] A. Sárkány, O. Geszti, G. Sáfrán, *Appl. Catal. A* **2008**, *350*, 157-163.
- [46] M. Bowker, C. Morgan, V. P. Zhdanov, *Phys. Chem. Chem. Phys.* **2007**, *9*, 5700-5703.
- [47] S. Nakamura, T. Yasui, *J. Catal.* **1970**, *17*, 366-374.
- [48] S. A. H. Zaidi, *J. Catal.* **1981**, *68*, 255-263.
- [49] S. B. Ziemecki, G. A. Jones, D. G. Swartzfager, R. L. Harlow, J. Faber, *J. Am. Chem. Soc.* **1985**, *107*, 4547-4548.
- [50] M. Bonarowska, A. Malinowski, W. Juszczak, Z. Karpiński, *Appl. Catal. B* **2001**, *30*, 187-193.
- [51] M.-M. Pohl, J. Radnik, M. Schneider, U. Bentrup, D. Linke, A. Brückner, E. Ferguson, *J. Catal.* **2009**, *262*, 314-323.

## 4.6. Appendix

## In Situ X-Ray Diffraction Programs

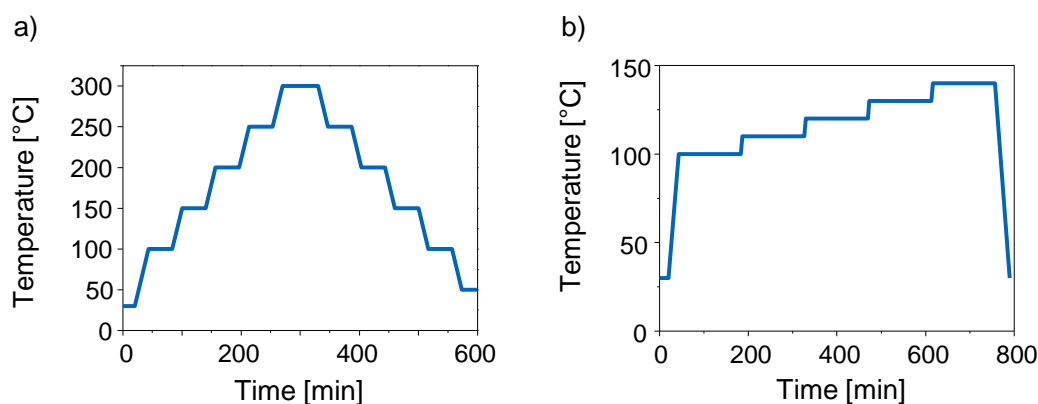


**Figure A4.1.** In situ XRD temperature programs. (a) The temperature was increased from 30 to 300 °C and cooled to 50 °C with a heating/cooling rate of 3 °C/min. At each temperature level, a 20 min XRD pattern was recorded after equilibrating the temperature for 20 min. (b) The temperature was raised from 30 °C to 100 °C and then in steps of 10 °C to 140 °C (heating rate 3 °C/min). In contrast to program (a), the temperature was equilibrated for 2h prior to a 20 min XRD measurement.

### XAFS Functions at the Pd-K and Au-L<sub>3</sub> Edge of Unpromoted and Li-acetate Promoted PdAu/SiO<sub>2</sub>

The  $k^2$  weighted EXAFS functions of (a) Au and (b) Pd edges differ slightly between unpromoted (blue) and LiOAc promoted (violet) PdAu/SiO<sub>2</sub> catalysts. The addition of LiOAc to PdAu/SiO<sub>2</sub> qualitatively induced no changes in metal-metal distances. Additional oscillations might reveal changing surroundings of Pd and Au.

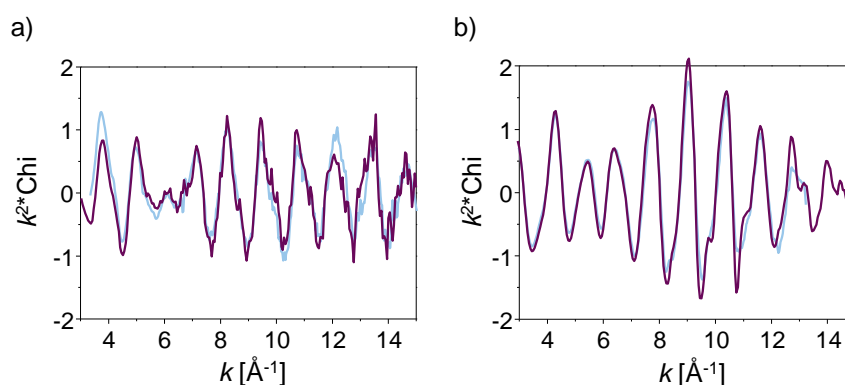


**Figure A4.2.** EXAFS function at the a) Pd-K and b) Au-L<sub>3</sub> edge of PdAu/SiO<sub>2</sub> (blue) and PdAu/LiOAc/SiO<sub>2</sub> (violet),  $k^2$  weighted.



## In situ X-Ray Diffraction Studies

Radius dependent Pd(111) peak shifts were investigated by applying (a) LiOAc, (b) NaOAc, (c) KOAc and (d) CsOAc impregnated PdAu/SiO<sub>2</sub> to the in situ XRD program in Figure A4.1b.

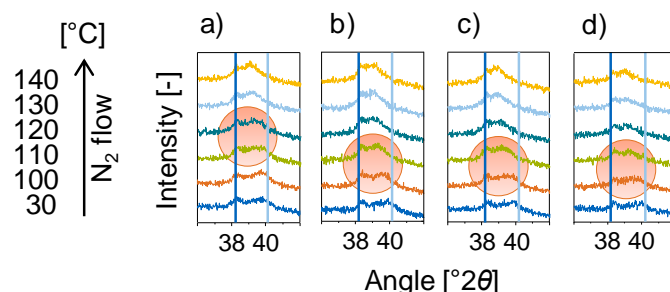


**Figure A4.3.** In situ XRD profiles for Pd<sub>x</sub>Au<sub>y</sub>(111) of (a) PdAu/LiOAc/SiO<sub>2</sub>, (b) PdAu/NaOAc/SiO<sub>2</sub>, (c) PdAu/KOAc/SiO<sub>2</sub> and (d) PdAu/CsOAc/SiO<sub>2</sub> in flowing N<sub>2</sub>. The bimetallic phase is located between those of the pure metals: Au(111) ( $2\theta = 38.3^\circ$ , blue bar) and Pd(111) ( $2\theta = 40.1^\circ$ , bright blue bar).

Figure A4.4 depicts the peak position of Pd(111) of (a) unpromoted as well as alkali acetate promoted PdAu/SiO<sub>2</sub> and (b) of KOH, K<sub>2</sub>CO<sub>3</sub>, K<sub>2</sub>C<sub>2</sub>O<sub>4</sub> and KOAc impregnated PdAu/SiO<sub>2</sub> as function of the temperature for the in situ XRD program in Figure A4.1a.

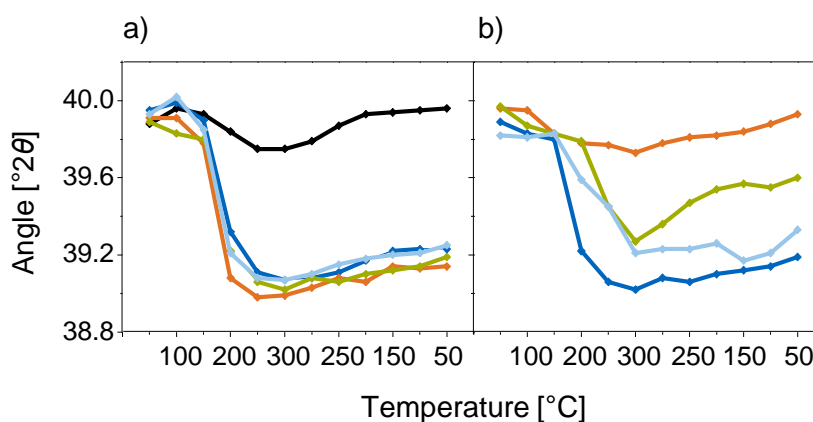


**Figure A4.4.** Temperature dependent position of Pd(111) of PdAu/SiO<sub>2</sub> promoted with (a) promoter free (black), LiOAc (blue), NaOAc (orange), KOAc (green), CsOAc (bright blue) and (b) KOAc (blue), KOH (orange), K<sub>2</sub>CO<sub>3</sub> (green), K<sub>2</sub>C<sub>2</sub>O<sub>4</sub> (bright blue).

## In Situ X-Ray Diffraction Studies on Pd Carbide, Hydride and Oxide Formation

Adsorbed carbon from decomposed acetates<sup>[1-2]</sup> migrates to the Pd bulk to form PdC<sub>x</sub> leading to a downshift of the Pd reflections corresponding to a Pd-Pd bond enlargement of 0.075 Å.<sup>[3-4]</sup> The presence of PdC<sub>x</sub> instead of a Pd/K<sup>+</sup> mixed adlayer was not only excluded because of the difference in Pd bond enlargement (0.055 Å compared to 0.075 Å) but also by several independent experiments. Pd(OAc)<sub>2</sub> impregnated Pd/SiO<sub>2</sub> should

show the Pd(111) shift in the absence of KOAc due to Pd(OAc)<sub>2</sub> decomposition that creates PdC<sub>x</sub>. (Figure A4.5a) Decomposition of thermally unstable Pd(OAc)<sub>2</sub> above 140 °C led to the expected, however reversible in contrast to the irreversible Pd(111) shift for PdAu/KOAc/SiO<sub>2</sub>. The absence of PdC<sub>x</sub> from decomposed acetate was confirmed by applying NH<sub>4</sub>OAc impregnated PdAu/SiO<sub>2</sub> (Figure A4.5b). NH<sub>4</sub>OAc decomposed, but generated tetragonal PdO at 34.0, 54.8 and 60.8 °2θ<sup>[5]</sup> and no shift of Pd(111) due to PdC<sub>x</sub>. Additionally, possible PdC<sub>x</sub> species in PdAu<sup>[6]</sup> can be removed by H<sub>2</sub> treatment at 180 °C.<sup>[7]</sup> Thus, PdAu/KOAc/SiO<sub>2</sub> was heated in N<sub>2</sub> to observe the downshift of Pd(111) and then in H<sub>2</sub> to remove possible PdC<sub>x</sub> species (Figure A4.5c). As expected, the Pd(111) peak shift occurred above 150 °C in N<sub>2</sub> but it was irreversible in H<sub>2</sub> strongly suggesting the absence of PdC<sub>x</sub>.

Pd-hydride formation in H<sub>2</sub>/N<sub>2</sub> as cause for the irreversible downshift of Pd(111) in PdAu/KOAc/SiO<sub>2</sub> is also excluded since hydrides decomposed above 150 °C leading to reversible Pd(111) shifts (Figure A4.5d).

Formation of PdO on Pd(111)<sup>[8-11]</sup> was reported to form above 470 K and 2 · 10<sup>-2</sup> Pa.<sup>[12]</sup> In order to check for PdO, in situ XRD was performed with PdAu/KOAc/SiO<sub>2</sub> in synthetic air (Figure 4.5e). The Pd(111) peak did not shift but became lower in intensity as soon as additional peaks for tetragonal PdO<sup>[5]</sup> formed. Consequently, the formation of bulk PdO can be excluded.

Summarily, our findings on the nature of interstitial PdC<sub>x</sub> species, on Pd oxide and hydride species and the general finding that Au suppressed carbide formation in PdAu particles<sup>[13-14]</sup> led us to the conclusion that exclusively M<sup>+</sup> from MOAc (M<sup>+</sup> = Li<sup>+</sup>, Na<sup>+</sup>, K<sup>+</sup>, Cs<sup>+</sup>) induced the Pd-Pd bond enlargement.

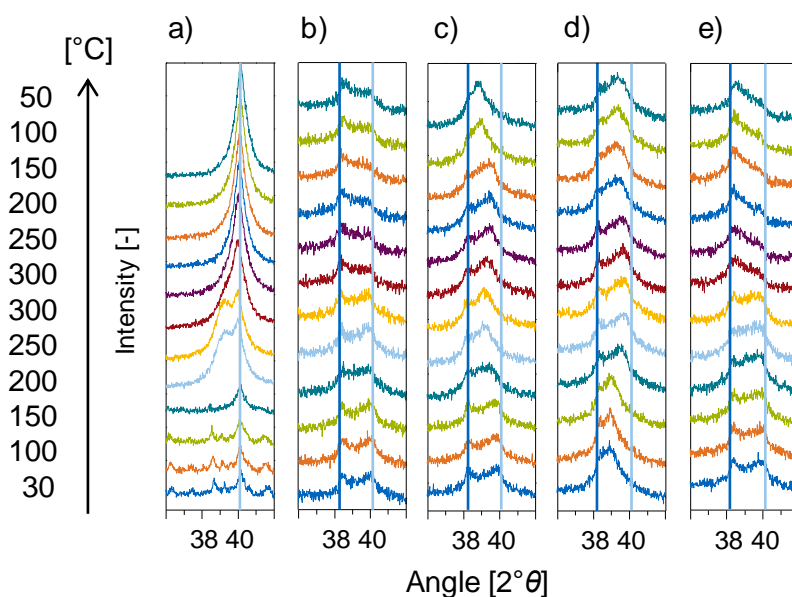


**Figure A4.5.** Temperature dependent In situ XRD studies with (a) Pd/Pd(OAc)<sub>2</sub> in N<sub>2</sub>, (b) PdAu/NH<sub>4</sub>OAc in N<sub>2</sub>, (c) PdAu/KOAc in N<sub>2</sub>/H<sub>2</sub>, (d) PdAu/KOAc in H<sub>2</sub>/N<sub>2</sub> and (e) PdAu/KOAc in synthetic air. The bimetallic phase is located between those of the pure metals: Au(111) ( $2\theta = 38.3^\circ$ , blue line) and Pd(111) ( $2\theta = 40.1^\circ$ , bright blue line).

## Temperature Dependent CO Adsorption on Au/SiO<sub>2</sub>, Pd/SiO<sub>2</sub> and PdAu/SiO<sub>2</sub> Followed by IR Spectroscopy

In order to determine the effect of temperature<sup>[15]</sup> on CO band positions, CO was adsorbed on Au/SiO<sub>2</sub>, Pd/SiO<sub>2</sub> and PdAu/SiO<sub>2</sub> at -89, -50, 0, 50 and 100 °C (Figure A4.6). On Au/SiO<sub>2</sub>, CO linearly adsorbed at 2104 cm<sup>-1</sup> while the broad bands at 2020 and 1890 cm<sup>-1</sup> derived from subtraction errors with the spectrum of the activated sample measured at 50 °C (Figure A4.6a). CO linearly adsorbed on Pd at 2109 and 1991 cm<sup>-1</sup> at -89 °C (Figure A4.6b). With increasing temperature, the CO band areas and frequencies decreased due to lower CO coverages and thus less CO dipole coupling.<sup>[15-17]</sup> In the bimetallic case (Figure A4.6c), CO adsorbed on Au in contact to Pd at 2109 cm<sup>-1</sup> and on Pd close to Au at 2083 cm<sup>-1</sup> at -89 °C. Thus, the contact of Au with Pd leads to an increase and the contact of Pd to Au to a decrease of CO band frequencies according to the electronic Pd-Au interactions described in the two band model.<sup>[18-19]</sup> However, an increase in temperature leads to a slight upshift of CO on Au (~3 cm<sup>-1</sup>) like observed from Rainer<sup>[20]</sup> and France et al.<sup>[21]</sup> and a downshift of linear CO on Pd (~7 cm<sup>-1</sup>). CO/Au shows a large negative shift which offsets the positive dipolar shift as CO coverage increases. The upshift can be explained by the weakening of the Au-C bond upon temperature increase. The downshift of CO on Pd might be due to the reduction in CO dipole couplings (transition from a compressed to an uncompressed CO overlayer).

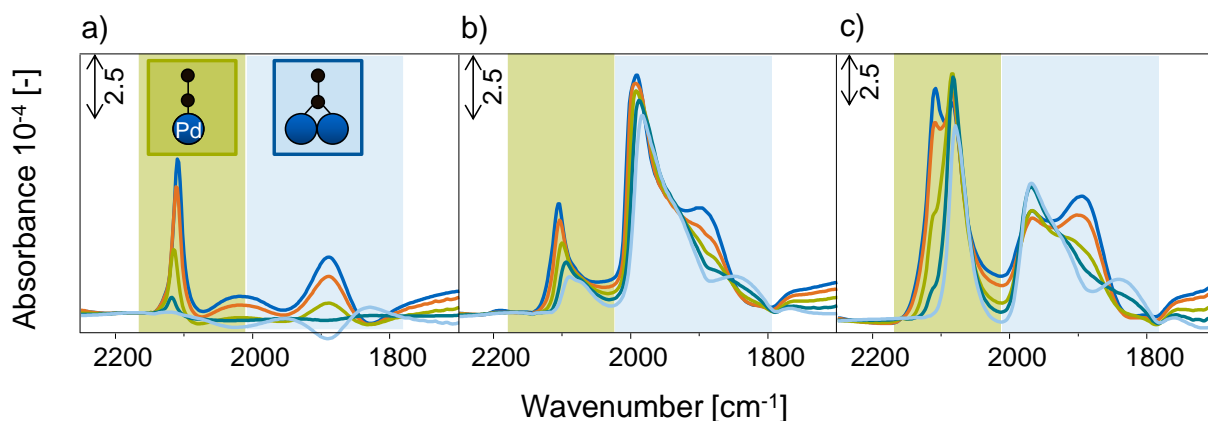


**Figure A4.6.** IR spectra of 1.0 mbar CO adsorbed on (a) Au/SiO<sub>2</sub>, on (b) Pd/SiO<sub>2</sub> and on (c) PdAu/SiO<sub>2</sub> at -89 °C (blue), -50 °C (orange), 0 °C (green), 50 °C (dark green) and 100 °C (bright blue).

At 100 °C, linear and bridged adsorption modes were observed at 2090 cm<sup>-1</sup> and 1984 cm<sup>-1</sup> on Pd/SiO<sub>2</sub>, whereas on Au/SiO<sub>2</sub>, CO adsorbed only in a linear mode at 2118 cm<sup>-1</sup> (50 °C).<sup>[22]</sup> The temperature dependent spectra revealed that CO adsorbed exclusively on Pd above 50 °C.

---

**References**

- [1] N. Aas, M. Bowker, *J. Chem. Soc., Faraday Trans.* **1993**, 89, 1249-1255.
- [2] M. Bowker, C. Morgan, V. P. Zhdanov, *Phys. Chem. Chem. Phys.* **2007**, 9, 5700-5703.
- [3] M. Bowker, C. Morgan, J. Couves, *Surf. Sci.* **2004**, 555, 145-156.
- [4] S. B. Ziemecki, G. A. Jones, D. G. Swartzfager, R. L. Harlow, J. Faber, *J. Am. Chem. Soc.* **1985**, 107, 4547-4548.
- [5] J. Waser, H. A. Levy, S. W. Peterson, *Acta Crystall.* **1953**, 6, 661-663.
- [6] M. Bonarowska, A. Malinowski, W. Juszczak, Z. Karpiński, *Appl. Catal. B* **2001**, 30, 187-193.
- [7] M. Bonarowska, J. Pielaszek, V. A. Semikolenov, Z. Karpiński, *J. Catal.* **2002**, 209, 528-538.
- [8] H. Conrad, G. Ertl, J. Küppers, E. E. Latta, *Surf. Sci.* **1977**, 65, 245-260.
- [9] B. A. Banse, B. E. Koel, *Surf. Sci.* **1990**, 232, 275-285.
- [10] S. Yang, A. Maroto-Valiente, M. Benito-Gonzalez, I. Rodriguez-Ramos, A. Guerrero-Ruiz, *Appl. Catal. B* **2000**, 28, 223-233.
- [11] A. M. Venezia, L. F. Liotta, G. Pantaleo, V. La Parola, G. Deganello, A. Beck, Z. Koppány, K. Frey, D. Horváth, L. Guzzi, *Appl. Catal. A* **2003**, 251, 359-368.
- [12] E. H. Voogt, A. J. M. Mens, O. L. J. Gijzeman, J. W. Geus, *Surf. Sci.* **1997**, 373, 210-220.
- [13] Y. F. Han, D. Kumar, C. Sivadinarayana, A. Clearfield, D. W. Goodman, *Catal. Lett.* **2004**, 94, 131.
- [14] M. Bowker, C. Morgan, *Catal. Lett.* **2004**, 98, 67-67.
- [15] W. K. Kuhn, J. Szanyi, D. W. Goodman, *Surf. Sci.* **1992**, 274, L611-L618.
- [16] R. P. Eischens, S. A. Francis, W. A. Pliskin, *J. Phys. Chem.* **1956**, 60, 194-201.
- [17] M. Primet, *J. Catal.* **1984**, 88, 273-282.
- [18] N. F. Mott, *Proc. Phys. Soc.* **1935**, 47, 571-588.
- [19] P. Liu, J. K. Nørskov, *Phys. Chem. Chem. Phys.* **2001**, 3, 3814-3818.
- [20] D. Rainer, *J. Vac. Sci. Technol. A* **1997**, 15, 1653-1662.
- [21] J. France, P. Hollins, *J. Electron. Spectrosc. Relat. Phenom.* **1993**, 64-65, 251-258.
- [22] E. L. Kugler, M. Boudart, *J. Catal.* **1979**, 59, 201-210.

# Chapter 5

## Summary

Vinyl acetate (VA) synthesis over SiO<sub>2</sub> supported bimetallic PdAu catalysts is a well-established industrial process. Two neighbored Pd atoms, separated by inert Au atoms on the PdAu particle surface were identified as highly active and selective ensembles. Catalyst structures dynamically form in the presence of the alkali acetate promoter, potassium acetate (KOAc). KOAc is essential to obtain high activities and selectivities and, thus, KOAc was hypothesized to profoundly influence reordering of the PdAu bulk and surface structures. However, PdAu catalysts suffer from a gradual loss of KOAc which may cause long time deactivation.

So the goals of this study were to (1) resolve the catalyst structure under working conditions in absence and presence of the promoter KOAc, (2) to identify reactive intermediates in an overall reordering PdAu network, (3) to evaluate the influence of the nature of alkali acetate MOAc (M<sup>+</sup> = Li<sup>+</sup>, Na<sup>+</sup>, K<sup>+</sup>, Cs<sup>+</sup>) promoters on deactivation of PdAu and (4) to address the (temperature dependent) interaction of the promoter with PdAu.

We were able to derive a restructuring mechanism for bimetallic PdAu catalysts, by applying various surface and bulk sensitive characterization techniques on as synthesized and used samples as well as under operating conditions of vinyl acetate synthesis.

Reordering of PdAu particles is attributed to the adsorbate-induced segregation of Pd<sup>0</sup> to the PdAu particle surface and its oxidation to Pd<sup>2+</sup>. In absence of KOAc, trimeric inactive Pd<sub>3</sub>(OAc)<sub>6</sub> and in presence of KOAc, active K<sub>2</sub>Pd<sub>2</sub>(OAc)<sub>6</sub> complexes form by reaction with the reactants. Subsequent extraction of these homogeneous complexes from the bimetallic particles into the liquid phase consisting of AcOH and H<sub>2</sub>O generates Pd depleted PdAu particles. In presence of KOAc, an equimolar ~Pd<sub>50</sub>Au<sub>50</sub> phase forms whereas in absence of the promoter, bimetallic particles with Au enriched Pd<sub>40</sub>Au<sub>60</sub> compositions were generated. PdAu particles do not completely dissolve in acetic acid under reaction conditions since Pd<sup>2+</sup> species can be reduced to Pd<sup>0</sup> via the homogeneous pathway to VA and Pd<sup>0</sup> can reincorporate into Pd<sub>x</sub>Au<sub>y</sub>. As Pd<sub>3</sub>(OAc)<sub>6</sub> is stable in acetic acid in contrast to reactive K<sub>2</sub>Pd<sub>2</sub>(OAc)<sub>6</sub>, reincorporation of Pd<sup>0</sup> from Pd<sub>3</sub>(OAc)<sub>6</sub> into PdAu is hindered and thus, Au enriched but thermodynamically stable Pd<sub>40</sub>Au<sub>60</sub> particles are formed. Additionally, the Pd leaching is slowed down as soon as the surface is Pd enriched but intermixed, since the electronic influence of Au on Pd reduces the oxidizability of Pd. Moreover a saturation concentration of the Pd acetate species in the

liquid surface layer limits further Pd extraction from the bimetallic particle into the liquid surface layer. Summarily, the overall catalyst activity consists from Pd<sup>0</sup> ensembles on solid PdAu surfaces and from less active Pd<sup>2+</sup> homogeneous species. The rate enhancing role of KOAc is to convert inactive Pd<sub>3</sub>(OAc)<sub>6</sub> trimers to active K<sub>2</sub>Pd<sub>2</sub>(OAc)<sub>6</sub> dimers, to stabilize Pd<sup>0</sup> on the active surface and to transfer acetates/acetic acid to Pd<sup>0</sup> on PdAu thereby favoring the coupling to vinyl acetate rather than the unselective combustion of ethene to CO<sub>2</sub>.

Reordering of PdAu particles and thus, the activity and long-term deactivation was shown to depend on the nature of promoter metal M<sup>+</sup> varying from Li<sup>+</sup>, Na<sup>+</sup>, K<sup>+</sup> to Cs<sup>+</sup>. The different solvation energies of M<sup>+</sup> influence the equilibrium constant *K* of the conversion from leached Pd<sub>3</sub>(OAc)<sub>6</sub> with MOAc to M<sub>2</sub>Pd<sub>2</sub>(OAc)<sub>6</sub>. The equilibrium shifts to active M<sub>2</sub>Pd<sub>2</sub>(OAc)<sub>6</sub> from Li<sup>+</sup> to Cs<sup>+</sup> lowering the possibility for M<sup>+</sup> to leach into the fluid phase, decreasing the concentration of inactive Pd<sub>3</sub>(OAc)<sub>6</sub> and thus, abating deactivation of solid PdAu particles. The activity of LiOAc promoted PdAu decreased drastically in parallel to the dramatic loss of the promoter which concentration became finally too low to maintain a Pd enriched PdAu surface. Thus, activity as well as selectivity dropped markedly.

The temperature dependent interaction of MOAc with PdAu induces reordering of PdAu accompanied by Pd surface segregation and the formation of a mixed Pd/M<sup>+</sup>-oxidic adlayer as shell on the PdAu particle. This adlayer offer elongated Pd-Pd bond lengths which causes the Fermi level within the Pd d-band to rise enhancing the atomic-like character of Pd atoms. Correspondingly, the Pd surface lattice mismatch induced by KOAc confines reactants in a small region, weakens binding toward reactants and thus, increase the catalytic activity especially in structure sensitive reactions like in vinyl acetate synthesis.

# Chapter 6

## Zusammenfassung

Die Synthese von Vinylacetat (VA) über  $\text{SiO}_2$  getragerte, bimetallische PdAu Katalysatoren ist ein fest etablierter großindustrieller Prozess. Zwei benachbarte, durch inerte Au Atome getrennte, Pd Atome auf der PdAu Partikeloberfläche wurden als hochaktive und selektive Zentren identifiziert. Die Katalysatorstrukturen bilden sich dynamisch durch die Anwesenheit des Alkaliacetat-Promoters, Kaliumacetat (KOAc). Die Zugabe von KOAc ist essentiell, um hohe Aktivitäten- und Selektivitäten zu erhalten. Deswegen wurde vermutet, dass KOAc die Reorganisation des PdAu Partikelkerns und der -oberfläche tiefgreifend beeinflusst. Die PdAu Katalysatoren verlieren allmählich KOAc unter Reaktionsbedingungen, was Langzeitdeaktivierung hervorrufen könnte.

In diesem Zusammenhang waren die Ziele der vorliegenden Arbeit (1) die Katalysatorstruktur unter Reaktionsbedingungen in An- und Abwesenheit des Promoters KOAc aufzuklären, (2) reaktive Intermediate innerhalb eines Restrukturierungsnetzwerks von PdAu zu identifizieren, (3) den Einfluss der verschiedenen Alkaliacetat-Promotoren MOAc ( $M^+ = \text{Li}^+, \text{Na}^+, \text{K}^+, \text{Cs}^+$ ) auf die Deaktivierung von PdAu herauszufinden und (4) die temperaturbedingte Wechselwirkung zwischen dem Promotor und PdAu zu untersuchen. Der Mechanismus, nach dem bimetallische Katalysatoren unter Reaktionsbedingungen restrukturieren, wurde anhand der Charakterisierung der Proben vor, während und nach der Reaktion bestimmt, wobei sowohl Oberflächen- als auch Partikelkern-sensitive Methoden angewendet wurden.

Die Restrukturierung der PdAu Partikel wurde auf die adsorbatinduzierte Segregation von  $\text{Pd}^0$  auf die Partikeloberfläche und dessen Oxidation zu  $\text{Pd}^{2+}$  zurückgeführt. In Abwesenheit von KOAc entsteht trimeres, inaktives  $\text{Pd}_3(\text{OAc})_6$  und in Anwesenheit von KOAc, aktive  $\text{K}_2\text{Pd}_2(\text{OAc})_6$  Komplexe durch die Reaktion mit den Reaktanten. Das anschließende Herauslösen dieser homogenen Komplexe aus den bimetallischen Partikeln in die Flüssigphase aus Essigsäure und Wasser generiert Pd verarmte PdAu Partikel. Durch KOAc bilden sich PdAu Partikel in äquimolarer Zusammensetzung,  $\text{Pd}_{50}\text{Au}_{50}$ , wohingegen sich in Abwesenheit von KOAc goldreiche Partikel der Zusammensetzung  $\text{Pd}_{40}\text{Au}_{60}$  bilden. Die PdAu Partikel lösen sich unter Reaktionsbedingungen nicht vollständig in Essigsäure auf, weil die  $\text{Pd}^{2+}$  Spezies über den homogenen Mechanismus zu VA zu  $\text{Pd}^0$  reduziert werden und sich  $\text{Pd}^0$  in PdAu wiedereinlagern kann. Dadurch, dass

$\text{Pd}_3(\text{OAc})_6$  im Gegensatz zu reaktiven  $\text{K}_2\text{Pd}_2(\text{OAc})_6$  stabil in Essigsäure ist, ist die Einlagerung von  $\text{Pd}^0$  aus  $\text{Pd}_3(\text{OAc})_6$  in PdAu unterdrückt und deswegen bilden sich thermodynamisch stabile, aber goldreiche  $\text{Pd}_{40}\text{Au}_{60}$  Partikel. Zusätzlich verringert sich das Herauslösen von Palladium, sobald die Metalloberfläche Pd-reich aber gut vermischt ist, da der elektronische Einfluss von Au auf Pd die Oxidierbarkeit des Palladiums herabsetzt. Außerdem verlangsamt eine hohe Konzentration der gebildeten Palladiumacetat-Spezies innerhalb des Flüssigfilms den Extraktionsvorgang. Kurzgefasst, die Gesamtaktivität des Katalysators rührt von  $\text{Pd}^0$  Anordnungen auf der PdAu Oberfläche und von weniger aktiven, homogenen  $\text{Pd}^{2+}$  Spezies her. KOAc erhöht die Rate zu VA, weil es inaktive  $\text{Pd}_3(\text{OAc})_6$ -Trimere zu aktiven  $\text{K}_2\text{Pd}_2(\text{OAc})_6$ -Dimeren umwandelt,  $\text{Pd}^0$  auf der aktiven Oberfläche stabilisiert und Acetate bzw. Essigsäure zur PdAu Oberfläche transferiert. Dadurch wird die Kupplung zu VA im Gegensatz zur unselektiven Verbrennung von Ethen zu  $\text{CO}_2$  begünstigt.

Die Restrukturierung und deshalb auch die Aktivität sowie Langzeitdeaktivierung der PdAu Partikel hängt von dem Promotormetall  $\text{M}^+$  ( $\text{Li}^+$ ,  $\text{Na}^+$ ,  $\text{K}^+$  to  $\text{Cs}^+$ ) ab. Die unterschiedlichen Solvatationsenergien von  $\text{M}^+$  beeinflusst die Gleichgewichtskonstante  $K$  der Umwandlung von  $\text{Pd}_3(\text{OAc})_6$  mit MOAc zu  $\text{M}_2\text{Pd}_2(\text{OAc})_6$ . Von  $\text{Li}^+$  zu  $\text{Cs}^+$  liegt das Gleichgewicht zunehmend auf der Seite von aktiven  $\text{M}_2\text{Pd}_2(\text{OAc})_6$ . Dadurch erniedrigt sich nicht nur die Wahrscheinlichkeit für das Leachen von  $\text{M}^+$ , sondern auch die Konzentration von inaktiven  $\text{Pd}_3(\text{OAc})_6$  und dadurch die Deaktivierung der PdAu Partikel. Die Aktivität LiOAc promotierter PdAu Katalysatoren sank erheblich durch den erhöhten Promotorverlust, sodass die Promotorkonzentration schließlich zu klein war, um eine Pd reiche PdAu Oberfläche zu erhalten.

Die temperaturabhängige Wechselwirkung von MOAc mit PdAu initiiert die Restrukturierung von PdAu, die mit der Pd Oberflächenanreicherung und der Bildung einer gemischten Pd/ $\text{M}^+$ -oxidischen Adlayer als Schale auf den PdAu Partikeln einhergeht. Diese Adlayer zeigte aufgeweitete Pd-Pd Abstände auf, welche das Fermi-niveau innerhalb des Pd-d Bandes anhebt und so den atomaren Charakter von Pd erhöht. Gleichermaßen begrenzt die fehlerhafte Anordnung der Pd Atome durch KOAc die Reaktanten in einer kleinen Region, schwächt Reaktantbindungen und steigert so die katalytische Aktivität speziell von struktursensitiven Reaktionen wie der Vinylacetatsynthese.



# Curriculum Vitae

## Persönliche Daten

---

Name Elisabeth Katharina Hanrieder  
Geburtsdatum /-ort 08.09.1986, Freising  
Familienstand Ledig  
Nationalität Deutsch

## Berufserfahrung

---

08/2015 – heute **Anton Paar Switzerland AG**  
Produktspezialistin für Präzisionslabormessgeräte

10/2011 – 05/2015 **Technische Universität München**  
Promotion am Lehrstuhl für Technische Chemie II in Kooperation mit der Wacker Chemie AG

08/2010 - 09/2010 **Industriepraktikum bei der Süd-Chemie AG, Heufeld/Bruckmühl**

## Studium / Schule

---

10/2009 – 08/2011 **Technische Universität München**  
**Masterstudium Chemie** (Note 1,3)

- Schwerpunkte: Anorganische Chemie, Katalyse und Reaktionstechnik
- Masterarbeit: Promoted bimetallic PdAu catalysts for gas phase vinyl acetate synthesis (Note 1,0)

10/2006 – 08/2009 **Technische Universität München**  
**Bachelorstudium Chemie** (Note 2,0)

- Bachelorarbeit: Synthese und Charakterisierung Fe-getauschter Zeolithe (Note 1,7)

09/1997 - 06/2006 **Josef-Hofmiller-Gymnasium, Freising**

- Allgemeine Hochschulreife (Note 1,7)

## Auszeichnungen

---

03/2015 Posterpreis der Deutschen Gesellschaft für Katalyse auf dem 48. Jahrestreffen Deutscher Katalytiker, Weimar

10/2011 Wacker Presidential Science Award als Promotionsstipendium im Institut für Siliciumchemie

## Auslandserfahrung

---

08/2014 Vortrag auf dem ACS Meeting, San Francisco, USA

# Liste der Publikationen

## Publikationen in Fachzeitschriften

- ACS Catal.*                    E. K. Hanrieder, A. Jentys, J. A. Lercher  
Atomistic Engineering of Catalyst Precursors - Dynamic Reordering of PdAu Nanoparticles during Vinyl Acetate Synthesis enhanced by Potassium Acetate, *ACS Catalysis* **2015**, 5776.
- J. Catal.*                        E. K. Hanrieder, A. Jentys, J. A. Lercher  
Impact of Alkali Acetates on Deactivation of PdAu during Vinyl Acetate Synthesis, *J. Catal.* **2016**, 333, 71.
- to be submitted                E. K. Hanrieder, A. Jentys, J. A. Lercher  
Interaction of Alkali Acetates with PdAu.
- to be submitted                E. K. Hanrieder, A. Jentys, J. A. Lercher  
Influence of the Promoter and Reactant Concentrations on the Reordering of PdAu during Vinyl Acetate Synthesis.

## Vorträge

- 2015                                E. K. Hanrieder, A. Jentys, J. A. Lercher  
48. Jahrestreffen Deutscher Katalytiker, Weimar, Deutschland  
Formation of a Mixed Pd/K<sup>+</sup> Phase on the PdAu Catalyst during Vinyl Acetate Synthesis.
- 2014                                E. K. Hanrieder, A. Jentys, J. A. Lercher  
248<sup>th</sup> ACS National Meeting and Exposition, San Francisco, USA  
Interaction of the Alkaline Acetate Promoter with Bimetallic PdAu Catalysts for Vinyl Acetate Synthesis.

## Posterpräsentationen

- 2015                                E. K. Hanrieder, A. Jentys, J. A. Lercher  
48. Jahrestreffen Deutscher Katalytiker, Weimar, Deutschland  
Formation of a Mixed Pd/K Phase on the PdAu Catalyst during Vinyl Acetate Synthesis.
- 2014                                E. K. Hanrieder, A. Jentys, J. A. Lercher  
47. Jahrestreffen Deutscher Katalytiker, Weimar, Deutschland,  
Interaction of the Acetate Promoter with Bimetallic PdAu Catalysts for the Gas Phase Vinyl Acetate Synthesis.
- 2013                                E. K. Hanrieder, S. Reiner, A. Jentys, J. A. Lercher  
46. Jahrestreffen Deutscher Katalytiker, Weimar, Deutschland  
Adsorption Studies of Ethylene and Acetic Acid on SiO<sub>2</sub> and Alkali Acetate Promoted SiO<sub>2</sub>.